SOME EFFECTS OF MAGNETIC IMPURITIES ON SUPERCONDUCTIVITY

a thesis submitted

by

JOHN ROBERT COOPER.

for the

Degree of Doctor of Philosophy

of the University of London

Department of Physics.

Imperial College of Science and Technology

London

1969

ABSTRACT

Using a He^3 cryostat, measurements of superconducting transition temperature (T_c) or critical field (H_c) have been made on three types of alloy system.

(1) Results of T_c measurements on $La_{1-x}R_xAl_2$ alloys (R is a rare earth element) have been correlated with the crystal field levels of the R^{+++} ion deduced from magnetic susceptibility measurements on $La_{.98}Tm_{.02}Al_2$. Experiments relating to the theory of Abrikosov-Gorkov (32) for magnetic impurities in superconductors are discussed and this theory is then used to calculate the effect of the lower crystal field levels on T_c. Good agreement with theory is only obtained when the expected isolation of the lowest level is large ($\gtrsim 10^{\circ}K$). When this is $\simeq 3^{\circ}K$ there is evidence that fluctuations in the magnetic moment of the ground state must be considered.

(2) The results of measurements of T_c (or of an upper limit to T_c) for a series of $MgCu_2$ structure XCo_2 compounds (X=Ce, Ti, Zr, Sc, Hf and Nb) are briefly discussed with reference to their enhanced Pauli paramagnetic susceptibilities. There is evidence that Fe in $CeCo_2$ causes an extremely strong depression in T_c ($\simeq 10^3 - 10^4$ $^{\circ}K$/at.%).

(3) $H_c(T)$ measurements have been made on AlZn, AlMn and AlCr alloys all with $T_c \simeq 1^{\circ}K$. Within the accuracy of measurement ($\pm$ 0.003 in $H_c(T)/H_c(0)$) there are no deviations from the theory of BCS (1) which can be attributed to localised spin fluctuations.

ACKNOWLEDGEMENTS

I would like to thank Professor B.R. Coles for his supervision and cheerful encouragement at all stages of this work. Helpful suggestions from Drs. J.G. Park, A. D. Caplin and D. Griffiths are also gratefully acknowledged. Among the past and present research students in the Metal Physics group I would particularly like to thank Mr. J. B. Dunlop for making measurements of magnetic susceptibility on two $LaAl_2$ based alloys and Dr. D.P. Jones for the use of his integrating magnetometer.

The computer program of Dr. L.L. Hirst and Dr. G. Williams for the calculation of crystal field levels has also been most useful. Several people have kindly lent me alloys and these are acknowledged in the text.

Financial support was received from the Science Research Council for the first three years and subsequently from the U.K.A.E.A., Harwell. Finally I would like to thank Miss Joy Dunning for typing this thesis quickly and efficiently.

CONTENTS

	Page
ABSTRACT	2
ACKNOWLEDGEMENTS	3
CONTENTS	4
LIST OF TABLES	10
LIST OF FIGURES	11
INTRODUCTION	13
CHAPTER 1 — SUPERCONDUCTING PROPERTIES AND SYSTEMS OF INTEREST	16
1.1 Introduction	16
1.2 Theoretical M(H,T) Curves	17
1.3 M(H) Curves Observed Experimentally	22
1. Non-ideal behaviour in M(H,T) curves for type II superconductors	23
2. Non-ideal behaviour in T_c and H_{c2}	24
1.4 Types of Alloy System Studied	26
CHAPTER 2 — EFFECTS OF ALLOYING: THEORY AND EXPERIMENT	29
2.1 General Theories	29
2.2 Mean Free Path Effects on T_c and H_c	31

Page

CHAPTER 2 - (Continued)

2.3 Mean Free Path Effects on k 35

2.4 Valence Effects 37

2.5 Localised Impurity States 40

1. Non-magnetic virtual bound state 40
2. Magnetic virtual bound state 42
3. Localised moments - the Abrikosov-Gorkov (AG) theory 43
4. AG expression for T_c-theory and experiment 44

2.6 Other Tests of the AG Theory 52

1. H_c measurements 52
2. Tunnelling measurements 53
3. Other depairing effects 54
4. Specific heat measurements 57
5. k parameters for magnetic impurities 58

2.7 Concluding Remarks and Summary of this Chapter 60

CHAPTER 3 - RARE EARTH IMPURITIES IN SUPERCONDUCTORS 61

I - INITIAL AIMS, EXPERIMENTAL METHODS 61

3.1 Crystal Field Effects in Metals and Salts 61

3.2 Initial Aims 66

3.3 Choice of System 69

Page

CHAPTER 3 - (Continued)

3.4 Experimental Details 71

1. Alloy preparation 71
2. Metallographic examination 74
3. Electron probe analysis 76
4. Effects of annealing the specimens 80
5. Measurement of T_c 81
6. Magnetisation measurements 86

3.5 Results 88

1. Magnetisation curves 88
2. Discussion of the magnetisation results 89
3. T_c measurements for $La_{1-x}R_xAl_2$ alloys 93
4. Susceptibility measurements 94

CHAPTER 4 - RARE EARTH IMPURITIES IN SUPERCONDUCTORS 96

II - RESULTS, ANALYSIS AND DISCUSSION 96

4.1 $La_{1-x}Gd_xAl_2$ (including a discussion on the sign of J_{eff}) 96

4.2 $La_{1-x}Tm_xAl_2$, Susceptibility Results (including the method of fitting χ to the crystal field model) 101

1. Results of the crystal field fit 101
2. The isotropy of the susceptibility 112

4.3 T_c Measurementsfor $La_{1-x}R_xAl_2$ Alloys 117

Page

CHAPTER 4 - (Continued)

4.4 Calculation of dT_c/dx for Known Crystal Field Levels 118

4.5 Discussion of These Results 124

4.6 Results of Other Workers for $LaAl_2$ Based Systems 134

1. $La_{1-x}Ce_xAl_2$ 134
2. $La_{1-x}Pr_xAl_2$ 136

4.7 Results of Other Workers for Similar Systems 137

4.8 Concluding Discussion and Summary for Rare Earth Impurities 142

1. T_c and susceptibility measurements 142
2. Crystal field effects 144

CHAPTER 5 - DILUTE ALLOYS CONTAINING 3d TRANSITION ELEMENTS 148

5.1 Introduction 148

I CRITICAL FIELD MEASUREMENTS ON AlT ALLOYS 151

5.2 Experimental Details 151

1. Measurement of H_c 151
2. Thermal contact measurements 154
3. Other experimental precautions 155

Page

CHAPTER 5 - (Continued)

5.2	4.	Temperature measurement	156
	5.	Temperature control	159
	6.	Secondary thermometers	159
5.3	Results and Analysis		160
	1.	Magnetisation curves	160
	2.	Critical field measurements	162
	3.	Methods of finding H_o	165
5.4	Discussion of Results		169
	1.	Experimental errors	169
	2.	Values of H_o^2/T_c^2 and D_o obtained	170
	3.	Conclusions for alloys with $T_c \sim 1^\circ K$	171
	4.	The Al 0.1 at. % Mn alloy	172
II	THE DEMAGNETISATION CRYOSTAT		174
5.5	Introduction		174
5.6	Design Criteria		175
	1.	Choice of paramagnetic salt	177
5.7	Experimental Details		182
	1.	The magnetising field	182
	2.	The saltpill assembly	185
	3.	Temperature measurement and detection of superconductivity	186
	4.	Secondary thermometer	189
5.8	Performance of the Apparatus and Experimental Procedure		190

Page

CHAPTER 5 - (Continued)

5.9 Results 192

5.10 Conclusions and Final Suggestions 193

CHAPTER 6 - INTERMETALLIC COMPOUNDS OF TRANSITION METALS 195

6.1 Reasons for Interest 195

6.2 Experimental Details 198

6.3 Results and Discussion 200

APPENDIX I TRANSITION TEMPERATURES OF $LaAl_2$ and $La_{1-x}R_xAl_2$ ALLOYS 210

REFERENCES 217

LIST OF TABLES

			Page
CHAPTER 3 -	3.1	Crystal Field Parameters Obtained by Williams and Hirst	63
CHAPTER 4 -	4.1	Crystal Field Levels for Tm^{+++} in $LaAl_2$	109
	4.2	Comparison of the Measured and Calculated Values of dT_c/dx for $La_{1-x}R_xAl_2$ Alloys	125
	4.2 (Continued)	Predicted Crystal Field Levels for $La_{1-x}R_xAl_2$ Alloys	126
	4.3	dT_c/dx Values for Other Rare Earth/ Superconductor Systems	140
CHAPTER 5 -	5.1	Summary of $H_c(T)$ Data for Al and Al Alloys	168
CHAPTER 6 -	6.1	T_c Measurements on Intermetallic Cobalt Compounds	201
	6.2	Paramagnetic Susceptibilities of $MgCu_2$ Structure Intermetallic Compounds at 300°K	206
APPENDIX -	I	Transition Temperatures of $LaAl_2$ and $La_{1-x}R_xAl_2$ Alloys	210

LIST OF FIGURES

		Page
CHAPTER 1 -	1.1 to 1.3 Ideal M(H) Curves for Type I, Type I-II and Type II superconductors	20
CHAPTER 2 -	2.1 The Abrikosov-Gorkov Universal Curve for T_c vs Concentration	50
	2.2 Results of Guertin and Parks for $Th_{1-x}Er_x$	50
CHAPTER 3 -	3.1 The Phase Diagram of the Lanthanum-Aluminium System (after Buschow (63))	75
	3.2 Apparatus Used for T_c Measurements	82
	3.3 Superconducting M(H) Curve for $LaAl_2$	87
	3.4 Critical Field Curves for $LaAl_2$	90
CHAPTER 4 -	4.1 $(\chi - \chi_o)T$(x 10^{-4} emu/gm) vs T for $La_{0.98}Tm_{.02}Al_2$ (20°K to 300°K)	107
	4.2 $(\chi - \chi_o)T$ vs T for $La_{.98}Tm_{.02}Al_2$ (3°K to 20°K)	108
	4.3 to 4.8 $T_{co} - T_c$(°K) vs x(%) for $La_{1-x}R_xAl_2$ (R is Tb, Tm, Ho, Pr, Lu and Er respectively)	127/131

Page

CHAPTER 4 (Continued)

4.9 χT vs T for $La_{1-x}Ce_xAl_2$ 135

CHAPTER 5 –

5.1 Apparatus Used for $H_c(T)$ Measurements on Al Alloys 152

5.2 M(H) Curve for 5N Aluminium 161

5.3 M(H) Curve for Al .023 at. % Mn 161

5.4 D(h) vs t^2 for Al.023 at. % Mn 165

5.5 D(h) vs t^2 for Al .095 at. % Cr 165

5.6 'Sheahen' Fit for 5N Al 166

5.7 D(h) vs t^2 for Al .23 at. % Zn 166

5.8 D(h) vs t^2 for Al 0.1 at. % Mn (I_o = 3.174 amps) 167

5.9 D(h) vs t^2 for Al 0.1 at. % Mn (I_o = 3.04 amps) 167

5.10 The Demagnetisation Cryostat (Scale 1:3) 180

5.11 The Saltpill Assembly 181

5.12 Current Supply Circuit for the Superconducting Solenoid 184

5.13 The Hartshorn Bridge Circuit 187

CHAPTER 6 –

6.1 T_c, χ and γ vs Electron Density for some 4d and 5d Alloys 196

INTRODUCTION

The systematic studies of Matthias and co-workers (23) first showed that:

(a) except for rare earth impurities in a very limited concentration range, magnetic order and superconductivity were incompatible.

(b) if magnetic impurities retained a magnetic moment in solid solution in a superconductor, they caused a strong reduction in the superconducting transition temperature (T_c).

Since then T_c has been measured for many alloys and intermetallic compounds containing transition metals. In conjunction with measurements of normal state properties such as specific heat, magnetic susceptibility and electrical resistance, this information has given a better understanding of their magnetic properties and of the factors which suppress superconductivity.

For example, it was the absence of superconductivity at the end of the 4d and 5d transition series, despite the increased electronic density of states there, which led to the concept of

spin fluctuations in the d-band of Pd metal (Doniach (20) 1966)

Furthermore, the presence of short range magnetic moment correlations between rare earth impurities above the magnetic ordering temperature has been deduced from T_c measurements (40).

In the work described in this thesis, attempts have been made:

(a) to obtain information about the properties of magnetic impurities, in particular the strength and temperature dependence of their interaction with the conduction electrons, from their effect on the superconducting host metal.

(b) to correlate this with the results of resistivity and susceptibility measurements made in this laboratory on these alloys and similar non-superconducting ones.

In chapter 1 the superconducting properties of interest and the types of alloy system measured are classified, and in chapter 2 the relevant theories are mentioned. The predictions of the theory of Abrikosov-Gorkov (32) for localised magnetic impurities in superconductors are stated and the experimental

tests of them are reviewed.

Chapters 3 and 4 are devoted to rare earth impurities and some results of T_c measurements on $LaAl_2$-rare earth alloys are interpreted in terms of crystal field splittings deduced from magnetic susceptibility measurements.

Some critical field measurements have been made on superconducting alloys of aluminium containing dilute concentrations of 3d transition elements. These are described in chapter 5; in addition the design and construction of an adiabatic demagnetisation stage for the He^3 cryostat is also described there.

Finally, in chapter 6, the results of some T_c measurements down to $0.4^{\circ}K$ on intermetallic XCo_2 compounds are given and briefly discussed.

CHAPTER 1

SUPERCONDUCTING PROPERTIES AND SYSTEMS OF INTEREST

1.1 Introduction

Since the discovery of the Meissner effect in 1933 it has been recognised that the superconducting state is a definite thermodynamic phase of many metallic and, more recently, of some semiconducting systems. Therefore at a constant temperature T the equilibrium response of a superconductor to a static magnetic field H is fixed by the condition that the total Gibbs free energy of the system is a minimum. This response is that of expelling some or all magnetic flux and is equivalent to a certain magnetisation M(H,T) per unit volume. If M(H,T) is known for both the normal,(n), and the superconducting,(s), phases from T=0 to T_c (the superconducting transition temperature) then the "equation of state" is known and so the free energy difference for the two phases, $G_s - G_n$, and all other thermodynamic functions of state, can be found. In fact M_n is usually negligible compared with M_s, although for some high field superconductors the Pauli paramagnetism of the 'electron gas' gives a contribution to G_n which is

sufficient to limit the upper critical field, H_{c2}. In the presence of paramagnetic impurities, which also polarise the electron gas, this can be one of the mechanisms leading to non-monotonic $H_{c2}(T)$ curves.

The response of a super-conductor to many other perturbations has now been measured experimentally and calculated theoretically from the BCS pairing theory (1) and its subsequent extensions. Among the more interesting perturbations are electron transfer (tunnelling measurements), lattice vibrations (ultrasonic attenuation), electromagnetic radiation (microwave and infra-red absorption), and transport currents. The response to these perturbations gives much more information, especially on a microscopic scale, but will not be considered in this thesis.

1.2 Theoretical M(H,T) Curves

Theoretical magnetisation curves were first derived by Abrikosov (2) from the Ginzburg -Landau (GL in future) equations. These have been derived by Gorkov (3) from the BCS theory although they were suggested before this by GL from general considerations of second order phase changes. From the equations, which are only valid within a certain temperature range near T_c, (this

range is called the GL regime and becomes larger as the electronic mean free path of the metal is reduced), it follows that the shape of the $M_s(H,T)$ curve is determined by the GL parameter $\kappa(T)$.

This parameter is defined by the relation

$$\kappa(T) = \frac{\lambda(T)}{\xi(T)} \qquad 1.1$$

where, in the conventional notation, $\lambda(T)$ is the low magnetic field penetration depth and $\xi(T)$ is the superconducting coherence length at a temperature T.

The scale of the M(H) curve, for a given κ, is determined by the thermodynamic critical field $H_c(T)$ since, from elementary thermodynamics, the area under the curve equals $H_c^2/8\pi$, H_c is defined in terms of the Gibbs free energy difference per mole by the formula:

$$\frac{H_c^2}{8\pi} V_{mol} = G_n(H_c,T) - G_s(0,T) \qquad 1.2$$

$$\simeq G_n(0,T) - G_s(0,T)$$

where V_{mol} is the molar volume.

It also follows from the GL theory that the upper critical fields H_{c2} and H_{c3}, for the occurrence of bulk and surface superconductivity respectively, are related to H_c and κ by the formulae

$$\kappa = 0.417 \frac{H_{c3}}{H_c} = 0.707 \frac{H_{c2}}{H_c}$$

Therefore there are three ranges of κ for which different types of magnetic behaviour (type I, I-II, and II) occur, and typical curves for these three cases are shown in Figs 1.1 to 1.3. For type II superconductors the structure of the mixed state, (which occurs when the lower critical field for flux penetration $H_{c1} < H < H_{c2}$) was shown theoretically by Abrikosov (2) and later verified experimentally (8), to consist of normal filaments of radius $\sim \xi$ occupying a triangular lattice structure. Supercurrents circulate around each normal core and the total flux associated with each vortex is ϕ_o, the flux quantum. $\phi_o = 2.07 \times 10^{-27}$ gauss cm^2. At H_{c2}, where the bulk superconductor becomes normal, the cores are packed as closely as possible giving $H_{c2} = \frac{\phi_o}{2\pi(\xi(T))^2}$. κ also affects the shape of the magnetisation curve through the relation:

$$\left(\frac{dM}{dH}\right)_{H_{c2}} = \frac{1}{1.16(2\kappa^2-1).4\pi}$$

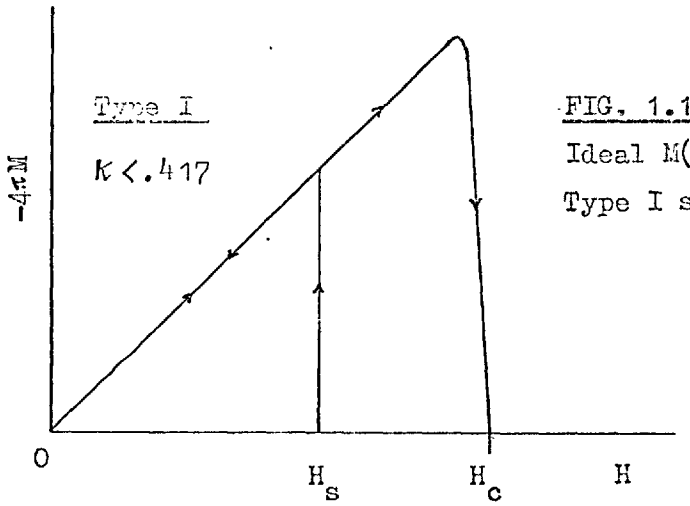

FIG. 1.1
Ideal M(H) curve for a Type I superconductor

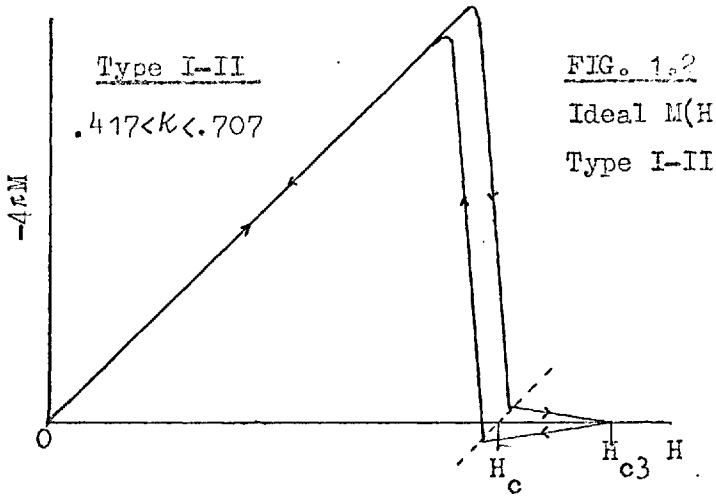

FIG. 1.2
Ideal M(H) curve for a Type I-II superconductor

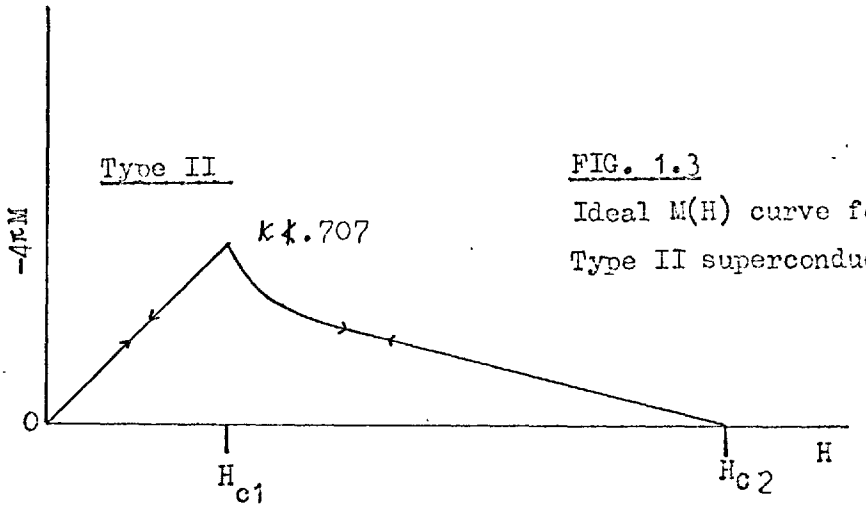

FIG. 1.3
Ideal M(H) curve for a Type II superconductor

This theory has now been extended away from the GL region, that is for all electron mean free paths and all temperatures, by various authors. No drastic changes occur but different aspects of the ideal M(H) curve are now used to define various $\kappa_1(T)$, $\kappa_2(T)$ .... parameters which, although they all have a different temperature dependence, have the same limiting value, κ, at T_c. For example from the work of Maki (4):

$$\kappa_1(T) = 0.707 \frac{H_{c2}(T)}{H_c(T)} \qquad 1.3$$

$$\left.\frac{dM}{dH}\right)_{H_{c2}} = \frac{1}{4\pi\beta(2\kappa_2^2-1)} \qquad 1.4$$

($\beta = 1.16$ for a triangular vortex lattice)

$$\frac{H_{c1}(T)}{H_c(T)} = f(\kappa_3(T)) \qquad 1.5$$

where $f(\kappa_3) \doteq (\ln \kappa_3)/(\sqrt{2}\,\kappa_3)$ for $\kappa_3 \gg 1$.

As a general rule increases in κ_1 and κ_2 of between 20 and 60% occur as T falls from T_c to $0^\circ K$, as shown by Eilenberger

(5) for weak-coupling superconductors containing non-magnetic impurities. Therefore only in exceptional cases does the character of the M(H) curve change with temperature, although minor changes in shape occur because of the temperature dependence of the various k-parameters.

For the purposes of this thesis the changes in the thermodynamic properties which occur on alloying can be classified as:

(i) changes in T_c

(ii) changes in free energy, i.e. in H_c

(iii) changes in M(H) curves, i.e. in k

It is from these changes that attempts have been made to obtain information about the properties of various magnetic impurities in superconductors.

1.3 M(H) Curves Observed Experimentally

These are always irreversible to some extent and so, strictly speaking, application of the preceding thermodynamics is invalid. Some irreversibility, for example that associated with supercooling in type I materials and with surface screening currents in type I-II (and possibly type II) materials, can be

understood in terms of the GL theory and still represents ideal behaviour. Superheating effects are nearly always negligible for type I superconductors (6) and so, for these, the determination of H_c is reasonably simple. To check that inhomogeneities or strains are not broadening the transition at H_c it is better to have a specimen with a known demagnetising factor. The supercooling field measured is rarely the ideal one (H_{c3}) unless special methods are used, so that no κ parameters can be determined for type I superconductors.

For type I-II materials, H_c can be found from the M(H) curve by the construction shown in Fig. 1-2, or for extremely accurate measurements (7) the surface sheath can be suppressed by plating with a magnetic metal. $H_{c3}(T)$ and hence κ can be measured although sensitive apparatus and a good specimen surface are required.

1. Non-Ideal behaviour in M(H,T) curves for type II superconductors

In practice it is difficult to obtain accurate values of $H_c(T)$ for type II superconductors from the area of the M(H) curves. This is because defects in the specimen act as traps for the vortex lines (especially near H_{c1} where the specimen surface may also have an effect) and prevent them from taking up the thermodynamically

favoured structure. Unless a particular flux pinning model is assumed, irreversibilities from this source cannot be estimated from the GL equations. For the arc melted specimens which we have measured these defects were probably small cavities and regions of a normal phase remaining at the grain boundaries. The radius of a vortex line is approximately $\xi(T)$ which increases considerably as $T \rightarrow T_c$, therefore a defect of a given size should become less effective as a trap near T_c and the flux trapping in zero field (a measure of the irreversibility) should decrease.

Near H_{c2}, as already mentioned, the flux lines are closely packed, despite the defects. Reasonably defect free, homogeneous specimens therefore usually exhibit reversible behaviour near H_{c2}, enabling it to be measured reasonably accurately, and κ_2 can be found from the slope $(dM/dH)_{Hc2}$, according to equation 1.4.

Anomalous values of H_{c2} and H_{c3} will be found if different regions, especially the surface, have different impurity concentrations or electronic mean free paths and hence different κ values.

2. Non-Ideal behaviour in T_c and H_{c2}

A small amount of superconducting second phase multiply-connected throughout the sample can screen out applied fields

(both AC and DC) from the bulk material, giving erroneous values of T_c and H_{c2}. Some workers have overcome this by remeasuring T_c after powdering the alloy. Care has to be taken that the particle size is less than the grain size (typically 100 μ or more) and yet still considerably greater than the penetration depth $\lambda(T)$ at a few millidegrees K. from T_c (this is not likely to be greater than 10 μ even for the dirtiest superconductors).

Erroneous values of T_c have been found to arise from surface inhomogeneity in some measurements made here and will be discussed in chapter 3.

Specific heat measurements have several advantages in this respect:-

(i) The superconducting properties of the bulk system are definitely measured. If two or more phases are present their transitions can often be unambiguously identified because their magnitudes are proportional to the relative volumes present.

(ii) H_c can be determined, even if there is irreversible magnetic behaviour, by use of the thermodynamic equations, such as 1.2.

On the other hand such measurements are more tedious and

larger samples, often of expensive materials, are needed.

1.4 Types of Alloy System Studied

In order to classify the effects of alloying on the superconducting properties, it is useful to distinguish between the localised or itinerant nature of the extra electron (or hole) states introduced when the impurity atom is substituted for a solvent atom. If the correlations which exist between electrons in a particular shell of the free atom are retained in the metal then these states are 'localised'. Conversely, if the outer electronic structure of the impurity atom is similar to that of the host metal then the impurity electron states can be considered to be part of the conduction band of the host metal, they are 'itinerant'. It is not possible to classify all systems this way but there are good examples of each type which are usually quite well described by the existing theories.

Rare earth impurities are the best example of the 'localised' category. Although the dominant effects on superconductivity arise from the magnetic moment of the 4f shell, the small 4f-shell radius (0.4 Å), combined with the shielding effect of the outer $5p^6$ and $5s^2$ closed shells, enables the conduction electrons (responsible for

superconductivity) and the 4f electrons to be considered separately. The 4f states are believed to form real bound states (that is states below the bottom of the conduction band in energy) or very narrow virtual bound states (v.b.s.) degenerate with the conduction band. According to Blandin (9) the width of these states in energy is only $\simeq 100^{\circ}K$. (It is not thought that such a width is incompatible with well-defined crystal field splittings which are often deduced to be $\sim 1^{\circ}K$ from magnetic susceptibility measurements. The reason for this is that the width of the virtual bound state represents the probability that a 4f electron will hop into the conduction band. As long as the same 4f level is reoccupied the crystal field picture will be unchanged).

Results of measurements for a system of this type, namely $La_{1-x}R_xAl_2$ where R is a rare earth element, are given in chapters 3 and 4.

3d transition elements dissolved in simple metal hosts (for example ZnMn) and in transition elements well separated from them in the periodic table (for example MoFe) are other examples of localised behaviour. Some $H_c(T)$ measurements on AlT alloys, where T is a 3d transition metal, are reported in Chapter 5.

On the other hand, in alloys of neighbouring early members of the 3d, 4d and 5d transition elements, d electrons of both elements seem to enter a collective band. These alloys have the same crystal structure (usually b.c.c.) as their constituent metals.

As will be discussed in chapter 2, in many of these alloys, rather surprisingly, the rigid band model applies.

Alloys of 'simple' metals, and intermetallic compounds not containing rare earths, will also be placed in the 'itinerant' category. Measurements of T_c (or in most cases of an upper limit to the possible value of T_c) for a system of this type, the Laves phase cobalt compounds XCo_2 (X=Ce, Ti, Zr, Sc, Hf and Nb), will be reported in chapter 6.

CHAPTER 2

EFFECTS OF ALLOYING: THEORY AND EXPERIMENT

2.1 General Theories

The basic pairing theory of superconductivity is due to Bardeen, Cooper and Schrieffer (1957) (ref. 1). The main result of this is that, in the superconducting state, electrons of opposite spin ($\downarrow,\uparrow$), and wavevectors ($-\underline{k},\underline{k}$) are paired in the sense that the states $\underline{k}\uparrow$ and $-\underline{k}\downarrow$ are more likely to be simultaneously occupied than in the normal state. This pairing arises from the attractive electron-electron interaction via the phonons of the lattice, although other mechanisms have occasionally been proposed. By taking a constant attractive electron-electron interaction, V, BCS derived the following formula for T_c, valid for weak coupling superconductors ($N(0)V \ll 1$):

$$T_c = 1.14\ \Theta_D \exp(-1/N(0)V)$$

Where Θ_D is the Debye temperature and $N(0)$ is the electron density of states at the Fermi level. T_c (or V) is the only variable

parameter in the BCS theory, once this is specified all other quantities, for example $H_c(T)$, are given in terms of the reduced temperature T/T_c. Nevertheless the BCS theory adequately describes many properties, for example thermal conductivity, specific heat, tunnelling density of states and ultrasonic attenuation, of weak-coupling superconductors. Since 1957 the BCS theory has been extended in many ways. The main ones of interest here are:

1. The derivation and use of more generalised Ginzburg Landau equations enabling $H_{c1}(T)$ and $H_{c2}(T)$ to be calculated for type II superconductors at all temperatures and for arbitrary impurity concentrations. For example, see Eilenberger (5).

2. Modification of BCS in order to apply it to specific metals. This involves a more realistic treatment of the electron-phonon interaction, especially for strong coupling superconductors. The effective coulomb repulsion U_{eff} between the conduction electrons is also included. Recent work along these lines (1968) has been done by Macmillan (10).

3. Theories which work within the original BCS approximations and combine the BCS Hamiltonian with various model Hamiltonians used to describe localised impurity states in the normal metal. For example the theory of Abrikosov and Gorkov (AG) (32) using the $-J_{eff}\ \underline{S}.\underline{s}$ Hamiltonian for a localised magnetic moment, and that of Ratto and Blandin (11) using the Anderson Hamiltonian (12) for a non-magnetic virtual bound state, will be discussed in more detail later in this chapter. Similarly, Maki(13) has combined the scattering theory of Suhl (14), for systems with a strong 'local moment-conduction electron' interaction, with the BCS theory to calculate T_c and the tunnelling density of states.

4. Minor modification of BCS to allow for the anisotropy of the electron-electron interaction V. That is, the dependence of V on $(\underline{k},\underline{k}')$, the wavevectors of the interacting electrons. The original theory here was due to Markowitz and Kadanoff (15) for the calculation of T_c, and to Clem (16) for the calculation of H_c.

2.2 Mean Free Path Effects on T_c and H_c

It was first shown by Anderson (17) that non-magnetic impurites will not break up the superconducting pairs but will

just cause combinations of $\underline{k}\uparrow$, $\underline{k}'\uparrow$, $\underline{k}''\downarrow$ ... states to be paired with their time reversed partners, the same combinations of $-\underline{k}\downarrow$, $-\underline{k}'\downarrow$, $-\underline{k}''\uparrow$ ... states. It follows from this that for an isotropic interaction, V, there is no depression in T_c proportional to the residual resistivity of the impurity. The depression in T_c which is in fact observed was first explained quantitatively by Markowitz and Kadanoff (MK) (15) in terms of the mean square anisotropy, $\langle a^2 \rangle$, of the superconducting energy gap, but here the more compact formula of Fulde (18) is used:

$$\ln \frac{T_{co}}{T_c} = \langle a^2 \rangle \left\{ \psi(\tfrac{1}{2} + \rho/2) - \psi(\tfrac{1}{2}) \right\} \qquad 2.1$$

In this formula:

T_{co} is the transition temperature of the pure host metal,

ψ is the digamma function (19), which has the initial expansion

$\psi(\frac{1}{2}+x) - \psi(\frac{1}{2}) = \frac{\pi^2 x}{2}$ as $x \longrightarrow 0$, and $\rho = \frac{\hbar}{2\pi k T_c \tau_1}$.

$\frac{1}{2\tau_1}$ is the scattering rate due to the impurities and is assumed to be proportional to the resistivity. (see below).

In terms of the electron mean free path l and the coherence

length of the pure metal at zero temperature , ξ_o, $\rho/2 \simeq \xi_o/l$. Since ξ_o is typically 10^3 - 10^4 Å, and $l \simeq 300$ Å for a residual resistivity, ρ_r, $\sim 1 \mu\Omega$cms, even the most concentrated alloys ($\frac{c}{r} \simeq 10\ \mu\Omega_{cms}$) have $l \sim \xi_o/100$. The maximum change in T_c from this mechanism is therefore given by

$$\Delta T_c = -T_{co} \langle a^2 \rangle \{ \psi(100) - \psi(\tfrac{1}{2}) \}$$

$$\simeq -6 \langle a^2 \rangle T_{co}$$

Since $\langle a^2 \rangle$ is usually $\simeq 10^{-2}$, the maximum value of ΔT_c is 6% of T_{co}. In fact $\psi(x)$ varies more slowly for large x and so 66% of the maximum depression in T_c has occurred at $l = \xi_o/10$.

Clem (10) has shown that, because of anisotropy, $H_c(T)$ is altered on alloying. A fractional increase of the order $\langle a^2 \rangle$ occurs in the quantity $H_c(0)^2/\gamma T_c^2$ (γ is the coefficient of the electronic specific heat).

In addition a reduction of the order $\langle a^2 \rangle$ occurs in the deviation function, $D(h) = 1-h-t^2$, on alloying, (h is the reduced field $H_c(T)/H_c(0)$ and t is the reduced temperature, $t=T/T_c$), that is, $D(\frac{1}{2}) \rightarrow D(\frac{1}{2}) - \langle a^2 \rangle$.

To the writer's knowledge values of $\langle a^2 \rangle$ have not been

obtained by measurements of $H_c(T)$ for superconducting alloys. However, Mapother et al (101) have explained deviations from BCS theory in $H_c(T)$ data for aluminium by taking $\langle a^2 \rangle = 0.013$, in agreement with the value obtained by Markowitz and Kadanoff (MK) (15) from the T_c measurements of other workers.

In fact MK introduced another parameter λ_i relating $1/\tau_1$, the scattering cross-section for smoothing out anisotropy, to the scattering cross-section obtained from residual resistivity measurements. λ_i varies from 0.5 to 2.0 for various impurities in Al, and only the quantity $\lambda_i \langle a^2 \rangle$ can be determined from T_c measurements. For more concentrated alloys H_c data should, according to the theory, give $\langle a^2 \rangle$ directly. This point will occur again in chapter 5 in the discussion of the $H_c(T)$ measurements for Al alloys.

The effect of magnetic impurities can simply be added to the anisotropy effect by adding another $\left(\psi(\frac{1}{2}+\rho_s/2)-\psi(\frac{1}{2})\right)$ term to the right hand side of equation 2.1. Here ρ_s is the scattering cross-section associated with that part of the interaction which is not time reversal invariant. Since ρ_s is often $\simeq 10^{-2}\rho$ for rare earth impurities and non-magnetic virtual bound state impurities, the initial depression in T_c from the 'magnetic' term

is the same order of magnitude as the 'anisotropy' term in these cases. In practice, for the rare earth impurities studied here, this is no problem because (a) there are no limits on solid solubility, therefore the $\langle a^2 \rangle \Psi$ term 'saturates' long before the magnetic Ψ term; (b) the mean free path l of the host matrix is probably short enough to smooth out most of the anisotropy before alloying. Conditions (a) and (b) were certainly not satisfied by the AlT systems studied by Boato, Rizzuto and Gallinaro (21) and corrections for anisotropy had to be made.

2.3 Mean Free Path Effects on κ

For non-magnetic impurities the changes in κ are well described by the Gorkov-Goodman formula, derived by Gorkov from the BCS theory. (De Gennes p.224) (22)

$$\kappa = \kappa_0 + 7.5 \times 10^{-3} \gamma^{\frac{1}{2}} \rho_r \qquad 2.2$$

Where,

ρ_r is the residual resistivity (in $\mu\Omega$cms)

γ is the coefficient of the electronic specific heat (ergs/cc/ $^oK^2$)

κ_0 is the Ginzburg-Landau parameter of the host metal.

In terms of ξ_0 and l it follows that:

$$\frac{\kappa - \kappa_0}{\kappa_0} = \frac{\xi_0}{l}$$

Therefore for extremely type I host metals (such as aluminium, for which $\kappa_0 \simeq .01$) most of the effect of anisotropy on T_c has been washed out before the first change in the M(H,T) curve, the appearance of a surface sheath, occurs. This would not be so for materials with $\kappa_0 \simeq .05$ or more.

To give an idea of the order of magnitude of $\kappa - \kappa_0$ for Al, equation 2.2 gives $\kappa - \kappa_0 = 0.4$ for $\rho_r = 1.5\ \mu\Omega$ cms. Hence for Al Zn alloys one first expects the appearance of a surface sheath at about 10 at. % Zn.

Eilenberger (5) has calculated $\kappa_1(T)$ and $\kappa_2(T)$ for arbitrary non-magnetic impurity concentrations and finds considerable difference in these parameters if he includes p-wave electron scattering as well as s-wave. Presumably non-magnetic virtual 3d states would also give anomalous temperature dependence of the κ parameters although no work has been done on this to the writer's knowledge.

The question of the κ parameters for systems containing localised moments is postponed until after the discussion of the AG theory later in this chapter.

2.4 'Valence' Effects

In additionto the mean free path effects there are gradual changes in T_c and H_c dependent on the particular impurity, the so-called 'valence' effects. These are usually linear in impurity concentration and can be estimated from T_c measurements on dilute alloys after using the procedure of MK to allow for anisotropy. These changes are usually less than $0.1^{\circ}K$/at.% for alloys of non-transition elements, but they cannot usually be followed out to concentrations larger than a few per cent because of solid solution limitations and the formation of new phases with different crystal structures. They are generally, rather loosely, ascribed to gradual changes in the BCS parameters $N(0)$, V, and θ_D.

On the other hand transition elements have extensive ranges of mutual solid solubility. For these alloys, and many intermetallic compounds, empirical correlations between T_c, electron concentration, electron specific heat and crystal structure have been found by Matthias and co-workers. A review of these rules is given by Matthias et al (1963 ref.(23)) and also, for intermetallic compounds, by Roberts. (1964 ref.(24)).

A good example of this kind of work has been given recently

(1968) by MacMillan (10) for alloys of the 3d, 4d and 5d transition elements. Most of the alloys he discussed were between elements in the same row of the periodic table. For example, he has used the measured transition (T_c) and Debye (Θ_D) temperatures for a series of Hf-Ta-W-Re alloys to obtain empirical values of the electron-phonon coupling constant λ from his theoretical formula for T_c. By dividing the measured electronic specific heat for the alloys by $1+\lambda$ he obtained the 'bare' electronic density of states. This is the electronic density of states unenhanced by the electron-phonon interaction. The resulting plot of 'density of states' versus 'electron per atom ratio' was found to be in remarkably good agreement with the calculated band structure of W, confirming the validity of the rigid band model for these alloys.

MacMillan also allowed for the effective electron-electron coulomb repulsion (U_{eff}) which opposes the attractive electron-electron interaction and reduces T_c. This is the other important parameter in the theory of the superconductivity of transition elements and their alloys. As first shown by Garland (26) this can be responsible for a different dependence of T_c on the isotopic mass M. BCS predicts $T_c \propto M^{-1/2}$, whereas for many transition metals, and some non-transition metals, it is

found experimentally that $T_c \propto M^{-\beta}$, where β is less than $\frac{1}{2}$.

U_{eff} is responsible for electron spin correlations in the appropriate band. If it is large enough compared with the bandwidth, ferromagnetism of the band occurs below a certain temperature. As U_{eff} approaches this critical value spin fluctuations within the band become longer lived and give an additional suppression of superconductivity. This mechanism is believed to be responsible for the absence of superconductivity in Pd, which according to the rules of Matthias would be expected to become superconducting.

It will be seen later on that there are analogous effects for localised impurities. U_{eff} is then the coulomb repulsion between two electrons on a 3d site. This initially gives a 'static' depression in T_c according to the model of Ratto and Blandin. As U_{eff} increases further, localised spin fluctuations become longer lived giving an additional depression in T_c. Finally the Anderson (12) criterion for the appearance of a localised magnetic moment is satisfied and a permanent local moment appears, depressing T_c very quickly.

2.5 Localised Impurity States

1. Non-magnetic virtual bound state

Boato et al (21) measured T_c and the residual resistivity ρ_r of a series of dilute AlT alloys (T is a 3d transition element). After applying the analysis of MK they found anomalously large 'valence' effects. ($\simeq 6^{\circ}K$/at. % for Mn). This was later explained by Ratto and Blandin (11) using the Anderson model (12) for the localised non-magnetic state. Reasonable agreement was found using a value of 1 to 1.5 eV for Γ, the half width of the virtual bound state, for all alloys except Al Mn whose value of $dT_c/d\rho_r$ was still a factor of two too small. As distinct from those used in the earlier theory of Zuckermann, the above values of Γ were approximately constant through the series, and when used in Anderson's criterion for the occurrence of a local moment, correctly predicted "no moment".

Physically the large depression is caused by the effective coulomb repulsion (U_{eff}) between $\uparrow$ and $\downarrow$ spin electrons of the bound pair when one of them occupies the impurity site. Zuckermann (27) has shown that, within the model of Ratto and Blandin, no deviations from BCS are expected in the thermodynamic properties of these alloys, other than a small change in γ

associated with the v.b.s., but that there may be a region of gaplessness which could be detected by tunnelling experiments.

It has recently been suggested by several authors (28) that the extra $dT_c/d\rho_r$ observed in Al Mn and Zn Fe alloys could be associated with localised spin fluctuations(l.s.f.) on the impurity site. If the lifetime (τ_o) of the l.s.f. is $\geq \hbar/kT_c$ then there will be an additional pair breaking mechanism to the one considered above. For, in this case the occupancy of a d state by a $\underline{k}\uparrow$ electron will affect not only its partner $-\underline{k}\downarrow$ but also all other pairs, in the same way that a permanent local moment does. However, the theory has not yet been worked out in the limit $\tau_o \simeq (\hbar/kT_c)$ so at the moment the order of magnitude of this effect cannot be estimated reliably. (28(c)).

An alternative viewpoint of the Al Mn system was given by Schrieffer (29), namely that it is a Kondo spin-compensated state with a large Kondo temperature T_K. Similarly recent measurements on the Zn Al Mn system by Rizzuto (30) can possibly be interpreted on the basis of T_K rising through T_c. At the moment the connection of this approach with that of localised spin fluctuations is not very clear.

2. Magnetic virtual bound state

These states have the strongest effect on superconductivity because they combine a localised magnetic moment with a strong interaction with the conduction electrons, for example in ZnMn dT_c/dx is $-300^{\circ}K$/at. % (21).

Until recently such systems were discussed from the viewpoint of the AG theory, using the scalar $J_{eff}\underline{S}.\underline{s}$ interaction between the localised spin $\underline{S}$ and the conduction electron spin $\underline{s}$. This will be done here but more recent treatments of Maki (13) and Coqblin and Schrieffer (31) will also be mentioned.

3. Localised magnetic moments - the AG theory

As already stated the theory assumes a scalar 'impurity-conduction electron' interaction which can be written in second quantised form as:

$$-\sum_{\underline{k}\underline{k}'}\sum_{n} J(\underline{k},\underline{k}')\left\{(a^{+}_{\underline{k}'+}a_{\underline{k}+}-a^{+}_{\underline{k}'-}a_{\underline{k}-})S^{z}_{n} + a^{+}_{\underline{k}'+}a_{\underline{k}-}S^{-}_{n} + a^{+}_{\underline{k}'-}a_{\underline{k}+}S^{-}_{n}\right\}$$

(Yosida (76))

where: $\underline{k}\pm$, label the conduction electron states with wave vector $\underline{k}$, and z component of spin $\pm\frac{1}{2}$,

$a^{+}_{\underline{k}+}$, $a_{\underline{k}+}$ are the usual Fermion creation and annihilation operators, $\underline{S}_n$ is the local impurity spin operator on the n^{th} magnetic site, with components S^x_n, S^y_n and S^z_n ; and $S^{\pm}_n$ are the raising and lowering operators given by, $S^{\pm}_n = S^x_n \pm iS^y_n$.

There are two contributions to $J(\underline{k},\underline{k}')$:

1. The Heisenberg exchange contribution from the coulomb repulsion (in practice a screened potential) between the conduction electron wavefunctions $\psi_{\underline{k}}$ and the localised ψ_{4f} states. (These could alternatively be 3d states)

This is given by:

$$J(\underline{k},\underline{k}') = \int \psi^*_{\underline{k}}(\underline{r}_1)\,\psi^*_{4f}(\underline{r}_2)\,\frac{e^2}{|\underline{r}_1-\underline{r}_2|}\,\psi_{\underline{k}'}(\underline{r}_2)\,\psi_{4f}(\underline{r}_1)\,d^3r_1\,.\,d^3r_2$$

To arrive at this formula it has already been assumed that the coulomb exchange repulsion between 4f wavefunctions and conduction electron wavefunctions based on different sites can be neglected. (Doniach ref.(33)).

The Heisenberg contribution to $J(\underline{k},\underline{k}')$ is always positive.

2. The negative, mixing contribution to $J(\underline{k},\underline{k}')$ for a virtual bound state which is given by $J(\underline{k},\underline{k}') = V_{\underline{k}d}\,V_{\underline{k}'d}\,\frac{U}{E_d(E_d+U)}$,

where $E_d = E - E_F$ is the (negative) energy separation of the v.b.s. from the Fermi energy. U is the repulsive interaction between ↑ and ↓ spin electrons on the impurity site. $V_{\underline{k},d}$ is the 'conduction electron - localised state' mixing term first proposed by Anderson (12). The latter author defines

$$V_{d\underline{k}} = \int \psi^{*}_{4f}(\underline{r})\, V(\underline{r}) \sum'_{\underline{Rn} \neq 0} e^{i\underline{k}.\underline{Rn}} \alpha(\underline{r}-\underline{Rn})\, d^3r$$

Where $\alpha(\underline{r}-\underline{Rn})$ is a Wannier conduction electron wavefunction based on the $\underline{Rn}^{th}$ lattice site. (Replacing ψ_d in Anderson's formula by ψ_{4f}). $V(\underline{r})$ is the selfconsistent (Hartree Fock) potential. Note that in the above sum $\underline{Rn} = 0$ is excluded, according to Anderson because of the different symmetry of $\psi_{4f}(\underline{r})$ and $\alpha(\underline{r})$, so that, in contrast to the previous case, it is the overlap of the localised (in this case 4f) wavefunctions with the neighbouring conduction electron wavefunctions which leads to the $V_{\underline{k}d}$ term. Thus, for 3d elements, $V_{\underline{k}d}$ is typically $\simeq$ 2 eV whereas it is probably $\simeq 0.2$ eV or less for rare earth impurities, with their tightly bound 4f wavefunctions.

4. AG expression for T_c - Theory and Experiment

(1) Theory - Treating the above interaction in the first order

Born approximation (that is, using first order perturbation theory for the scattered wavefunction). AG obtained

$$\ln \frac{T_{co}}{T_c} = \psi\left(\frac{1}{2} + \frac{\rho_s}{2}\right) - \psi\left(\frac{1}{2}\right) \qquad 2.3$$

using the previously mentioned digamma (ψ) function.

In this formula:

$$\rho_s = \frac{\hbar}{\pi \gamma_s k T_c}$$

and $1/\gamma_s$ is the difference in scattering cross-sections for spin↑ and spin↓electrons which is given by $1/\gamma_s = \frac{\pi}{\hbar} . x . n(E_F) J_{eff}^2 \, S(S+1)/4$, in this approximation. Here:

$$J_{eff}^2 = 4 \langle J(\underline{k},\underline{k}')^2 \rangle$$

where $\langle \rangle$ represents an average over the Fermi surface, i.e. an average value for the electrons responsible for superconductivity. $n(E_F)$ is the electrohic density of states, for both spin directions, at the Fermi energy. x is the magnetic impurity concentration and S is the impurity spin.

Liu (34) has shown that the coulomb exchange interaction $J_{eff}\ \underline{S}.\underline{s}$ can be replaced in the case of strong spin-orbit coupling by the operator $(g_J-1)J_{eff}\ \underline{J}.\underline{s}$, where g_J is the free ion Lande' g-factor and $\underline{J}$ is the total angular momentum of the impurity ion ($\underline{J} = \underline{L} + \underline{S}$), but only under certain conditions. These conditions are: (i) the conduction electrons are s-like in their region of overlap with the impurity 4f shell.

(ii) the wavelength of the conduction electrons (at $k=k_F$) is large compared with the size of the 4f shell.

These are quite good approximations for the heavier rare earth elements, after gadolinium.

Therefore one obtains, for strong spin-orbit coupling:

$$\frac{1}{\tau_s} = \frac{\pi}{4\hbar}\left\{x\ \ n(E_F)\ J_{eff}^{\ 2}\ (g_J-1)^2\ J(J+1)\right\}$$

This formula is used in chapter 4 in the form

$$\frac{dT_c}{dx} = \frac{\pi^2}{4k}\left\{n(E_F)\ \frac{J_{eff}^{\ 2}}{4}\ (g_J-1)^2\ J(J+1)\right\}$$

The AG formula, for T_c versus concentration of magnetic impurities, can also be expressed as a universal function.

Using the asymptotic expansion (19)

$$\psi(\tfrac{1}{2} + x) - \psi(\tfrac{1}{2}) \longrightarrow \ln 7.125\, x \qquad \text{as } x \longrightarrow \infty$$

it follows from equation 2.3 that there is a maximum value of $1/\tau_s$ given by:

$$\left(\frac{1}{\tau_s}\right)_{cr} = \frac{1}{7.125}\,\frac{2\pi k T_{co}}{\hbar}$$

above which superconductivity is suppressed completely. $1/\tau_s$ is proportional to the impurity concentration x, therefore in terms of the critical concentration x_{cr}, the AG formula is:

$$\ln \frac{T_{co}}{T_c} = \psi\left(\tfrac{1}{2} + 0.140\,\frac{x}{x_{cr}}\cdot\frac{T_{co}}{T_c}\right) - \psi(\tfrac{1}{2}) \qquad 2.4$$

This formula is also used in chapter 4 and is plotted in Fig. 2.1, p51.

If the dominant contribution to $J(\underline{k},\underline{k}')$ is from the Anderson mixing term then it now seems unlikely that the previous expression for τ_s is valid. For Coqblin and Schrieffer (31), in a recent paper, have allowed for strong spin-orbit coupling before using the Schrieffer-Wolff transformation to go from the

Anderson Hamiltonian to an 'exchange type' interaction. (The Schrieffer-Wolff transformation is one method of obtaining the relation:

$$J(\underline{k},\underline{k}') = \frac{V_{\underline{k}d}\, V_{d\underline{k}'} \cdot U}{E_d(E_d+U)}$$

given previously). They find that the expressions for the depression of T_c (dT_c/dx), the magnetic resistivity (ρ_m), the Kondo term in the resistivity and <u>especially</u> the Ruderman-Kittel-Yosida (RKY) interaction are radically altered. Their calculation is only valid for a one electron (or one hole) 4f shell, that is Ce^{+++} (or Yb^{+++}), and according to the authors, extension to a many-electron 4f shell will be very complicated. Evidence is presented in chapter 4 which shows that J_{eff} may well be positive for the $La_{1-x}R_xAl_2$ system, despite some experimental indications to the contrary, so for the present the validity of the (g_J-1) J_{eff} $\underline{J}.\underline{s}$ interaction has been assumed.

The modifications to the theory of AG for T_c in the presence of crystal field effects, using the (g_J-1) J_{eff} $\underline{J}.\underline{s}$ Hamiltonian, are discussed in Chapter 4.

(2) Experiment - The detailed form of the AG expression for T_c (equation 2.4) has been verified by M. B. Maple (35) for $La_{1-x}Gd_xAl_2$ alloys in the temperature range $1 \geqslant T_c/T_{co} \geqslant 0.1$ to within the widths of the superconducting transitions, $\Delta T_c = \pm .005\ T_{co}$. This is in marked contrast to the other systems studied so far, namely the $La_{1-x}Gd_x$ (0.5), $La_{3-x}Gd_xIn$ (0.4), $La_{1-x}Gd_xSn_3$ (0.25), $La_{3-x}Gd_xAl$ (0.65) and $Th_{1-x}Er_x$ (0.4) systems. The figures in brackets are the reduced transition temperatures (T_c/T_{co}) at which deviations from AG start to occur. The respective references for these systems are (36) to (40) inclusive. It is now well established from measurements of susceptibility in the normal state that these departures are associated with correlations between the magnetic moments of the paramagnetic ions.

The precise nature of these correlations is not as clear. Certainly the results of Guertin and Parks (40) for the $Th_{1-x}Er_x$ system show clearly that the short-range spin correlations set in at temperatures an order of magnitude higher than long range order. These short range correlations show up as departures from Curie-Weiss behaviour in the susceptibility (χ) versus temperature plot, at a particular temperature T_M. As shown in

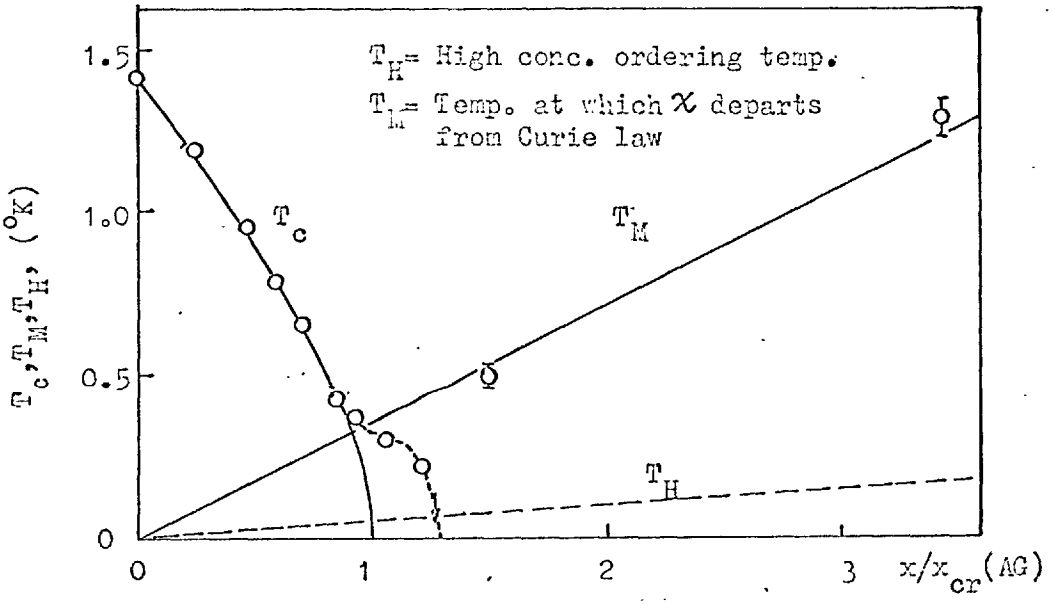

FIG. 2.2 Results of Guertin and Parks for $Th_{1-x}Er_x$

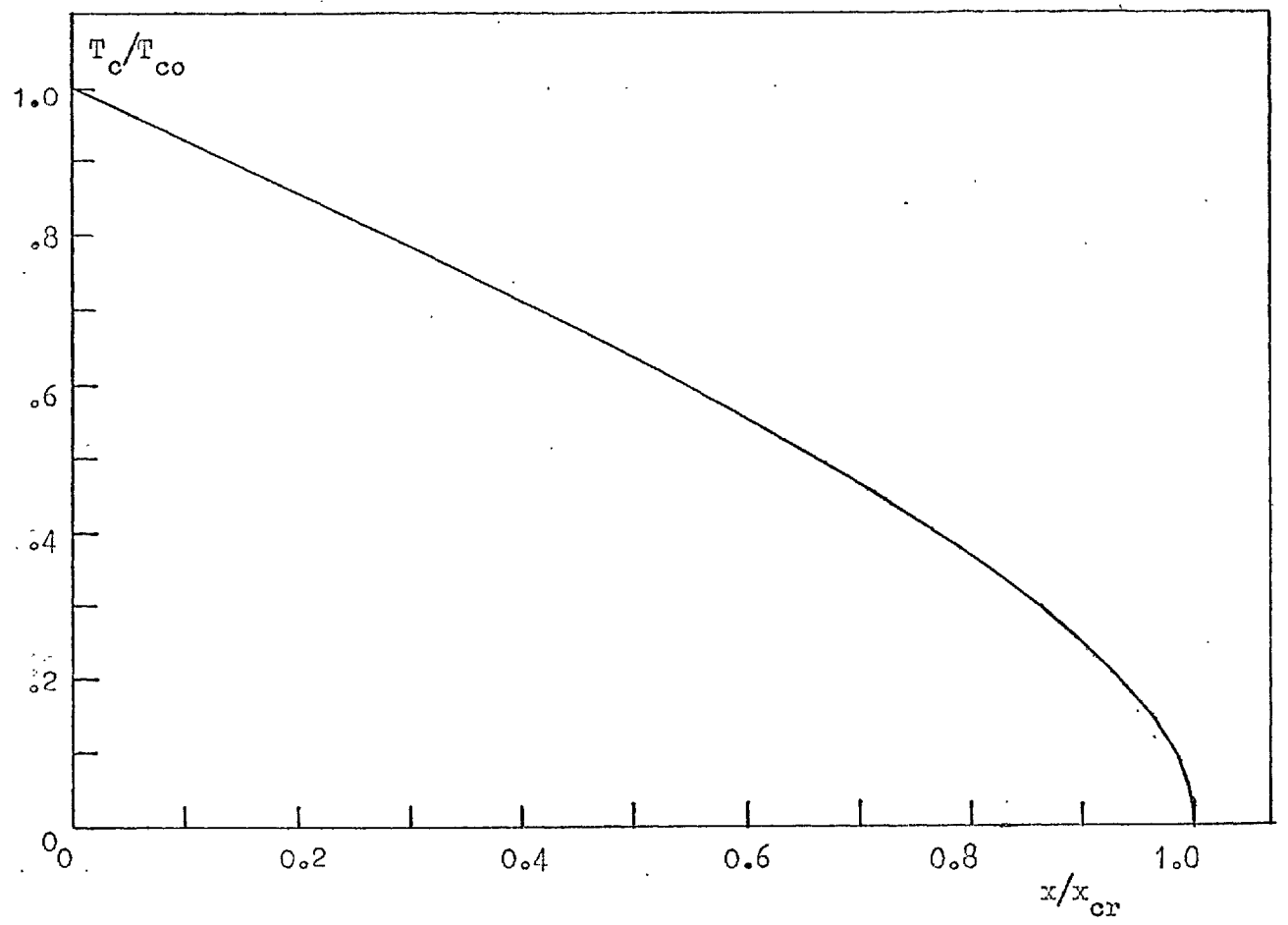

FIG. 2.1 The Abrikosov-Gorkov universal curve for T_c vs concentration

Fig. 2.2 where these results are quoted, the T_M vs concentration (x) plot intersects the T_c vs x curve in the same region where the deviations from AG begin. Short range local moment correlations have also been invoked by Toxen et al (38) for the $La_{1-x}Gd_xSn_3$ system; in this case the long range ordering is antiferromagnetic and the (negative) Curie-Weiss temperature versus x plot intersects the AG curve at temperatures well above the deviating region.

Bennemann (41) originally (1966) discussed the results for the $La_{3-x}Gd_xIn_3$ and $La_{1-x}Gd_x$ systems in terms of a combination of long range spin ordering and the polarisation of the conduction electrons. However, a more recent (1968) paper (25) by the same author invokes a complicated ordering process involving magnetic clustering, in order to explain the observed giant moments and $H_{c2}(T)$ curves for the $La_{3-x}Gd_xIn$ system. Presumably his previous, less complicated, considerations no longer apply to this particular system.

Nevertheless, one can say qualitatively that deviations from AG are caused when the impurity spins start to be correlated by interactions.

Usually these deviations take the form of a slower decrease

in T_c (versus concentration) than predicted by the AG theory, probably associated with a reduced 'spin-flip' scattering cross section. This is often followed by a sharper decrease, probably due to the polarisation of the conduction electrons.

2.6 Other Tests of the AG Theory

1. H_c Measurements

The only rare earth impurity system which has so far been obtained sufficiently pure and defect free to exhibit type I or type I-II magnetic behaviour is the ThGd system studied by Finnemore et al (43). These authors found good agreement between the measured values of $H_c(T)$ and the AG theory. In fact, the deviations from BCS are not remarkable. For example, these authors found that for $Th_{0.98}Gd_{.02}$ ($T_c/T_{co} = 0.64$) the extrapolated $H_c(T)$ curve gave H_o=73 gauss, in agreement with AG. From the BCS theory, which predicts a constant H_o^2/T_c^2 for all alloys, one would expect H_o=80 gauss. A more sensitivetest is the slope $(dH_c/dT)_{T_c}$ which is related thermodynamically to the specific heat jump, ΔC, at T_c. The BCS, AG and measured values of ΔC, expressed as a fraction of the observed value for pure thorium, were 0.51, 0.35 and 0.362 respectively which represents good

agreement between the AG theory and experiment.

2. Tunnelling experiments

One of the most interesting predictions of the AG theory is that, for any finite concentration of magnetic impurity below x_{cr}, there is always a temperature range where gapless superconductivity occurs.

In this range the order parameter remains finite but, as distinct from a BCS superconductor where the single particle excitation energies are given by $E_{\underline{k}} = \sqrt{(\varepsilon_{\underline{k}}^2 + \Delta^2)}$, in the gapless region there are some states for which $E_{\underline{k}} = 0$.

In the above formula $\varepsilon_{\underline{k}}$ is the energy of the conduction electron state $\underline{k}$ in the normal metal (measured from the Fermi level) and Δ is the superconducting energy gap.

Reif and Woolf (44) verified this aspect of the AG theory by tunnelling measurements on Pb Gd films but disagreement was found for In Mn and Sn Mn films. More recently Edelstein (45) has measured the tunnelling characteristics of La Ce films. Again he finds disagreement with the AG theory at all concentrations. The form of the discrepancy is that more states are found within the gap than predicted by AG, especially at higher temperatures.

It now seems that this discrepancy is associated with the large values of J_{eff}, that is, with 'Kondo' anomalies in such systems. The recent theory of Maki (13), applying Suhl's (14) scattering theory to the superconducting state and treating J_{eff} to higher order does give more states within the gap.

3. Other depairing effects

In their extension of the theory of Gorkov and Rusinov (46) for the co-existence of ferromagnetism and superconductivity, Fulde and Maki (47) showed that, in the limit of extreme type II behaviour, the effect of several different pair breaking mechanisms is additive. The above limit was defined by them to occur when ξ_o was much greater than both the electronic transport mean free path l, and the spin-orbit scattering mean free path l_{so}. The result of this additive property is that the transition temperature T, in the presence of various pair breaking parameters, α_j, is still given by the formula:

$$\ln \frac{T_{co}}{T} = \Psi\left(\tfrac{1}{2} + 0.140 \cdot \frac{T_{co}}{T} \cdot \sum_{j=1}^{3} \frac{\alpha_j}{\alpha_j^{cr}}\right) - \Psi\left(\tfrac{1}{2}\right) \qquad 2.5$$

In this formula T_{co} is, as usual, the transition temperature of

the host metal and ψ is the digamma function. $\alpha_j cr$ is the value of α_j needed to suppress superconductivity at all temperatures in the absence of any other pair breaking mechanisms. The pair breaking mechanisms considered were:

(i) Randomly oriented impurity spins interacting via the $J_{eff}\ \underline{S}.\underline{s}$ interaction with the conduction electrons. In the notation of equation 2.4, $\alpha_1/\alpha_{1cr} = x/x_{cr}$, and, of course, if the remaining α_j are zero the AG result (equation 2.4) is retrieved.

(ii) The pair breaking effect of a magnetic field near H_{c2}. Here $\alpha_2/\alpha_{2cr} = H_{c2}(T)/H_{c20}(0)$. $H_{c2}(T)$ is the upper critical field when impurities are present, but $H_{c20}(0)$ is the upper critical field for the host metal at T=0. If the other α_j are zero one obtains the usual result for $H_{c2}(T)$ for a 'dirty' superconductor (67).

$$\ln \frac{T_{co}}{T} = \psi\left(\tfrac{1}{2} + 0.140.\frac{T_{co}}{T}.\frac{H_{c2\delta}(T)}{H_{c2\delta}(0)}\right) - \psi\left(\tfrac{1}{2}\right) \qquad 2.6$$

Of course this is in the same form as the AG expression for T_c, showing the equivalence of the two pair breaking mechanisms.

(iii) The effect of the spin polarisation of the conduction electrons caused by the $J_{eff}\underline{S}.\underline{s}$ interaction with the impurities. This spin polarisation, denoted by I, is assumed to be spatially uniform, that is the spatial average of the RKY (76) polarisation density is used.

In terms of the spin orbit scattering time τ_{so};

$$\frac{\alpha_3}{\alpha_{3cr}} = \frac{\tau_{so} I^2}{1.76 T_{co}} = \frac{\tau_{so}(\langle S_z \rangle \times J_{eff})^2}{1.76 T_{co}}$$

where: x is again the concentration of magnetic impurities, $\langle S_z \rangle$ is the average spin polarisation of the impurities. As before, in the absence of an external magnetic field and of magnetic order, $\langle S_z \rangle = 0$, and the original AG result is obtained.

Crow and Parks observed non-monotonic $H_{c2}(T)$ curves for $La_{3-x}Gd_xIn$ in an intermediate concentration range. These could be explained qualitatively as follows. For low concentrations $H_{c2}(T)$ is monotonic because $\alpha_2/\alpha_{2cr} >> \alpha_3/\alpha_{3cr} \cdot \langle S_z \rangle$ is strongly dependent on the external magnetic field and the temperature, with the usual Brillouin function dependence for a paramagnetic system. At intermediate concentrations $\alpha_2/\alpha_{2cr} \simeq \alpha_3/\alpha_{3cr}$, and α_3 is strongly

temperature dependent via $\langle S_z \rangle$, hence non-monotonic $H_{c2}(T)$ curves are obtained.

At higher concentrations, impurity-impurity interactions gradually set in, $\langle S_z \rangle$ is no longer very dependent on H or T, and monotonic $H_{c2}(T)$ behaviour is again expected, and obtained experimentally.

Crow and Parks did not obtain detailed agreement with theory and the same system has been the subject of the recent paper by Bennemann et al (25) referred to previously. These authors explained the departures from the above theory, and the giant magnetic moments observed by susceptibility measurements on this system, in terms of a complex ordering process involving long range order of 'clusters' of impurities.

To the writer's knowledge the only other 'depairing' investigation to date has been by Barth et Al (48) on the Mo Re Fe system. Again only qualitative agreement was found, which is not surprising in view of the tunnelling results for 3d transition metal impurities obtained by Reif and Woolf (44)

4. Specific heat measurements

In addition to the critical field results, Bennemann and

Garland (49) have also found reasonable agreement between their theory and the specific heat measurements of Finnemore et al for $La_{1-x}Gd_x$ (50). In this system recent neutron diffraction measurements (42) have shown the existence of 'giant local moments' so, as for $La_{3-x}Gd_xIn$, the normal state magnetic properties are complicated.

5. κ parameters for magnetic impurities

For these systems the description of M(H,T) behaviour in terms of the various κ parameters, described in chapter 1, (which was quite convenient for non-magnetic alloys) is not often used. It is also difficult experimentally to get $H_c(T)$ values for such extreme type II materials (they are necessarily type II in order to apply the theory) because of hysteresis.

It is easily shown from equation 2.5 that, neglecting interaction effects, the upper critical field in the presence of paramagnetic impurities, $H_{c2}(T)$, is given in terms of that of the host metal, $H_{c20}(T)$, by the formula:

$$H_{c2}(T) = H_{c20}(T) - \frac{x}{x_{cr}} \cdot H_{c20}(0) \qquad 2.7$$

Since the $H_{c20}(T)$ curve is the usual 'digamma' function (equation 2.6) and not a straight line, the above constant displacement along the H_{c2} axis alters the shape of the $H_{c2}(T)$ curve and therefore the temperature dependence of κ_1 must be altered.

Similarly, from the paper of Barth et al (48), it can be seen that the theoretical (and experimental) values of $\frac{\kappa_2}{\kappa}(T)$, defined in the usual way, no longer have the usual temperature dependence, and in fact $\frac{\kappa_2}{\kappa}$ is less than unity at T_c. (Here κ is the GL parameter of the host metal, κ_2 that of the magnetic alloy).

Before leaving this section on the depairing effects one puzzling result of Fulde and Maki (47) should be mentioned. This is their statement that 'in the limit of $l_{so} \longrightarrow 0$ (the spin-orbit mean free path) the alignment of the impurities does not reflect itself in the dependence of transition temperature on concentration'. It is not clear to the writer how this can be reconciled with the theory of Toxen et al and Bennemann referred to earlier in this chapter. For, in these theories, part of the anomalous T_c dependence is ascribed to the freezing out of the spin flip processes on ordering. It is difficult to see how large spin-orbit scattering could prevent this affecting T_c.

2.7 Concluding Remarks and Summary of This Chapter

Some theories for the effects of various impurities on superconductivity and examples of their experimental confirmation have been discussed, particularly the theory of AG for localised magnetic moments. It is apparent that detailed agreement with AG has only been found for tunnelling measurements on Pb Gd, $H_c(T)$ measurements on Th Gd and T_c measurements on $La_{1-x}Al_2Gd_x$. Certainly impurities having a magnetic virtual bound state are only qualitatively described by AG.

For rare earth impurities the observed deviations from AG in $H_{c2}(T)$ and T_c measurements provide good evidence for the coexistence of magnetic order and superconductivity. However, as in normal metals, the detailed nature of this ordering is difficult to determine.

As far as the 'depairing' effects are concerned, it would be of interest to attempt to verify the predictions of the theory, especially the non-monotonic $H_{c2}(T)$ curves, for a system such as $La_{1-x}Gd_xAl_2$ where the normal state magnetic properties are better understood and the impurity-impurity interactions are weaker than in the systems studied up to now.

CHAPTER 3

RARE EARTH IMPURITIES IN SUPERCONDUCTORS

I INITIAL AIMS, EXPERIMENTAL METHODS

Introduction

It has already been mentioned that the only superconductor-magnetic impurity systems quantitatively understood are those containing gadolinium as an impurity. For non-rare earth solutes departures from the Abrikosov-Gorkov (AG) theory are known to occur and for other rare earth solutes there are complications due to crystal field effects which will be discussed in this chapter and chapter 4.

3.1 Crystal Field Effects in Metals and Salts

Following the observation of electron paramagnetic resonance (e.p.r.) in a Ag Er alloy by Coles and Griffiths (51), the dilute ($\sim$0.5 at. %) alloys Ag R and Au R (where R is a rare earth element of atomic number greater than gadolinium) were also studied in this laboratory by Williams and Hirst (WH) (52).

From measurements of susceptibility (χ) between $1^{\circ}K$ and $300^{\circ}K$ and the e.p.r. g factor, if a resonance could be seen, WH (53) were able to set limits to the crystalline field parameters C_4 and C_6. The basic theory for these effects is given by Lea, Leask and Wolf (54) and in their notation $C_4 = B_4\langle r^4\rangle\beta$ and $C_6 = B_6\langle r^6\rangle\gamma$. Briefly then, in a cubic lattice these two parameters are sufficient to define an effective electrostatic field which partially raises the (2J+1)-fold degeneracy of the ground state of the trivalent R ion. (J is of course the total angular momentum, which remains a good quantum number, since in the rare earth ions L-S couplings are large, at least $3000^{\circ}K$, compared with typical crystal field splittings $\sim 100^{\circ}K$.)

It is usual to regard C_4 and C_6 as adjustable parameters and on this basis e.p.r. and susceptibility measurements for various salts of rare earth elements have been explained in terms of a smooth variation of these parameters along the series. (Low (55)). The values of (C_4, C_6) obtained by WH are given in table 3.1. It can be seen that the signs and orders of magnitude of these parameters are all the same, indicating that the dominant energy contribution is indeed electrostatic in origin, but for neighbouring impurities (e.g. Er^{+++} and Tm^{+++} in Ag)

Alloy	C_4(°K)	C_6(°K)	Ground State	Isolation (°K)	1st ex. State	x (Lea et al)
AgTb	-70	13	Γ_3	<1	$\Gamma_5^{(2)}$	.82
AgDy	-70	13	Γ_7	1	$\Gamma_8^{(1)}$	.57
AgHo	-70	13	$\Gamma_3^{(2)}$	<1	$\Gamma_4^{(2)}$	- .37
AgEr	-70 ± .2	13 ± .2	Γ_7	35	$\Gamma_8^{(1)}$	- .33
AgTm	-30	5.5 ± .1	Γ_2	22	$\Gamma_5^{(2)}$	.57
	-41	5.5 ± .1	Γ_2	20.5	$\Gamma_5^{(2)}$	.64
AuEr	-33 ± 4	6.5 ± .5	Γ_7	19	$\Gamma_8^{(1)}$	- .32
AuTm	-17 ± .5	2 ± .1	Γ_2	7	$\Gamma_5^{(2)}$	.66
AuYb	-27 ± .3	4.5 ± .3	Γ_7	79	Γ_8	.76

TABLE 3.1
Crystal Field Parameters obtained by Williams and Hirst

the parameters differ by a factor of two. The expected magnitudes of (C_4, C_6) are often calculated by the point charge model (in which charges of $\pm|e|$ are placed at all nearest neighbour lattice sites). In this case it gives values of $(+14, +1.5)^{\circ}K$ for (C_4, C_6) which are of the wrong sign and an order of magnitude too small. Obviously the defects in this model lie in the complete neglect of the conduction electrons of the host metal and of the closed $5s^2 5p^6$ shells of the rare earth ion. Williams and Hirst (53) suggested that in this case the dominant contribution to the fourth order part of the electrostatic potential (C_4) arises from the coulomb repulsion between the 4f electrons and the conduction electrons screening out the impurity potential. The latter charge density would probably be 5d-like, and be perturbed, according to the requirements of cubic symmetry, by neighbouring positive ions. The arguments for this are given in detail in their paper but it would certainly give the correct sign and magnitude for C_4 and could explain the observed variations. This proposition will be referred to again at the end of chapter 4.

The validity of the electrostatic model and attempts to calculate the crystalline field parameters are discussed for

rare earth salts by Wybourne (56) (1965) and for transition metal salts by Anderson (57). It is recognised that, expecially in the latter case, significant covalent mixing occurs between the magnetic wavefunctions and non-magnetic wavefunctions based on neighbouring atomic sites. However, the success of the electrostatic model is not solely due to the correct description of the point symmetry of the lattice, because the crystalline field parameters are usually reasonably constant for the various rare earth ions in the same environment. Moreover, this model does restrict the allowed energy levels quite considerably. For example consider the Tm^{+++} ion in a cubic environment. It is known from group theory that 6 irreducible representations (Γ_1, Γ_2, Γ_3, Γ_4 and $2\Gamma_5$) occur in the decomposition of the 13-dimensional representation of the cubic point group in terms of $|J=6, J_z\rangle$ basis vectors. Therefore for an arbitrary interaction (retaining cubic symmetry) there are $6\,!/2\,! = 360$ (Γ_5 occurs twice) possible permutations in energy of the 6 sets of degenerate levels. Examination of the tables of Lea, Leask and Wolf (54) reveals that "only" 20 of these remain for an electrostatic potential and that for 85% of the possible x values (x is the parameter defined by Lea et al which

is related to the ratio C_4/C_6) only 8 of these occur. Even with these limitations it is still not very easy to fix (C_4, C_6) accurately from susceptibility measurements. In this respect previous workers studying non-conducting salts were often helped by optical data and sometimes even by e.p.r. absorption of excited states. On the other hand such crystals often had lower symmetry than cubic and the number of parameters needed to define the electrostatic field was correspondingly larger. The particular method we have used to find (C_4, C_6) could be easily adapted so that susceptibility data could be used to find the best values by a computed least squares fit.

3.2 Initial Aims

It was decided that investigation of a similar system, a dilute solid solution of a rare earth in a metal of cubic symmetry would be of interest, especially if the metal were superconducting, for the following reasons.

(i) The depression of T_c resulting from the conduction electron-4f shell exchange interaction would obviously depend on the particular crystal field ground state of the rare earth ion. Especially, if the ground state were non-magnetic,

how small a dT_c/dx would be obtained ? This question has since been studied by Bucher, Andres et al (58) and their results are discussed in chapter 4.

(ii) Attempts had already been made in this laboratory (by R. J. Lowin) to measure the temperature dependent spin disorder resistivity associated with the exchange interaction. This was made difficult above $4^{\circ}K$ by deviations from Matthiesson's rule (whereby the impurity contribution can be separated from the lattice contribution to the resistivity). Below $4^{\circ}K$ small resistance minima were observed but these are believed to be due to 10 p.p.m. of Fe impurity. However, recent measurements by A. P. Murani (6) on Au Ho alloys (ground state isolation $\simeq 1^{\circ}K$) do show crystal field effects below $6^{\circ}K$. There is also the question of interference effects between the coulomb and exchange scattering contributions to the resistivity, which is not clear at present. The advantage of using a superconducting host metal is that, as discussed in chapter 2, the superconducting transition temperature (T_c) and critical field $H_c(T)$ are only altered by that part of the interaction which does not have time reversal symmetry,

that is the exchange part. By comparison with this, the effect of the coulomb potential of the impurity in smoothing out the energy gap anisotropy is negligible.

Specifically the initial aims were:

(1) To find a superconductor with a large value of T_c (say La_3In, $T_c \simeq 10^{\circ}K$) which would retain rare earth impurities in solid solution and to plot T_c versus concentration of rare earth (x), over a wide range of temperatures. Since a typical ground state isolation is $\sim 10^{\circ}K$ thermal population effects invisible by resistive measurements should show up as deviations from AG in the T_c versus x plots. It was not anticipated that critical field measurements would be possible for this system because an intermetallic compound with such a high value of T_c is likely to be extremely type II with a very large H_{c2}, and also highly irreversible.

(2) In several cases for the Ag and Au based systems, ground state isolations of $1^{\circ}K$ or less occur. Therefore if a type I superconductor, of cubic symmetry, could be made to dissolve up to 0.5 at. % of the rare earth elements, even if it had a lower T_c, crystal field effects and, at lower temperatures, interaction effects, could also be detected by measuring $H_c(T)$ between $3^{\circ}K$ and $0.4^{\circ}K$.

3.3 Choice of System

The only pure superconducting elements which are known (60) to dissolve appreciable (0.5 at. % or more) quantities of rare earths are

(i) Lanthanum, which has a crystallographic phase change (60) at 310°K. Above this temperature the cubic β-phase is stable and in practice it is difficult to retain this at lower temperatures without some of the hexagonal close packed α-phase being formed. The superconducting properties of this system have been studied fairly recently (1967) by Sugawara (64).

(ii) Thorium, T_c is 1.4°K for this element and it also has the face centred cubic structure. Some Th Er, Th Tm and Th Gd alloys were in fact purchased from Johnson Matthey Ltd. Their low temperature resistivities were $\sim 15\,\mu\Omega$ cms, which ruled out $H_c(T)$ measurements, since they were type II materials. T_c measurements were made using the He^3 cryostat but these, and subsequent electron probe analysis, revealed that there was no rare earth present and this project was shelved. Subsequently measurements on these systems have been reported by three workers and are referred to in chapter 4.

(iii) Other attempts at making solid solutions containing rare earths

According to the Darken-Gurry plot of electronegativity versus atomic radius, indium is a good candidate for dissolving the rare earth elements (see ref. 60 for example). In addition it is known that In forms solid solution with up to 400 p.p.m. (61) Ce and as for the Au and Ag systems the solid solution range could be considerably larger for the heavier rare earth elements. Attempts were therefore made to form In Gd and In Er solid solutions, starting from the pure materials at 500°C, and from $ErIn_3$ + Er at the same temperature and at 1000°C, but without success. One cursory attempt at forming arc melted Al 0.5 at. % Gd was also unsuccessful.

The system which was finally chosen represented a compromise between a 'dirty' high temperature superconductor and a purer low temperature one. This was the intermetallic Laves phase compound, La Al_2 which has the cubic Mg Cu_2 structure and a superconducting transition temperature of 3.24°K. This structure has a very high co-ordination number, each La atom having 12 nearest neighbour Al atoms at 3.33 Å and 4 La atoms

at 3.5 Å (62). As is well known the Laves phases are usually formed when the atomic diameters of the two pure metals have a certain ratio (ideally 1.225). The atomic diameters of each atom therefore remain about the same in La Al_2 as in the pure metals and as a result the electron density in La Al_2 is large (.14 electrons/$(A^o)^3$), approximately the same as for pure aluminium. Therefore the band structure of this compound is probably quite complex. All the other R Al_2 compounds have the same structure, and it is almost certain that the rare earth ion (R) goes into solid solution on a La lattice site.

From the work of Maple (35) (T_c vs x, and susceptibility measurements on $La_{1-x}Gd_xAl_2$) it is apparent that impurity-impurity interactions in La Al_2 are very small for Gd concentrations in the 0 to 1 at. % range.

3.4 Experimental details

1. Alloy preparation

Metallic lanthanum, in common with the other rare earths, oxidises very quickly in air, and at 1400°C, the melting point of La Al_2, it is extremely reactive. The two most

suitable methods of preparation are therefore by using a radio frequency levitation furnace or an argon arc furnace. Buschow et al (63) have found alumina crucibles suitable for annealing La-Al specimens. These authors made an accurate determination of the La-Al (and other rare earth - Al) phase diagram and needed to anneal some specimens for several weeks.

An argon arc furnace was used in this work. High purity argon was not used but both titanium and lanthanum getters were melted before melting the specimens. In order to make homogeneous compounds by this method, without further heat treatment, repeated turning and melting is needed. This is limited by weight losses due to evaporation, especially for Tm compounds, and by a tendency of the brittle intermetallic compounds to shatter on remelting.

With the above limitations in mind the final method of preparation was as follows:

Flat slices of 99.9% La, obtained from Rare Earth Products Limited, about 1 gm in weight, and 99.7% rare earth elements (Koch Light Trading Company Limited), about 50 mg, were cut from ingots using a carborundum wheel. They were cleaned by rubbing on fine emery paper under alcohol, weighed, and, to minimise oxidation, were kept under alcohol for the period of about one

hour before being melted in the arc furnace. None of the commonly available acids or alkalis was found suitable for cleaning the rare earths, all left a black surface deposit which could only be removed mechanically.

The binary alloy was turned and melted four times, it was then sliced up (0.2 to 0.6 gms) and cleaned, as before. The appropriate weight of 5N aluminium, in the form of sheet for easier weighing, having been cleaned in Na OH, was then melted with the ingot of binary alloy. For the more dilute (1%) alloys this binary alloy was first diluted even further with La. The compounds were less likely to shatter if they were indirectly heated by the arc for about 30 seconds before being remelted. This shattering was almost certainly caused by small amounts of second phase melting prematurely and expanding. Nevertheless shattering did occur occasionally and as a safeguard the compound was weighed after the first melt. It was then remelted and turned four times.

For alloys not containing thulium (Tm) weight losses were negligible (< 0.5 mg) in the absence of shattering, although occasional weight gains (~ 1 mg) occurred in melting the binary La based alloys. Special care had to be taken not to overheat the Tm alloys, especially on the first melt when the large

heat of formation of this phase is given out, since the vapour pressure of Tm is 35 mm Hg at 1400°C. Typical weight losses for the 4 to 8% Tm alloys were 1 mg per melt. The concentrations of these alloys were calculated by ascribing such losses to the evaporation of Tm alone.

2. Metallographic examination

All the La Al_2 specimens measured were examined microscopically, including those obtained from M. B. Maple, University of California, La Jolla. (These will be referred to as 'La Jolla' samples from now on).

The phase diagram determined by Buschow (63) is shown in figure 3.1. It can be seen from this that La Al_2 melts congruently at 1400°C. Despite this, microscopic examination revealed the four typical features shown below. Dilute (5% to 20%) aqueous or alcoholic HCl was used as an etchant, in general longer etching times were needed to reveal the microstructure in the La Jolla alloys. The features most often seen were:

(i)

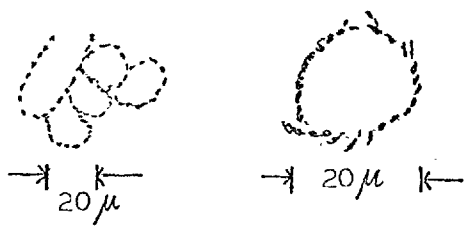

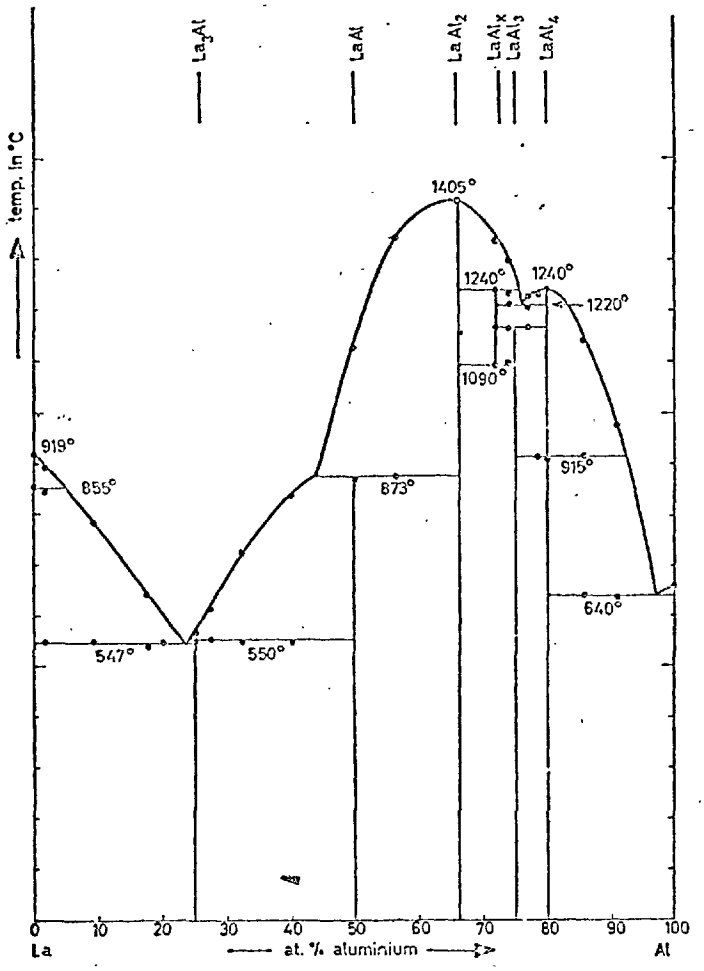

FIG. 3.1 The phase diagram of the lanthanum-aluminium system (after Buschow(63)).

Dendrites of La Al_2 outlined by a dark etching La-rich second phase which is probably the La-La_3 Al eutectic. These regions developed deep etch pits under longer etching.

(ii) 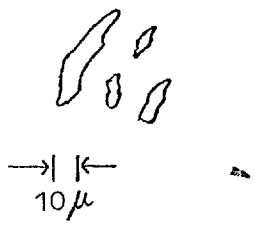

Light etching regions of Al rich second phase often in elongated shapes 10 μ by 100 μ. The electron probe analysis indicated various compositions for these regions ranging from La $Al_{2.5}$ to La Al_4, which is consistent with the various intermetallic compounds shown in the phase diagram.

(iii) 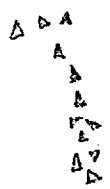

Strings of dark grey etching angular precipitate, about 100 μ overall length, the individual crystallites were 5 μ to 10 μ across.

(iv) 

Heavily etched regions (about 10 μ long) which were often needle shaped. These are probably La rich areas also, but are larger than the interdendritic regions in feature (i)

Features (i) and (iv) occurred to some extent in all the ternaryand pure $LaAl_2$ compounds. Feature (iv) occurred more in non-stoichiometric (La rich) compounds. Feature (i) was less well defined in the La Jolla alloys and needed a heavier etch to be revealed.

Feature (ii) occurred in both $La\ Al_2$ and ternary compounds but at most (in the $La_{1-x}\ Lu_x\ Al_2$ alloys) occupied 2-3% of the total volume. Feature (iii) was only observed in the ternary compounds made here, and was apparent even before etching. On the basis of electron probe analysis of several Tm and Lu alloys it is now thought that these crystallites correspond to rare earth oxide inclusions.

3. Electron probe analysis

Most of the specimens were finally analysed by the Analytical Services Laboratory, here at Imperial College, using an electron microprobe analyser. The results are summarised in Appendix I, together with a summary of T_c measurements and metallurgical data. Some difficulty has been found in correlating the observed microscopic features ((i) to (iv) previous section) with the results of electron probe analysis. It has

since been realised that facilities for simultaneous electron probe and microscopic examination are available but these were not used. The properties of some of the alloys, as determined by the probe, will be summarised here.

(i) La Jolla samples

The highest impurity concentration of these alloys was 2% and all electron probe analyses showed that this was uniform to within approximately 10%. There were occasional (<1%) 10μ regions of higher impurity concentration where the Al concentration remained the same.

(ii) $La_{1-x}Tm_xAl_2$ samples (1 at. % to 8 at. % Tm in La)

Alloys of less than 7% Tm were reasonably homogeneous (to within 10%) but there were occasional 10μ regions where the Tm concentration was up to twice the nominal value. These occurred in both the La Al_2 phase itself and in conjunction with Al rich phases. One of the most concentrated (7%) alloys had many (about 20%) Tm rich regions, about half of which were probably Tm inclusions (i.e. deficiencies of both Al and La). This particular alloy was the only one to show significant departure from the T_c versus concentration plot obtained for the remaining Tm alloys.

(iii) $La_{1-x}Lu_xAl_2$ (concentration range 0.5%to 5.%Lu in La)

These alloys had varying amounts of Lu rich regions although the Lu concentration in the La Al_2 matrix was uniform to within 10%. It was at first though that these regions corresponded to the Al rich phases observed optically (feature (ii) section 3.4.2). Further electron probe analysis revealed that this was not so, and that inclusions of Lu were present. It is difficult to estimate the amount of inclusions quantitatively and so there is an uncertainty in the Lu concentration of the La Al_2 matrix. The concentrations obtained from the probe were between 15% and 20% lower than the nominal ones but such a discrepancy by this method is not unusual. For, in this method, the concentrations are found by comparing the intensity of the characteristic X-rays from the Lu atoms in the sample with that from a pure Lu standard. These X-rays are produced by the incident beam of electrons exciting the Lu atoms. Corrections have to be made for various factors, back scattering of the electrons, X-ray absorption, etc. and an average concentration over an area of $5\mu x\ 5\mu$ is found. Nevertheless the relative values of concentration should be correct and in fact these agree with the nominal values.

Because of these uncertainties the nominal concentrations were taken as an upper limit and the electron probe concentrations as a lower limit when plotting T_c vs concentration for $La_{1-x}Lu_xAl_2$. This does not affect the overall conclusions but if the 'Lu correction' referred to in chapter 4 were made, J_{eff} for Tm would be reduced by a further 10%.

4. Effects of annealing the specimens

Initially 99.7% purity La was used to make the specimens. Pure $LaAl_2$ made from this had a transition temperature of 2.9°K compared with 3.24°K for 99.9% La. This is probably due to 0.1% of rare earth impurity, for example Gd. The additional depressions in T_c for Tm and Er specimens made with this starting material were consistent with those made from the later, higher purity, ingots of La and are therefore also plotted in Figs. 4.3 to 4.8. These alloys were used for some preliminary investigations. It was foundthat the La AL_2 and the ternary alloys which were only arc melted once and not turned had very broad transitions (200 to 400 millidegrees Kelvin). Attempts were made to homogenise them by annealing under vacuum (10^{-5} mm Hg) in alumina crucibles contained in sealed quartz

tubes. As expected, 12 hrs at 600°C had almost no effect. A 48 hours, 1000°C anneal resulted in the observation of two superconducting transitions for the $LaAl_2$ and $La_{.98}Er_{.02}Al_2$ alloys and an extremely broad transition, about 1°K wide, for the Tm alloy. However, metallographic analysis revealed no second phase, only small 'crows foot' areas indicative of premature melting of a second phase at the grain boundaries. It was then found that the spurious transitions were associated with the sample surface, when this was removed mechanically the expected T_c values and narrower transitions were obtained. The broad transition of the Tm alloy was due to evaporation of Tm from the surface of the specimen at 1000°C.

It would therefore have been possible to homogenise all the alloys, other than the Tm ones, provided the surface layer was afterwards removed. At the time this fact was slightly obscured by the lower value of T_c obtained for $LaAl_2$.

5. Measurement of T_c

A standard low frequency mutual inductance method was used to detect superconductivity. As shown in Fig. 3.2 the specimen, an arc melted lump about 3 mm across, was contained in a 350 turn secondary coil. The primary coil was wound on

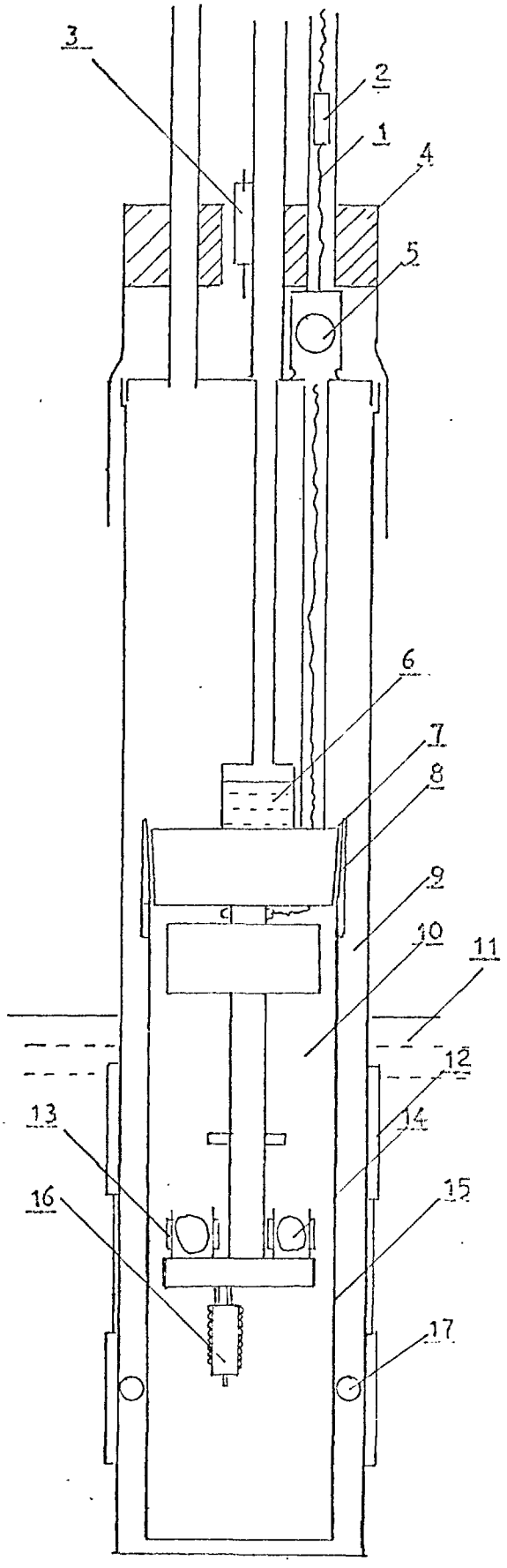

Key to Fig. 3.2

1 12x46 s.w.g. mangamin

2 Junction to copper wires

3 220 Ω Speer resistor (R_2)

4 Demountable copper block holding copper wires to the He bath

5 Copper thermal anchor

6 He^3 pot

7 Silicon vacuum grease

8 Copper cone joint

9 Vacuum space (He^3 runs), or 10 mm He^4 exchange gas

10 .02 mm He^3 gas (He^3 runs)

11 Typical He level

12 Primary coil

13 Secondary coil

14 Specimen

15 Vacuum can (for He^3 runs)

16 30 ohm Speer carbon resistor (R_1) in copper wire basket

17 Knotted nylon thread spacer (optional)

FIG. 3.2 Apparatus used for T_c measurements

the outer vacuum can of the He^3 apparatus. Five or six coils could be accommodated in the specimen chamber. The mutual inductance of each coil with the primary could be measured using a Hartshorn bridge based on a Tinsley 0.1μH to 1000μH variable mutual inductor. This system may seem excessively complicated for such simple measurements, but in fact it was originally designed to measure temperatures below 0.3°K, using crystals of cerium magnesium nitrate.

For the La Al_2 results given here the bridge was balanced at 94 c/s using a home-made tuned amplifier and an AC voltmeter. As described in chapter 5 a home-made phase-sensitive detector was used for measurements in the temperature range below 0.3°K when the primary coil current had to be reduced as much as possible. The output of this device was not sufficiently linear and so the AC voltmeter system was more convenient at higher temperatures. Subsequently a commercial phase sensitive detector became available and this was later used in conjunction with a chart recorder at various frequencies between 30 c/s and 180 c/s for the measurements reported in chapter 6.

The Hartshorn bridge circuit is given in chapter 5. All the specimen coils had one common lead and each one could be selected in turn using a switch at the top of the cryostat.

When the specimens became superconducting there was typically a change of 20 μH in the normal state mutual inductance of 200 μH. This change was later found to be slightly ($\sim$10% / octave) frequency dependent but empty coil measurements showed that this was caused by the phase shift induced by the brass can rather than by eddy currents in the La Al_2 specimens. Therefore the resistance of the specimens could not be estimated this way.

The earths field was balanced out to .01 g for these measurements although it was hardly necessary for such broad transitions.

Temperatures were measured by using the 30 ohm Speer carbon resistor calibrated against the He^4 vapour pressure (1958 scale), this resistor was not always reproducible from run to run. The correction for the density of mercury was not made. The temperature was controlled with a standard manostat and slowly lowered through the superconducting transition by pumping on the reference volume of the manostat through a needle valve.

As can be seen from the diagram the helium liquid level was below the top of the vacuum can during measurements. Despite the yoke of copper wires (needed to condense the He^3) the 220 ohm

Speer carbon resistor R_2 indicated that there were temperature gradients of about $0.15^{\circ}K$ along the can at $3^{\circ}K$ on some runs. This may have been the cause of the scatter ($\sim$10 md) obtained in the 30 ohm Speer resistor (R_1) calibration on some runs. However, the top of the can and the specimens were not in good thermal contact (otherwise the He^3 system would not have worked) and the level of the helium was above the level of the specimens. The can contained about 10 mm pressure of He^4 exchange gas. Moreover, on most runs a pure La Al_2 specimen was measured; for the same La purity (usually 99.9%) these had the same transition temperatures to within $.09^{\circ}K$ and measurements of T_c of the ternary compounds could be made relative to these. It is therefore felt that the experimental arrangement, although not ideal and rather wasteful of liquid helium, did not lead to significant errors compared with the width of the superconducting transitions themselves ($\sim$15 md or more).

A further check on the temperature calibration of the carbon resistor was made around $1.3^{\circ}K$ by comparing temperatures obtained from the He^3 and the He^4 vapour pressures on the same run. It was found that these agreed to within 20 md.

6. Magnetisation measurements

Measurements of the superconducting magnetisation curves could be made in fields of up to 1.2 kilogauss and at temperatures down to 1.4°K using the integrating magnetometer of Jones and Park (7). Two sets of coils were used for these measurements. With one set it was possible to change specimens with liquid He in the dewar. The other set was contained in a duralumin vacuum can and the specimen could be heated above T_c before each measurement, that is, a series of virgin magnetisation curves could be obtained. These were traced out on an x-y recorder, as described for the aluminium alloys in chapter 5. In this case the thermal contact of the specimens to the helium bath was better and so sweep rates of up to 500 gauss per minute could be used.

The temperatures were again determined from the 1958 He^4 vapour pressure scale using a mercury manometer.

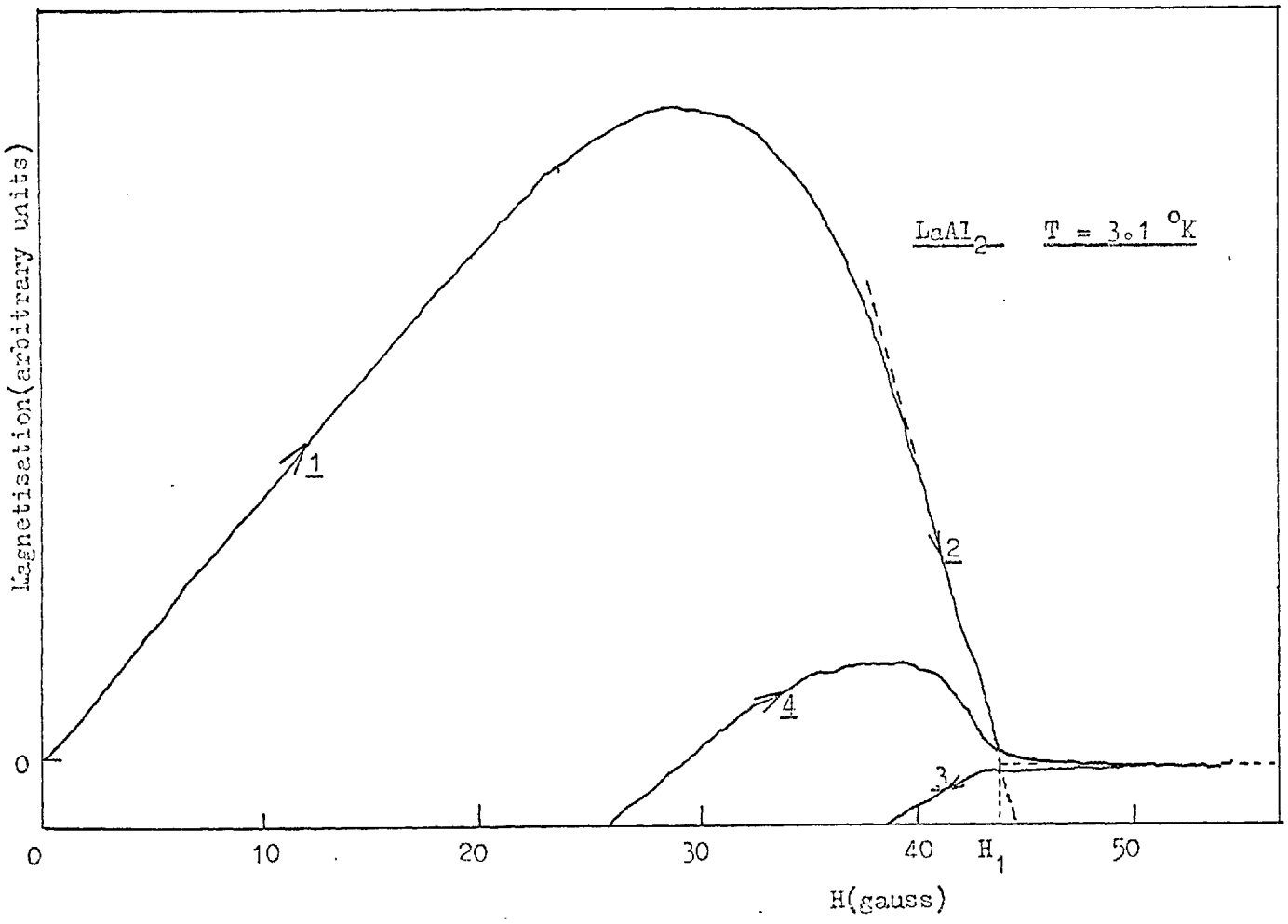

FIG. 3.3 Superconducting M(H) curve for $LaAl_2$

3.5 Results

1. Magnetisation curves

Only two specimens have been measured so far, a $La_{0.995}$ $Er_{.005}$ Al_2 specimen, kindly prepared by I. R. Harris, at Birmingham University, and the La Jolla La Al_2 specimen. The former specimen was ground into a powder of approximately 1/10 mm grain size and contained in a thin walled plastic tube. The M(H) curve was typical of type-II superconductor. At $2^{o}K$ ($T/T_c=0.66$), H_{c2}/H_{c1} was approximately 14 corresponding to a GL parameter κ of about 4. Measurements of H_{c2} could only be made down to $2^{o}K$ as below this H_{c2} exceeded 1.2 kilogauss, the maximum field which can be produced in the present apparatus. At this temperature trapped flux in zero applied field was relatively small, only about 30% of H_{c1}, probably because the specimen had been powdered.

The La Al_2 specimen was in the form of a spark machined cylinder, 2 mm long and 2 mm in diameter. In this case 'virgin' magnetisation curves were plotted, the specimen being raised above its transition temperature ($3.24^{o}K$) by a pulse of heat before each measurement. A typical M(H) curve for a reduced temperature of 0.96 is shown in Fig. 3.3. It can be seen that

there is a small surface sheath above a fairly well defined field H_1, where the magnetisation falls linearly to zero (neglecting the small contribution of the surface sheath). Detailed measurements on the surface sheath were not made because the short specimen resulted in a considerable loss in sensitivity. Moreover, no special efforts had been made to prepare a good specimen surface. In Fig. 3.4 the field H_1 is plotted against temperature T. Also plotted in Fig. 3.4 are two $H_c(T)$ curves, one is obtained from the area of the virgin M(H) curves, the other is $H_c=H_o(1-T^2/T_c^2)$. H_o has been chosen according to the discussion of section 3.5(2) to give the value of $\left(\frac{dH_c}{dT}\right)_{T_c}$ quoted there. For the La Al_2 specimen, which was not powdered, trapped flux was much larger. Even at $T/T_c=0.96$ it amounted to 75% of the maximum flux expelled (which was considerably greater than H_{c1} in fact), rising to 100% at $T/T_c = 0.66$.

2. Discussion of the magnetisation results

The M(H) curve shown in Fig. 3.3 ($T=3.1^{\circ}K$) has the shape and the area expected from a right circular cylinder of a type I-II superconductor whose thermodynamic critical field H_c equals H_1. However, from Fig. 3.4, H_1 is approximately linear in temperature down to a reduced temperature $t(t=\frac{T}{T_c})$ of 0.55. In

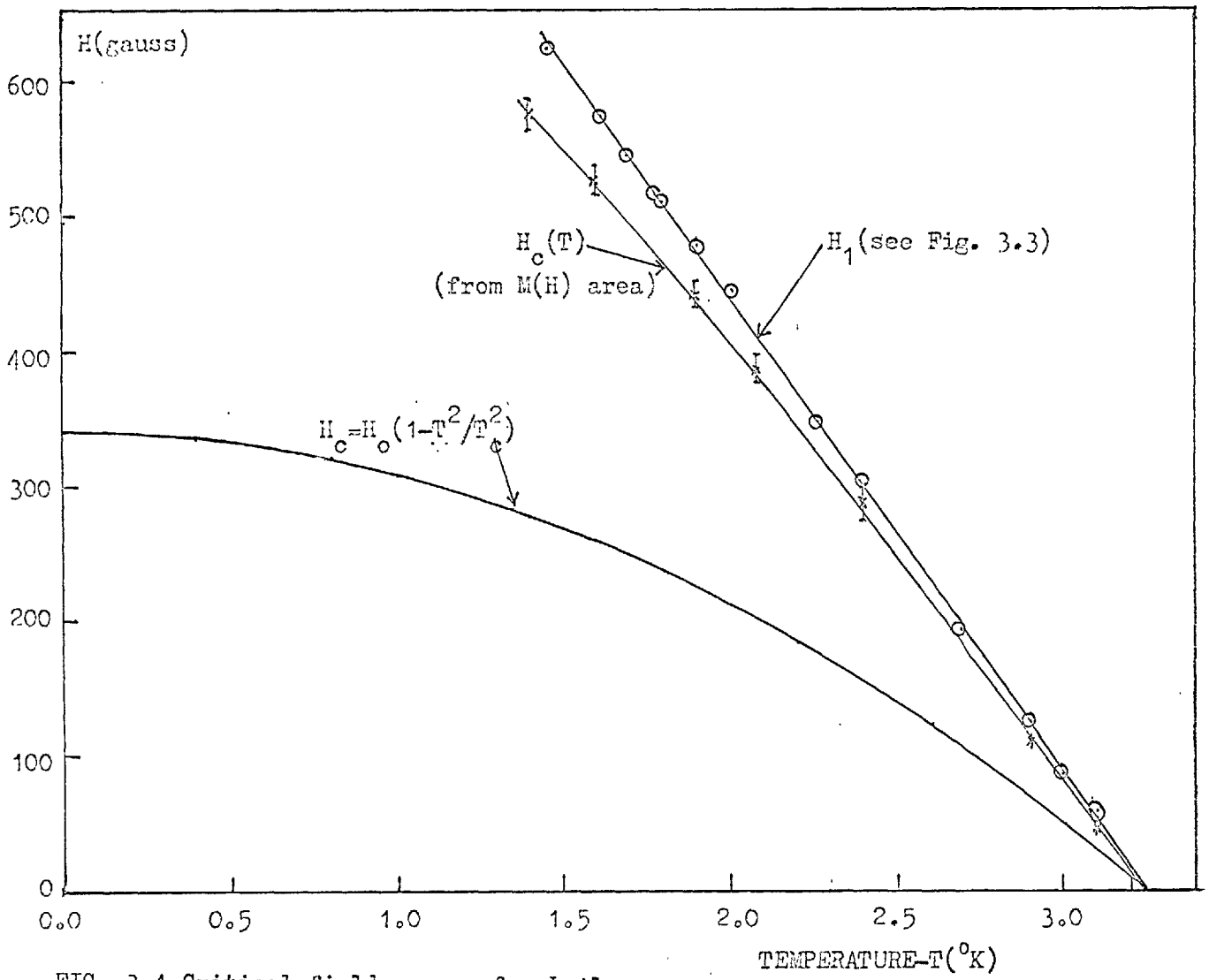

FIG. 3.4 Critical field curves for $LaAl_2$

addition the H_1 values determined from the areas of the M(H) curves are almost linearly dependent on T, rather than the T^2 dependence expected. One therefore concludes that the specimen is in fact type II but that the sharp fall in M(H) expected at H_{c1} is not observed because of defects in the specimen. Several examples of this behaviour have been observed, for example, J. D. Livingston (65), and explained in terms of flux trapping near the specimen surface. (Silcox et al (66)). A similar M(H) curve was obtained for La 1% Ce alloys by Sugawara. (64). He found that on powdering the alloy down to a 40 μ grain size the expected shape M(H) curve for a type II superconductor was obtained. The values of H_c determined from the area were then about a factor 2 smaller and the expected T^2 dependence of H_c was then observed. In addition the field H_{c2} for the powder corresponded to the field H_1 for the solid specimen.

Therefore in this case also it seems that the field H_1 is in fact H_{c2}. Theoretically $H_{c2}(T)$ is almost linear in T down to t=0.6 for all values of κ (67) (See also chapter 2). Therefore κ cannot be determined from $H_{c2}(T)$ alone and, in the absence of measurements on a powdered specimen which we hope to make shortly, $H_c(T)$ cannot be found for La Al_2 either.

We have made a rough estimate of H_c for the powdered $La_{0.995}\ Er_{.005}\ Al_2$ specimen. Here $\frac{H_{c2}}{H_{c1}} \simeq 14$, application of Makis' formulae for κ_2 and κ_3 (equations 1.4, 1.5) near T_c shows that $K \simeq 4$ (H_c cannot be estimated from the area of the M(H) curve because virgin curves were not plotted). Hence, for the dilute alloy, $\left(\frac{dH_c}{dT}\right)_{T_c} \simeq 200$ g/°K.

For such a small concentration of magnetic impurities $\frac{H_c}{T}$ will be the same as for pure La Al_2, this gives $\left(\frac{dH_c}{dT}\right)_{T_c} \simeq$ 290 gauss/°K for pure La Al_2. Thus, the pure La Al_2 specimen measured had $\kappa \sim 1.5$, which is not inconsistent with the measured M(H) curve, and the area of the virgin M(H) curve in Fig.3.3 is a factor of two too high because of flux pinning.

The specific heat jump ΔC at T_c is related to $\left(\frac{dH_c}{dT}\right)_{T_c}$ by the thermodynamic relationship:

$$\Delta C = \frac{T_c}{4\pi}\left(\frac{dH_c}{dT}\right)^2_{T_c}$$

Using the BCS formula; $\Delta C = 1.52\,\gamma T_c$, one obtains a value for γT, the electronic specific heat, and hence $n(E_F)$, the electronic density of states, of 1.4 states/ev/atom. This will be in error if La Al_2 is a strong coupling superconductor, and will

over-estimate $n(E_F)$, similarly 'phonon enhancement' of the specific heat will also cause too large a value of $n(E_F)$ to be found. Nevertheless, in the absence of specific heat data for La Al_2, this value has been used to calculate J_{eff} for La_{1-x} $Gd_x Al_2$ in chapter 4. It is about 3 times the free electron density of states, which is usually used for this system, corresponding to an effective mass ratio $m^*/m=3$. This is to be compared with the values $m^*/m=4.3$ from the specific heat of cubic β-La, and $m^*/m=2.2$ which we have calculated for the cubic, Cu_3 Au, compound La Pb_3 from the specific heat data of Bucher et al (58).

3. T_c measurements for $La_{1-x}R_xAl_2$ alloys

For ease of reference the T_c measurements are given in chapter 4 where they are analysed and discussed. They are plotted there as graphs of $T_{co}-T_c$ vs x (Figs. 4.3 to 4.8). T_{co} is the transition temperature of $LaAl_2$, which was 3.24^oK for $LaAl_2$ made from 99.9% La. The theoretical Abrikosov-Gorkov curve (p.50, chapter 2) is also plotted for each alloy, x_{cr} being chosen so that the initial slopes of the theoretical and experimental curves are equal. The transition temperature is

taken as the temperature of the midpoint of the inductive part of the transition. Also plotted on the graphs in the form of error bars is the temperature range over which 80% of the inductive transition occurs. In some cases this is asymmetric due to a low (or less often, high) temperature 'tail' to the transition.

In Appendix I all the transition temperatures are tabulated together with a summary of metallurgical examination results and electron probe analyses. The nominal concentrations (corrected for weight losses for the Tm alloys) are used throughout except for the La Jolla $La_{1-x}Tm_xAl_2$ alloy, where, as possible weight losses were not known, the value of x was found from the measured room temperature susceptibility.

4. Susceptibility measurements

The susceptibility (χ) of the La Jolla $La_{1-x}Tm_xAl_2$ alloy was kindly measured between 300°K and 3.2°K by Mr. J. B. Dunlop in this laboratory using a Faraday magnetometer, by which the force acting on the specimen in a non-uniform magnetic field is measured. Below 77°K the measuring field was 4.5 kilogauss. The results for χ are given in chapter 4, Figs 4.1 and 4.2.

M(H) curves were plotted up to 8 Kg at 77°K and up to 4.5 Kg at 4.2°K. Both of these are linear in field but in both cases there is a small positive intercept at H=0 amounting to .3% and .17% of the respective values of M at 4.5 Kg. The corresponding remanent moment at 77°K is very small. It is equivalent to a moment of $4.5 \times 10^{-5} \mu_B$ per $LaAl_2$ "molecule" and could be due to 10 p.p.m. of ferromagnetic inclusions. (Tm itself is paramagnetic above 56°K).

The "remanent moment" at 4.2°K is a factor of 7 larger and, since using this method the lowest measuring field is necessarily rather large (2.5 Kg in this case), this apparent intercept in fact arises from Brillouin curvature of the M(H) plot. This curvature amounts to a 0.17% reduction in χ at 4.5 Kg at a temperature of 4.2°K. This is consistent with that calculated by the program, which is 0.16% at 4°K for a measuring field of 4.5 Kg.

CHAPTER 4

RARE EARTH IMPURITIES IN SUPERCONDUCTORS

II RESULTS, ANALYSIS AND DISCUSSION

4.1 $La_{1-x}Gd_xAl_2$ (including a discussion on the sign of J_{eff})

Gd is an S state (L=0) ion and any crystal field splittings are negligibly small. This is verified experimentally by e.p.r. measurements (73) and by the 1/T dependence of χ in dilute $LaAl_2$ Gd (35), and Au Gd alloys (69) down to $1^{\circ}K$. Therefore the AG formula of chapter 2 can be applied:

$$\frac{dT_c}{dx} = \frac{-n(E_F)}{k} \frac{J_{eff}^2}{4} \frac{\pi^2}{4} (g_J-1)^2 J(J+1)$$

The most convenient units are:

$n(E_F)$ in states /eV/atom (of solvent)

kdT_c in eV

dx in concentration/atom (of solvent)

Then J_{eff} is obtained in eV/atom. (J_{eff} used here is equivalent to the quantity 2J in the notation of some authors, for example Yosida (76).) Since L=0 for Gd $(g_J-1)^2 J(J+1) = S(S+1)$.

Using the value $n(E_F)$=1.4 states/eV/atom (corresponding to m^*/m=3) and the measured value (35) of dT_c/dx (3.7°K/at. %) for Gd^{+++} in $LaAl_2$, one finds $|J_{eff}|$ = .084 eV/atom.

J_{eff} values have been obtained for various rare earth alloy systems by several methods. T_c measurements on Th Gd and La Gd yield values of $|J_{eff}|$ of 0.11 eV and 0.1 eV respectively, if values of $n(E_F)$ determined from the electronic specific heat are used. The latter value of J_{eff} disagrees with that calculated by Sugawara (68) from his own T_c data, even using the (lower) free electron value of $n(E_F)$ he found $|J_{eff}|$ = 0.04 eV.

According to the results of Freeman et al (70) such magnitudes of J_{eff} could arise from the usual Heisenberg exchange interaction, equivalent to the $4f^n$-6s exchange interaction in the free atom, in which case J_{eff} is >0 and parallel alignment of conduction electron and rare earth spin is favoured. In fact, the spectroscopic results quoted by Wybourne (71) (p.55) for the $4f^7 5s^2 5p^6 6s$ configuration of Gd^{++} rather surprisingly show that, in the free ion, the exchange energy between the 6s and $4f^7$ electrons is 0.3 eV. This is the difference in energy of the ^7S and ^9S levels. When this is put in the form of a J_{eff} $\underline{S}.\underline{s}$ interaction,

with $S=7/2$, and $s=\frac{1}{2}$, one obtains $J_{eff} \simeq 0.1$eV, and, as also mentioned by Wybourne, this integral is practically constant along the rare earth series for a given state of ionisation. In view of the complicated screening effects which occur in a metal, the probable increase in 4f radius in the solid state, and the anisotropy of $J_{eff}(\underline{k},\underline{k}')$ found by Freeman and Watson (70) such detailed agreement must be rather fortuitous.

As mentioned in Chapter 2, there is also a negative contribution to J_{eff} for a virtual bound state, arising from the mixing of the conduction electron and the 4f wavefunctions. This was first discussed by Anderson for 3d wavefunctions in 1961. (12). The formula $J_{eff} = \frac{2V_{kd}^2}{E(E+U)}$ has already been given in chapter 2. ($V_{kd} \longrightarrow V_{sf}$ here).

For rare earth ions $U \gg E$ and, as the energy of the virtual bound state approaches the fermi energy from below ($E \longrightarrow 0$ from below), large negative values of J_{eff} (~ -1 eV) can occur. In rare earths the maximum positive value of J_{eff} arising from the Heisenberg exchange interaction is ~ 0.2 eV.

It is not clear at present which sign of J_{eff} occurs in $La_{1-x}Gd_xAl_2$. Peter et al (73) found small negative g shifts in the e.p.r. absorption of Gd in $LaAl_2$ indicating $J_{eff} < 0$, but a

recent preliminary measurement by R. J. Lowin in this laboratory on the same system indicates that this shift may well be positive. Buschow et al (74) have interpreted the nuclear magnetic resonance data of Jaccarino (75) for R.E.Al_2 compounds and their own measurements of Curie temperature (θp), and spin disorder resistivity (ρm), for various diluted R.E.Al_2 compounds to give J_{eff}= -0.9 eV. However the procedure used to obtain this value was based on the theory of Rudermann Kittel and Yosida (76) (RKY) which predicts an oscillating conduction electron spin density associated with the $J_{eff}\ \underline{S}.\underline{s}$ perturbation. The authors did not apply RKY rigidly but varied k_F (the fermi wave vector), J_{eff} and m* (the effective electron mass), to obtain self consistent results for the various measurements.

Freeman and Watson (78) have shown that both the anisotropy of J_{eff} ($\underline{k}$,$\underline{k}'$), that is, the dependence of J_{eff} on the conduction electron wave vectors $\underline{k}$ and $\underline{k}'$, and the shielding of the 4f levels by the $5s^2\ 5p^6$ closed shells can alter the RKY polarisation density considerably. In addition the susceptibility response function is known to be extremely sensitive to the precise band structure, (79) whereas the RKY theory uses the free electron form for this function. A final objection to the

result of Buschow et al is that, as discussed in chapter 2, the recent paper of Coqblin and Schrieffer (31) shows that if $J_{eff} < 0$ the RKY polarisation density is severely modified.

Additional evidence that J_{eff} is positive for the $La_{1-x}Gd_xAl_2$ system comes from the recent work of Maple and Fisk (80). They find an increased paramagnetic moment per Gd^{+++} ion in solid solution in $LaAl_2$, 4-7% of the free ion value, and no resistance minimum is observed. From the enhanced moment, again using the value of $n(E_F)$ of 1.4 states/eV/atom, it is found that J_{eff} is positive and approximately 0.1 to 0.2 eV. Although this result again comes from RKY theory it is less open to objection, because, as shown by Freeman and Watson (78), the net conduction electron polarisation depends only in the static part of the electron gas susceptibility response function $\chi(0)$ and on $J_{eff}(0)$, and is independent of the precise spatial distribution of spin polarisation.

Although the criterion of 'no resistance minimum' is not always a good one for $J_{eff} > 0$ (for example, in the Pd Gd system $J_{eff} < 0$ from e.p.r. measurements, yet no resistance minima are seen in dilute alloys) because different bands of electrons could be responsible for the conducting and screening properties, and

have different J_{eff} values, in this case a minimum in $La_{1-x}Ce_xAl_2$ is observed by the same authors (80). The values of dT_c/dx are about the same in the two systems, hence one expects similar values of ρ_m, both being proportional to the 'spin flip' scattering cross-section. The logarithmic term in the resistance, which is responsible for the appearance of a minimum, is, according to Kondo (81), proportional to $\frac{J_{eff}}{E_F}\rho_m \ln T$. This should not be more than a factor of 10 smaller in Gd alloys than in Ce alloys and should be quite easily observable.

In view of these facts, especially the questionable validity of the $(g_J-1)\, J_{eff}\, \underline{J}\cdot\underline{s}$ Hamiltonian when J_{eff} arises from covalent mixing, the following results (except for the Ce^{+++} alloys) are discussed from the point of view that $J_{eff} > 0$.

4.2 $La_{1-x}Tm_xAl_2$, Susceptibility Results

The plots of $(\chi - \chi_o)T$ versus T for this alloy are shown in Fig. 4.1 (20°K to 300°K) and Fig. 4.2 (3°K to 20°K) p. 107. Above 100°K $(\chi - \chi_o)T$ is constant at $8.12 \pm .03 \times 10^{-4}$ e.m.u.°K/gm. The nominal concentration x, as determined from the initial weights of constituents before arc melting, was x=.03. However, the high temperature value of $(\chi - \chi_o)T$ gives x=.022 if one uses the free

ion value for the Tm^{+++} magnetic moment. This is consistent with the measured superconducting transition temperatures of the other $La_{1-x}Tm_xAl_2$ alloys, within the experimental errors, but is critically dependent on the value taken for χ_o the susceptibility of the pure $LaAl_2$ matrix. Maple's data (80) for $\chi_o(T)$ has been used, $\chi_o(T)$ increases by about a factor of two from 300°K to 4°K.

Since the La Jolla specimens were melted many more times than ours such a loss of Tm (about 2 mg is required) is perfectly feasible. From these measurements therefore, there is no evidence for any conduction electron polarisation, although this would have to be about 10% of the high temperature susceptibility to be detectable.

The susceptibility has been fitted to that expected from an assembly of free Tm^{+++} ions in an electrostatic field of cubic symmetry using the computer program of Williams and Hirst. $LaAl_2$ has the $Mg Cu_2$-type cubic structure and it has also been explicitly verified that the potential at the La site, arising from point charges at the neighbouring La and Al sites, does indeed have cubic symmetry. (Bleaney ref.(82)).

An outline of the method used to calculate χ is given

below:

(i) As already stated, spin-orbit coupling energies in the rare earths are considerably larger than crystal field energies Therefore, J remains a good quantum number and only rare earth ion states with the ground state value of J need to be considered. Even for Sm^{+++}, where the ground state (J=5/2) and the first excited state (J=7/2) are only separated by 1500°K, this is a good enough approximation as far as the effect on T_c is concerned, although there is an appreciable Van Vleck (83) contribution to the susceptibility in this particular case.

(ii) The effective electrostatic potential can be expanded in spherical harmonics about the rare earth site.

$$V(\underline{r}) = \sum_{\ell,m}' a_\ell^m P_\ell^{|m|}(\cos\Theta)\, r^\ell e^{im\phi}$$

Since the one electron 4f wave functions have $\ell=3$, these are only perturbed by components of V with $\ell \leqslant 6$. (Condon and Shortley (84) p.177). Furthermore, because $V(\underline{r})$ must have cubic point group symmetry, a_ℓ^m is only non-zero when $\ell=4$, $m=0,\pm4$, and $\ell=6$, $m=0,\pm4$. (Heine (85) p.150). Thus, in termsof the operator equivalents (O_4 etc.) and the multiplicative factors (β, γ) which are all tabulated by Stevens for the rare earth ions (86), and including a magnetic field $\mathcal{H}$ along one of the cubic axes, the z axis, the

Hamiltonian H is:

$$H = B_4'\langle r^4\rangle\beta\,(O_4^0 + 5.O_4^4) + B_6'\langle r^6\rangle\gamma\,(O_6^0 - 21.O_6^4) - g_J\mu_B\mathcal{H}\,J_z \qquad 4.1$$

In the notation used previously $C_4=B_4'\langle r^4\rangle$, and $C_6=B_6'\langle r^6\rangle$. The program contains all the relevant operator equivalents and multiplicative factors. Thus once the rare earth J value and the (C_4,C_6) parameters are specified the program works out the matrix of H with respect to $|J,J_z\rangle$ basis vectors.

The matrix is in turn diagonalized using the IBM Share Library program ASC MITRS number 3219 which converges on the correct eigen-values and vectors for degenerate and arbitrarily close roots. From these eigen-vectors the magnetic moment, in the finite field case, or the perturbative susceptibility, in zero field, including the 'Van Vleck' terms, is calculated by the program from the usual formulae (see for example, Van Vleck's book (83) chapter VII).

Williams (53) fitted his results graphically to $1/\chi$ vs T plots after finding preliminary values of (C_4,C_6) which gave the correct low temperature value of χT. This was probably to

allow for possible interaction effects (which on a molecular field model would just displace the $1/\chi$ vs T curves). Recent results obtained by A. P. Murani in this laboratory for the Au Gd system indicate that these effects are in fact negligible. 0.3 % Au Gd has a Curie temperature θ such that $|\theta| < 0.05^{\circ}K$. Using the above method it is difficult to systematically cover the (C_4, C_6) plane searching for the best fit. Accordingly a slightly different method was used, and is described below.

It follows from equation 4.1 that if C_4, C_6 and $\mathcal{H}$ are all multiplied by the constant α, the only change will be a scaling of all energy levels by α. If the exact energy eigenvalue (in the presence of a field $\mathcal{H}$) of the i^{th} state is E_i with average magnetic moment in the field direction, M_i, then the magnetic moment of the system is:

$$M = \frac{\sum_i M_i \exp(-E_i/kT)}{\sum_i \exp(-E_i/kT)}$$

Thus if $E_i \longrightarrow \alpha E_i$, M remains the same if $T \longrightarrow \alpha T$.

In terms of the susceptibility $\chi = M/\mathcal{H}$

$$\chi \longrightarrow \chi/\alpha$$

and so $$\chi T \longrightarrow \frac{\chi}{\alpha} \alpha T$$

The product χT remains the same also, so the shape of the χT vs log T plot only depends on the ratio C_4/C_6. Therefore by displaying the data on a χT vs log T graph one can easily see if a particular set of levels will fit the data for any scaling factor α. Or equivalently whether the data can be fitted for that particular value of the C_4/C_6 ratio. This effectively reduces the number of variables to one. This is an exact result, within the set of states with a given J, and therefore includes all higher terms (for example the Van Vleck terms) in the perturbative susceptibility, and is valid for the finite field case provided $\mathcal{H}$ is scaled as well. It is felt that this procedure could easily be programmed so that the best value of the ratio C_4/C_6 could be found by a least squares computer fit. Only one alloy had to be fitted in this study and so this was done graphically as shown in Figs 4.1 and 4.2.

1. Results of the crystal field fit

A good fit isobtained for $(C_4,C_6)=(-45,-13)^{\circ}K$, corresponding to x= -.437 (x is defined by Lea et al (54)). The composition of the lower levels, the limits on (C_4,C_6) and the ground

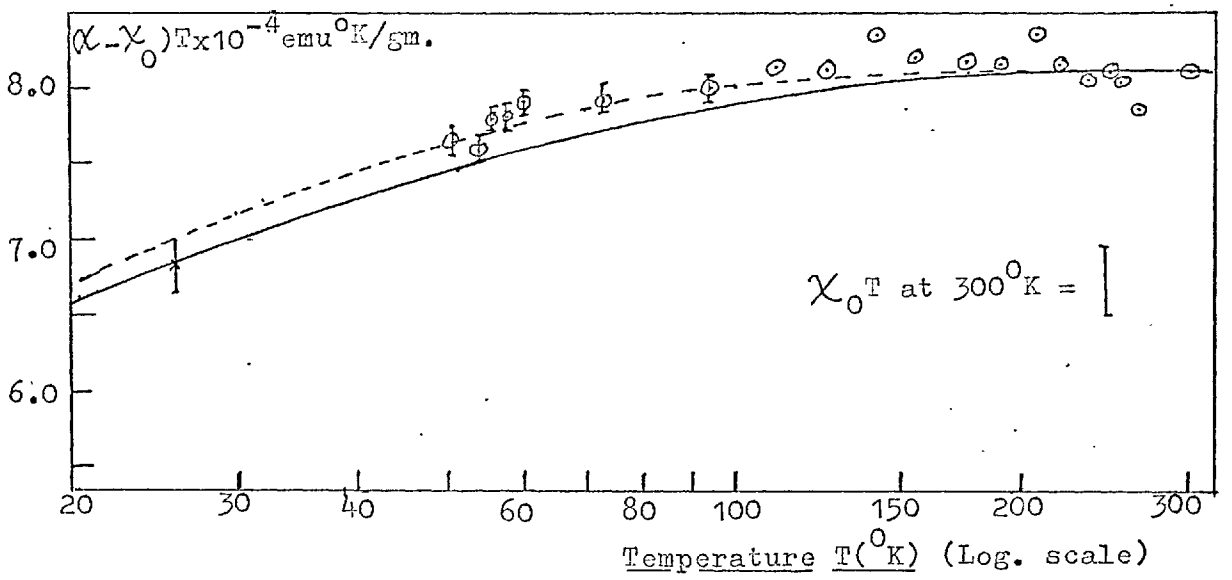

Key: ——— = calculated values for x(Lea et al definition)=-0.437

------ = calculated values, x=-0.40

⊙ = measured values in 6 kilogauss

× = measured value in 4.5 kilogauss

Fig. 4.1 $(\chi-\chi_0)T$ ($\times 10^{-4}$ emu °K/gm.) vs. T(°K) for $La_{.98}Tm_{.02}Al_2-$

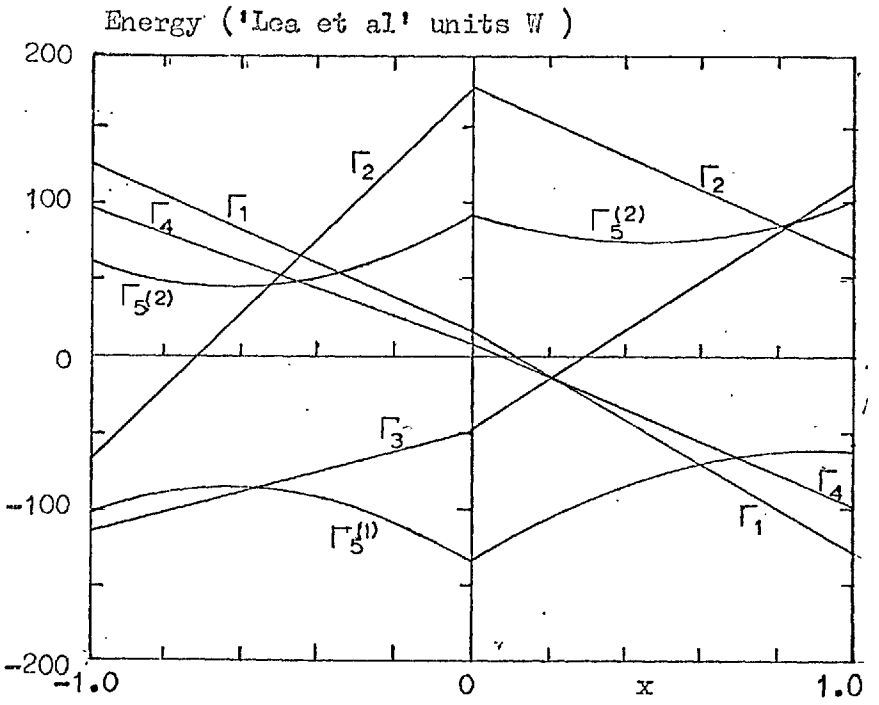

Energy levels of a J=6 ion (Tm^{+++} or Tb^{+++}) in a cubic field.

(Taken from Lea, Leask and Wolf(54).)

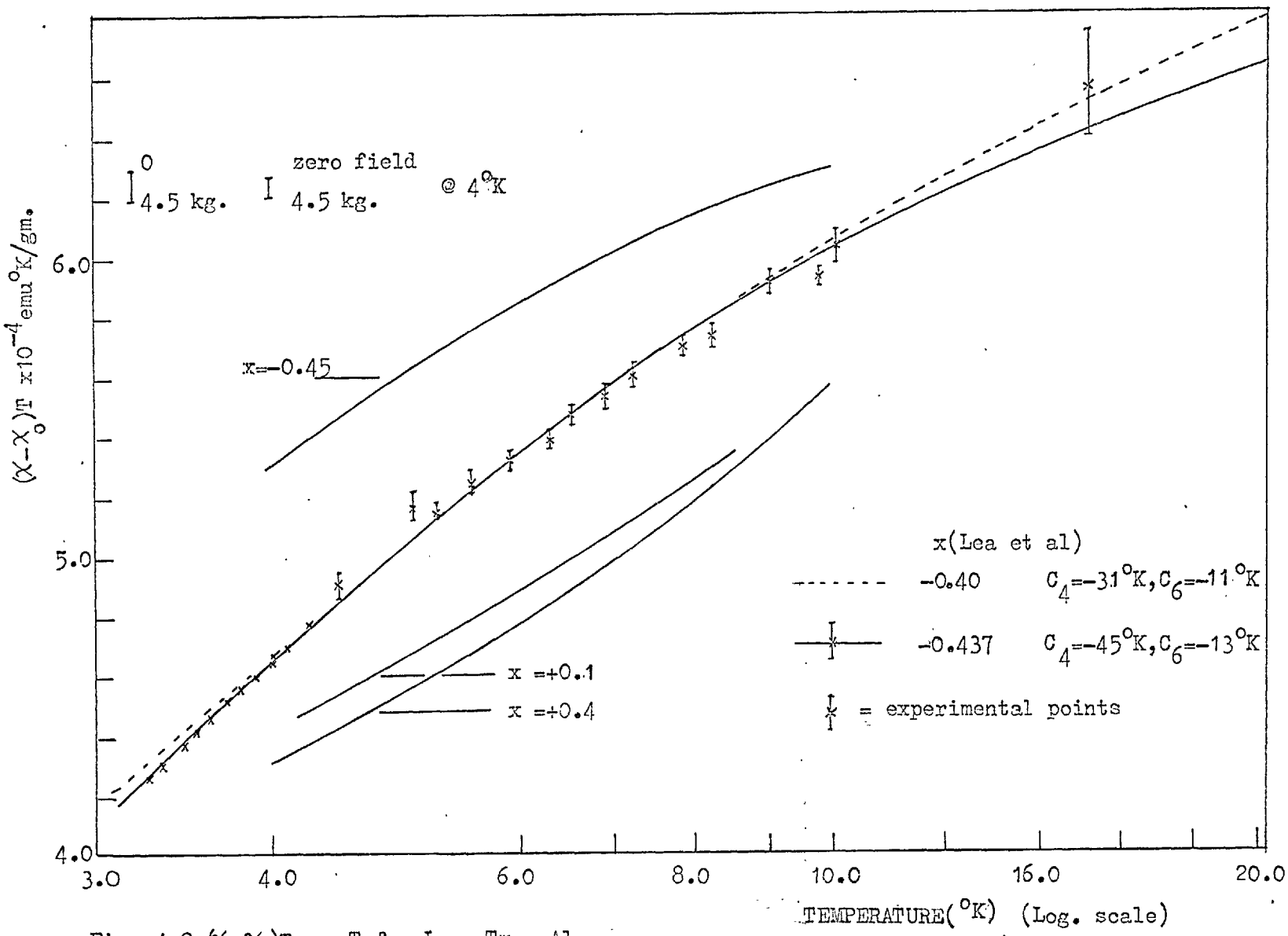

Fig. 4.2 $(\chi-\chi_o)T$ vs. T for $La_{.98}Tm_{.02}Al_2$

C_4 °K	C_6 °K	x (Lea et al)	Ground State	Isolation (°K)	Magnetic Moment μ_B	e.p.r. g factor (low field)	1st Ex. State	Overall Splitting (°K)
-45	-13	- .437	$\Gamma_5^{(1)}$	12.5	2.87 0 - 2.87	2.87	Γ_3	162
-31	-11	- 0.4	$\Gamma_5^{(1)}$	12.6		2.96	Γ_3	135

TABLE 4.1 Crystal Field Levels for Tm^{+++} in $LaAl_2$

TABLE 4.1 (Contd)

For $x = -.437$ the composition of the two lowest levels in terms of $|J=6, J_z\rangle$ basis vectors is as follows:

$$\Gamma_5^{(1)} \text{ triplet} \begin{cases} .5376|\pm 6\rangle + .4593|\pm 2\rangle - .4593|\mp 2\rangle - .537|\mp 6\rangle \\ .6038|+5\rangle + .7970|+1\rangle - .0130|-3\rangle \end{cases}$$

$$\Gamma_3 \text{ non-magnetic doublet} \begin{cases} .2500|4\rangle + .9354|0\rangle + .2500|-4\rangle \\ .5863|6\rangle + .3952|2\rangle + .3952|-2\rangle + .5863|-6\rangle \end{cases}$$

NOTE: in cubic symmetry the degeneracies of the represent-ations are:

Γ_1, and Γ_2 are non-magnetic singlet levels

Γ_3 is a non-magnetic doublet level

Γ_4, and Γ_5 are magnetic triplet levels

Γ_6, and Γ_7 are Kramers doublets

Γ_8 is a magnetic quartet level

state isolation are summarised in table 4.1. Referring back to Fig. 4.2 it can be seen that the parameters $(C_4,C_6)=(-31,-11)^{\circ}K$ (corresponding to x= -.40) are a slightly better fit at high temperatures but slightly worse at lower temperatures. Therefore these two values of x represent limiting values and the estimated errors in (C_4,C_6) are about $(\pm 7, \pm 2)^{\circ}K$. To show that this fit is unique, in Fig. 4.2 the low temperature values of χT arising from completely different level schemes (for example x=.4 giving the $\Gamma_5^{(1)}$ and Γ_1 levels) are shown.

The results therefore show that the $\Gamma_5^{(1)}$ triplet level lies lowest for Tm in $La_{1-x}Tm_xAl_2$, with an isolation of $12.5 \pm .1^{\circ}K$ from the non-magnetic Γ_3 doublet. Γ_5 occurs twice in the decomposition of the $|J=6,J_z>$ representation of the cubic point group so in this particular case the composition of the triplet depends on the C_4/C_6 ratio (i.e. on x). Despite this it was not found possible to fit (C_4,C_6) to better than $(\pm 7, \pm 2)^{\circ}K$ respectively. The presence of this magnetic low lying level also explains the fact that $TmAl_2$ orders ferromagnetically at $5^{\circ}K$ even though the exchange interaction (as deduced from T_c measurements) is small.

C_4 has the same sign, and approximately the same magnitude as obtained by Williams and Hirst for Ag and Au, but C_6 is

about a factor of two larger and of opposite sign. Bleaney (82) has used the point charge model for the Laves phase RNi_2 compounds (as usual R represents a rare earth) and using his results, in conjunction with the estimated $\langle r^4 \rangle$, $\langle r^6 \rangle$ values from the Hartree-Fock calculations of Freeman and Watson (87) and the lattice spacing data quoted by Wernick et al. (62), with point charges $+3\,|e|$ on both the La and Al nearest neighbour sites yields: $(C_4, C_6) = (-3.1, 0.45)^\circ K$.

The point charge model again gives values an order of magnitude too small. In contrast to the noble metal alloys, the point charges on the two types of lattice site (La and Al) in $LaAl_2$ contribute to C_4 in the opposite sense (the positive charges on the Al sites overcome the contribution from those in the La sites). Therefore one could explain the value of C_4 by using a different positive charge distribution. This is not so for C_6, where both contributions are of the same sign, and for this particular alloy it is the sign and magnitude of C_6 which reflect the inadequacy of the point charge model.

2. <u>The isotropy of the susceptibility</u>

The specimens used in this laboratory have always been polycrystalline and yet the computed susceptibilities have always been obtained for a field direction along one of the cubic axes

(the z axis). There are general arguments, related to the fact that χ is a second rank tensor, which show that χ is isotropic for a cubic system (88). However, the writer's attention was recently drawn to a paper by Trammell (89) in which he stated that such arguments are invalid if a degenerate ground state occurs. He specifically showed that the weak field susceptibility from a Γ_3 and Γ_4 level system (a non-magnetic doublet and a magnetic triplet) in cubic symmetry has an anisotropic, temperature independent (Van Vleck) part. Similar considerations, if correct, would show that χ is anisotropic for the Γ_5, Γ_3 lowest levels found here for Tm. In this case the calculated Van Vleck contribution is 40% of χT at $4^{\circ}K$ and any anisotropy in this would cause incorrect values of (C_4, C_6) to be obtained.

To check this the weak field susceptibility for an arbitrary field direction has been calculated from perturbation theory following the method of Van Vleck (83) (p.143). The result is that for all the sets of levels (Γ_1 .... Γ_8) occurring in cubic symmetry and for all the Van Vleck terms arising from mixing between them, χ is isotropic. (This is despite the fact that the Γ_8 levels do not have isotropic e.p.r. absorption spectra (90)). Thus the general 'cubic symmetry' arguments are confirmed and the

result of Trammell is contradicted.

The particular method used was as follows. If the field $\mathcal{H}$ is applied in an arbitrary direction $\hat{\underline{r}}$ with direction cosines (l, m, n) the perturbing Hamiltonian acting on the crystal field eigenstates is

$$-\mu_B \mathcal{H} g_J \underline{J}.\hat{\underline{r}}$$

Where g_J is the Landé g-factor and $\underline{J}$ is the angular momentum operator for the rare earth ions. μ_B is the Bohr magneton. Let the unperturbed crystal field eigenstates belonging to the n_d – dimensional irreducible representation Γ_d be called ψ_{di}, i=1 ... n_d.

These are n_d-fold degenerate with unperturbed energy E_d^o.

To second order in $\mathcal{H}$ the perturbed energies are E_{di},

$$E_{di} = E_d^o + E_{di}^{(1)}\mathcal{H} + E_{di}^{(2)}\mathcal{H}^2 + \ldots\ldots\ldots$$

and the magnetic moment M_{di} is given by:

$$M_{di} = E_{di}^{(1)} + 2E_{di}^{(2)}\mathcal{H} + \ldots\ldots$$

(Van Vleck p.143).

The average magnetic moment in the direction of $\mathcal{H}$ at temperature T is given by:

$$M = B'^{-1} \sum_{d,i} M_{di} \exp(-E_{di}/kT)$$

where

$$B' = \sum_{d,i} \exp(-E_{di}/kT)$$

and expansion in powers of $\mathcal{H}$ yields

$$M = \chi \mathcal{H} + O(\mathcal{H})^2 + \ldots\ldots\ldots$$

where

$$\chi = B' \sum_{d,i} \left\{ \frac{E_{di}^{(1)}}{kT}^2 - 2E_{di}^{(2)} \right\} \exp(-E_d^o/kT)$$

and

$$B = \sum_{d,i} \exp(-E_d^o/kT)$$

Now

$$E_{di}^{(1)} = g_J \mu_B \mathcal{H} \langle \psi_{di} | \underline{J} \cdot \hat{\underline{r}} | \psi_{di} \rangle$$

if the ψ_{di} are chosen so that:

$$\langle \psi_{di} | \underline{J} \cdot \hat{\underline{r}} | \psi_{dj} \rangle = 0, \text{ if } i \neq j \quad \ldots\ldots \quad 4.2$$

then

$$E_{di}^{(2)} = \sum_{\substack{b,j \\ b\neq d}} \frac{g_J^2 \mu_B^2 \left|\langle \psi_{di} | \underline{J}\cdot\hat{\underline{r}} | \psi_{bj} \rangle\right|^2}{E_d^o - E_b^o}$$

In fact $\sum_i E_{di}^{(2)}$ is not altered by taking a linear combination of ψ_{di} such that equation 4.2 holds. Thus, to calculate χ any orthogonal set of states can be used.

The computer program evaluates the matrix elements of J_x, J_y, J_z between the crystal field levels.

Since $\underline{J}\cdot\hat{\underline{r}} = lJ_x + mJ_y + nJ_z$, $\chi(l,m,n)$ could be evaluated for particular crystal field parameters (C_4, C_6). This was done for the Tm^{+++} levels $\Gamma_5^{(1)}$ and Γ_3, and for the $\Gamma_8^{(3)}$ ground state of Er^{+++}. In both cases χ was independent of (l, m, n), that is, isotropic. More recently the matrix elements of (J_x, J_y, J_z) tabulated by Statz and Koster (91) have been used and the aforementioned result that χ is independent of (l, m, n) for any of the Γ_1 .. Γ_8 levels in cubic symmetry and any Van Vleck mixing between them was obtained.

4.3 T_c Measurements for $La_{1-x}R_xAl_2$

The results of the T_c measurements and the computed crystal field levels are all summarised in table 4.2,p.125-6;graphs of $T_{co}-T_c$ (T_{co}=3.24°K for 3N La in $LaAl_2$ and 2.94°K for 2N7 La in $LaAl_2$) versus x (at. %) are plotted for the various systems in Figs 4.3 to 4.8. Also plotted for each alloy is the curve predicted from the AG theory (chapter 2).

$$\ln \frac{T_{co}}{T_c} = \psi(\tfrac{1}{2} + 0.140 \frac{x}{x_{cr}} \cdot \frac{T_{co}}{T_c}) - \psi(\tfrac{1}{2})$$

The initial slope of this curve is

$$\frac{dT_c}{dx} = -0.690 \frac{T_{co}}{x_{cr}}$$

x_{cr} is chosen so that the experimental and theoretical initial slopes are equal. These initial slopes are tabulated in 4.2 together with the values expected in the absence of crystal field splitting. The latter values were calculated by assuming that J_{eff} is the same for all the rare earth ions in $LaAl_2$ as for Gd and, according to the AG formula, scaling the measured value of dT_c/dx for Gd (3.7°K/at.%) by the ratio of the de Gennes factors $(g_J-1)^2J(J+1)$ i.e.

$$\frac{dT_c}{dx} = 3.7 \ (g_J-1)^2J(J+1) \ \frac{2}{7} \cdot \frac{2}{9} \quad {}^\circ K \ / \ \text{at.}\%$$

The assumption of a constant J_{eff} is doubtful of course, especially at the beginning of the series and here one needs respective values of J_{eff} 7.5, 1.7 and 1.3 times larger for Ce, Pr and Nd than for Gd, even in the absence of crystal field splitting. However, for Tm dT_c/dx is a factor of 3 lower than the 'De Gennes factor' prediction and possibly crystal field effects are also causing lower values in Dy, Tb and Sm alloys.

If the crystal field levels are known then dT_c/dx can be calculated (assuming a constant J_{eff}) as described in the following section.

To obtain exact agreement J_{eff} has then been adjusted slightly (by about 10%) and the values are also tabulated in 4.2 as a fraction of J_{eff} for gadolinium (J'_{eff}).

4.4 Calculation of dT_c/dx for Known Crystal Field Levels

It is known from the theory of AG and later workers (for example De Gennes (22) p.254) that the depression in T_c is proportional to a one electron scattering rate $1/\tau_s$ in the normal state. $1/\tau_s$ is due to that part of the conduction electron Hamiltonian which does not have time reversal symmetry, that is, the $J_{eff}\ \underline{S}.\underline{s}$ part (it was shown by Anderson that other perturbations do not have any effect on T_c for an isotropic energy gap). In fact $1/\tau_s$

has already been calculated by L. L. Hirst (93) in his calculation of the contribution of the $J_{eff}\ \underline{S}.\underline{s}$ interaction to the resistivity, for rare earth impurities in the presence of crystal field splitting. He assumed a free electron model (with an effective electron mass m*) and found the spin disorder relaxation time τ by using time dependent perturbation theory and including inelastic one electron scattering. The result is:

$$\frac{1}{\tau} = \frac{x\pi}{2\hbar} N(E_F)(g_J-1)^2 \sum_{\substack{I,I' \\ m,m'}} P(I) \frac{\Delta_{II'}}{kT(\exp(\frac{\Delta_{II'}}{kT}) - 1)} F_{kmI}^{k'm'I'}$$

where in this formula:

$$F_{kmI}^{k'm'I'} = \langle J_{eff}(k,k') \rangle^2 |\langle m;\ I'|\ \underline{J}.\underline{s}|m,I\rangle|^2$$

I,I' label the 4f ion states in the cubic crystalline field of respective energy E_I and E_I'.

$$\Delta_{II'} = E_I - E_{I'}$$

P(I) is the Boltzmann probability that the state $|I\rangle$ is occupied. $\underline{k},\underline{k}'$ are the conduction electron wave vectors. $m,m' = \pm\frac{1}{2}$ are the z components of the conduction electron spin (which are

assumed to be equally probable) $|m,I\rangle$ represents the state with s_z (conduction electron spin component)=m and the rare earth ion in the crystal field state $|I\rangle$.

$\langle J_{eff}(\underline{k},\underline{k}')^2\rangle$ is an average of $J_{eff}(\underline{k}\cdot\underline{k}')^2$ over the fermi surface. This is different for $1/\tau$ and $1/\tau_s$ because the transport cross section is a weighted average of the differential scattering cross section (Ziman (94) p.769). Often $J_{eff}(\underline{k},\underline{k}')$ is taken to be a constant, (this is implicitly assumed in much of this thesis) corresponding to a $J_{eff}\delta(\underline{r})$ interaction in real space, and then $1/\tau = 1/\tau_s$.

Finally x is, as usual, the concentration of rare earth impurities. Hence in order to find dT_c/dx the quantity

$$2(g_J-1)^2 \sum_{\substack{II' \\ mm'}} \frac{p(I)\,\Delta_{II'}}{kT\left\{\exp\frac{\Delta_{II'}}{kT}-1\right\}} \quad |\langle I',m'|\underline{J}\cdot\underline{s}|m,I\rangle|^2 \qquad 4.3$$

has to be calculated.

In the absence of crystal field splitting, or if $kT \gg \Delta_{II'}$, the above sum becomes $(g_J-1)^2 J(J+1)$ independent of temperature and thus one retrieves the usual 'De Gennes factor'

result. In the presence of crystal field splitting the above sum is temperature dependent. This dependence arises from the freezing out of certain scattering processes, both elastic and inelastic, by the combined effects of the Boltzmann population of the energy levels of the rare earth ions and the Fermi statistics of the conduction electrons. The computer program evaluates this sum for the particular levels given by the starting parameters (C_4, C_6), as a function of temperature T. In fact the program calculates it relative to the constant value for Gd (7/2.9/2) and this will be defined as $\rho(T)$. Therefore, assuming J_{eff} is the same as for Gd the initial slope of the T_c versus concentration (x) curve is given by:

$$\frac{dT_c}{dx} = 3.7\rho(T_{co})^{\circ}K/at.\ \%$$

(since the initial value of dT_c/dx for Gd is $3.7^{\circ}K/at.\ \%$).

If there are crystal field levels well separated from the ground state, compared to T_{co} then $\rho(T_{co})$ will be constant and reduced from its high temperature value of $4(g_J-1)^2J(J+1)/63$. However, if there are crystal field levels separated by an energy $\sim T_{co}$ from the ground state level then $\rho(T)$ will still be varying with temperature at T_{co}. It was this variation, which, it

was originally hoped, would lead to deviations from AG in the T_c versus x curves. (Strictly speaking T_c is given by the implicit formula:

$$\ln \frac{T_{co}}{T_c} = \psi\left(\tfrac{1}{2} + \frac{2.x}{\pi^2} \cdot \frac{3.7\,\rho(T_c)}{T_c}\right) - \psi\left(\tfrac{1}{2}\right)$$

However, in the temperature range above 1.5°K the initial expansion of the ψ function can be used).

To conclude this section, it should be mentioned that the writer had some difficulty in finding out whether or not non-spin flip processes should be included in the pair breaking mechanism, that is, whether or not the $J_z s_z$ matrix elements should be included in equation 4.3. According to Zuckermann (95) these should be included. However, it later transpired that for cubic symmetry the results were not altered by this.

This can be shown by using the expression for $\underline{J}.\underline{s}$ in terms of the raising and lowering operators $J^{\pm}$, $s^{\pm}$.

$$\underline{J}.\underline{s} = \tfrac{1}{2}(J^+ s^- + J^- s^+) + J_z s_z$$

The sum

$$\sum_{\substack{m' = \pm\frac{1}{2} \\ m = \pm\frac{1}{2}}} |\langle m'I' \mid \underline{J}.\underline{s} \mid m, I\rangle|^2$$

in equation 4.3 becomes:

$$\tfrac{1}{4}\left(\left|J^{+}_{II'}\right|^{2} + \left|J^{-}_{II'}\right|^{2} + 2\left|J^{z}_{II'}\right|^{2} \right)$$

(only one of the $J^{+}s^{-}$, $J^{-}s^{+}$, $J_{z}s_{z}$ elements are non-zero if m and m', the conduction electron spin components are fixed).

$J^{\pm} = J_{x} \pm iJ_{y}$, therefore the sum becomes:

$$\tfrac{1}{2}\left\{ \left|J^{x}_{II'}\right|^{2} + \left|J^{y}_{II'}\right|^{2} + \left|J^{z}_{II'}\right|^{2} \right\}$$

If this is summed over all the levels I within one representation and all the levels I' within another, then in cubic symmetry, in the absence of a magnetic field, all three x, y, z components give the same contribution. Thus, the scattering cross-section including the $J_{z}s_{z}$ term is the same as that involving just the spin flip $J^{+}s^{-} + J^{-}s^{+}$ terms, when expressed as a fraction of the Gd value.

In addition dT_{c}/dx is easily calculated for a well isolated ground state as it is proportional to $(g_{J}-1)^{2}\ \overline{\langle J_{z}\rangle^{2}}$, where $\langle J_{z}\rangle$ is the average value of J_{z} for one of the degenerate levels and the horizontal bar represents an average value for all the degenerate levels within a certain set (belong to a representation Γ). Therefore, for a well isolated magnetic ground state

(neglecting the 'Van Vleck' contribution to χ):

$$\frac{dT_c}{dx} = A \frac{(\chi T)_L}{(\chi T)_H}$$

where A is the value of dT_c/dx calculated from the de Gennes factor in the absence of crystal field splitting. $(\chi T)_{L,H}$ are the limiting values of χT at low and high temperatures, and are proportional to the square of the effective moment per atom in these two regimes.

4.5 Discussion of These Results

The $La_{1-x}Lu_xAl_2$ system was measured in order to allow for any depression in T_c which was non-magnetic in origin. However, the starting lutetium contained 2 wt % tantalum and in view of the results of Maple for $La_{1-x}Yb_xAl_2$ ($dT_c/dx \sim 0.01^{\circ}K/\%$) this correction will not be made.

Referring to table 4.2 it can be seen that for Tm^{+++}, where the crystal field levels are known reasonably accurately, the anomalously low value of dT_c/dx can be explained quantitatively with $J_{eff}/J_{eff}(Gd) = 1.0$, this ratio will be called J'_{eff} in future. (If the 'Lu correction' is madeone requires $J'_{eff} = 0.85$ which

Impurity	Measured $\frac{dT_c}{dx}$ (°K/at%)	dT_c/dx(°K/%) Calculated from De Gennes factor	dT_c/dx(°K/%) Calculated from crystal field levels	J'_{eff} (De Gennes factor)	J'_{eff} (crystal field levels)
Yb	.01	-	-	-	-
Tm	.106 ±.006	.28	.107	.61	1.0
Er	.48 ±.03	.58	.41	.91	1.08
Ho	.78 ±.03	.99	.58	.89	1.1
Dy	1.45 ±.03	1.55	1.25*	.96	1.15*
Tb	2.17 ±.03	2.56	1.6*	.92	1.15*
Gd	3.7 ±.03	3.7	3.7	1.0	1.0
Sm	.6 ±.03	.99	.65	.78	.95
Nd	.74 ±.03	.43	.31	1.3	1.5
Pr	.57 ±.03	.20	.12	1.7	2.2
Ce	2.4 ±.03	.042	.01	7.5	15
Lu	.03 ±.006	-	-	-	-

J_{eff}' = $J_{eff}/J_{eff}(Gd)$ ratio required for exact agreement between measured and calculated values of dT_c/dx. * $\rho(T)$ still falling at T_c

TABLE 4.2 Comparison of the measured and calculated values of dT_c/dx for $La_{1-x}R_xAl_2$ alloys

Impurity (R)	Ground State	Ground State Isolation (°K)	First Excited State	Calculated values of $\rho(T)$ T=3°K	T=1°K	Parameters Used C_4 °K	C_6 °K	x (Lea et al)	$\frac{dT_c}{dx} = 3.7\rho(T_\infty)$ °K/at %
Tm	$\Gamma_5^{(1)}$	12.5±.1	Γ_3	.027	.022	-45	-13	- .437	0.100
				.029	.024	-30	-11	- .399	0.107
Er	$\Gamma_8^{(3)}$	~70	Γ_6	.11	.11	-32	-10	.23	0.41
Ho	$\Gamma_5^{(1)}$	~40	$\Gamma_3^{(1)}$	.155	.155	-44	-13	- .72	0.58
Dy	$\Gamma_8^{(3)}$	~4	$\Gamma_8^{(2)}$	.33	.165	-44	-13	- .45	1.25
Tb	Γ_3	~4	$\Gamma_5^{(1)}$	.44	.1*	-32	-10	.73	1.6
Gd	-	-	-	1.0	1.0	-	-	-	3.7
Sm	Γ_8	~40	Γ_6	.175	.175	-44	-	1.0	0.65
Nd	$\Gamma_8^{(3)}$	~1.0	Γ_6	.082	.083	-44	-13	.3	0.3
Pr	Γ_5	?	Γ_3	.032	.032	<-50	$\simeq -10$	$<-.7$	0.12
Ce	Γ_6	200	Γ_8	.0026	.0026	+93	-	1.0	0.01

* $\rho(T) \longrightarrow 0$ as $T \longrightarrow 0$

TABLE 4.2 (contd) Predicted Crystal Field Levels for $La_{1-x}R_xAl_2$ Alloys

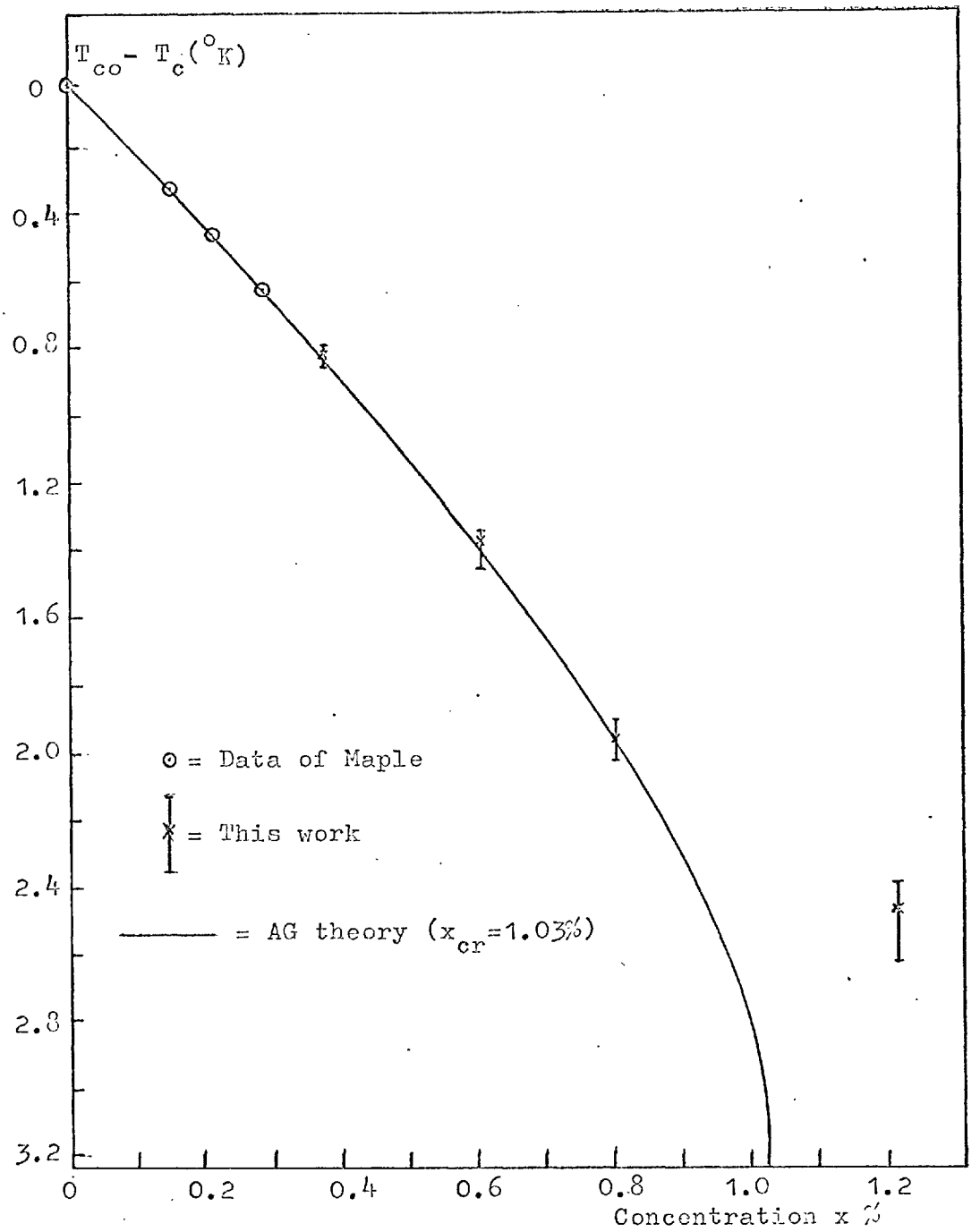

Fig. 4.3 $T_{co}-T_c(^{\circ}K)$ vs. x(%) for $La_{1-x}Tb_xAl_2$

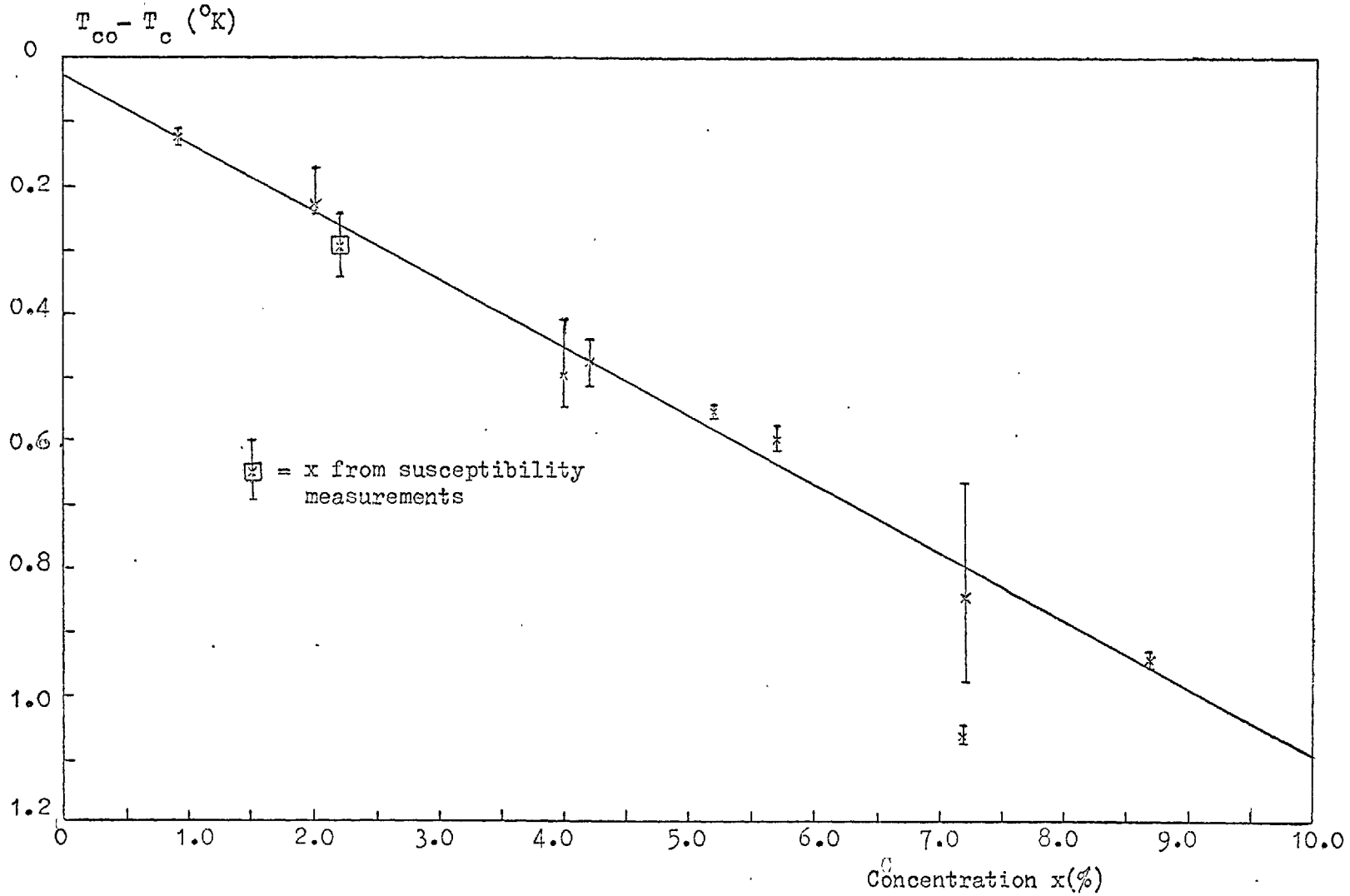

Fig.4.4 $T_{co} - T_c$ vs. x(%) for $La_{1-x}Tm_xAl_2$

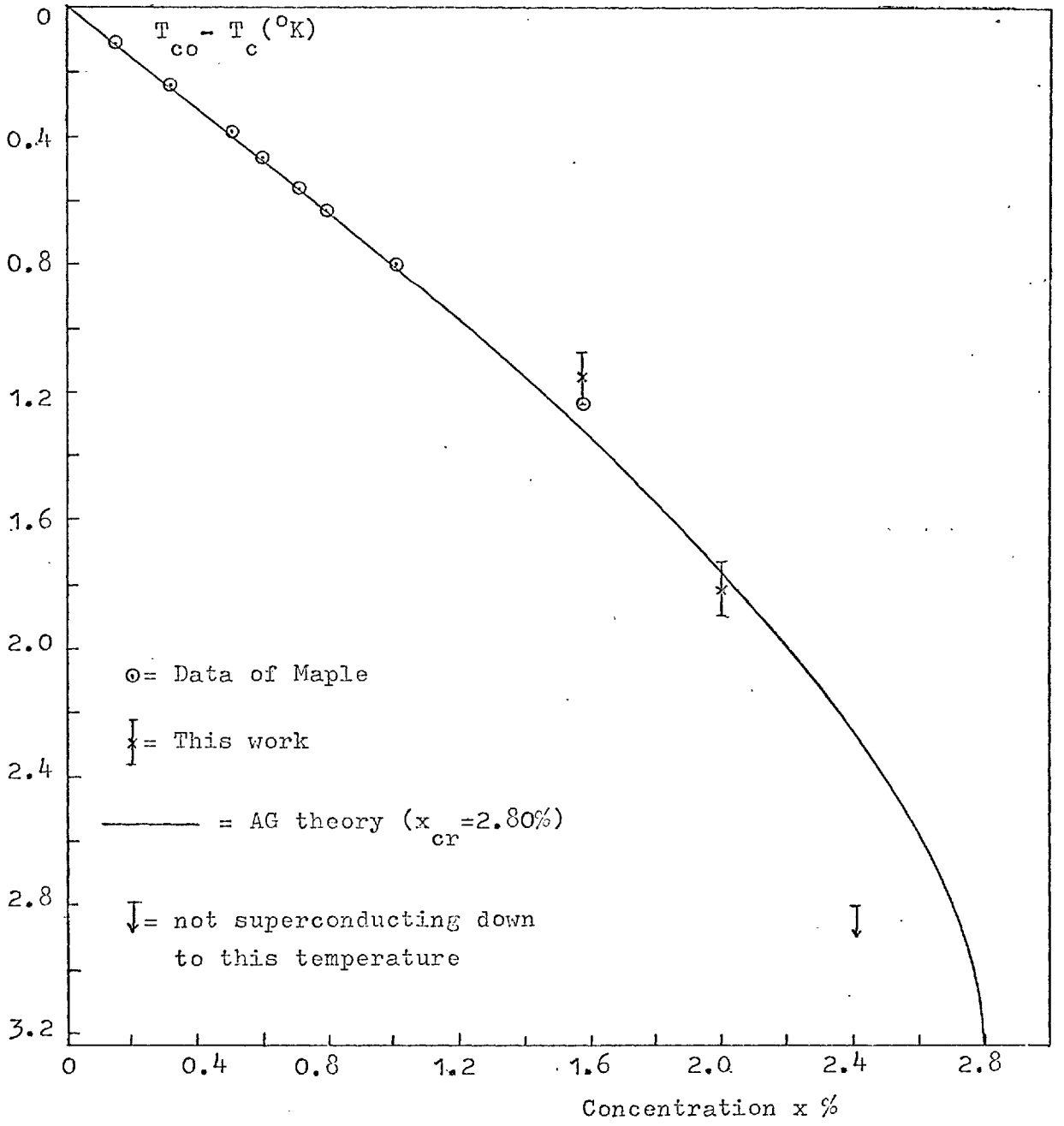

Fig. 4.5 $T_{co} - T_c$(°K) vs. x(%) for $La_{1-x}Ho_xAl_2$

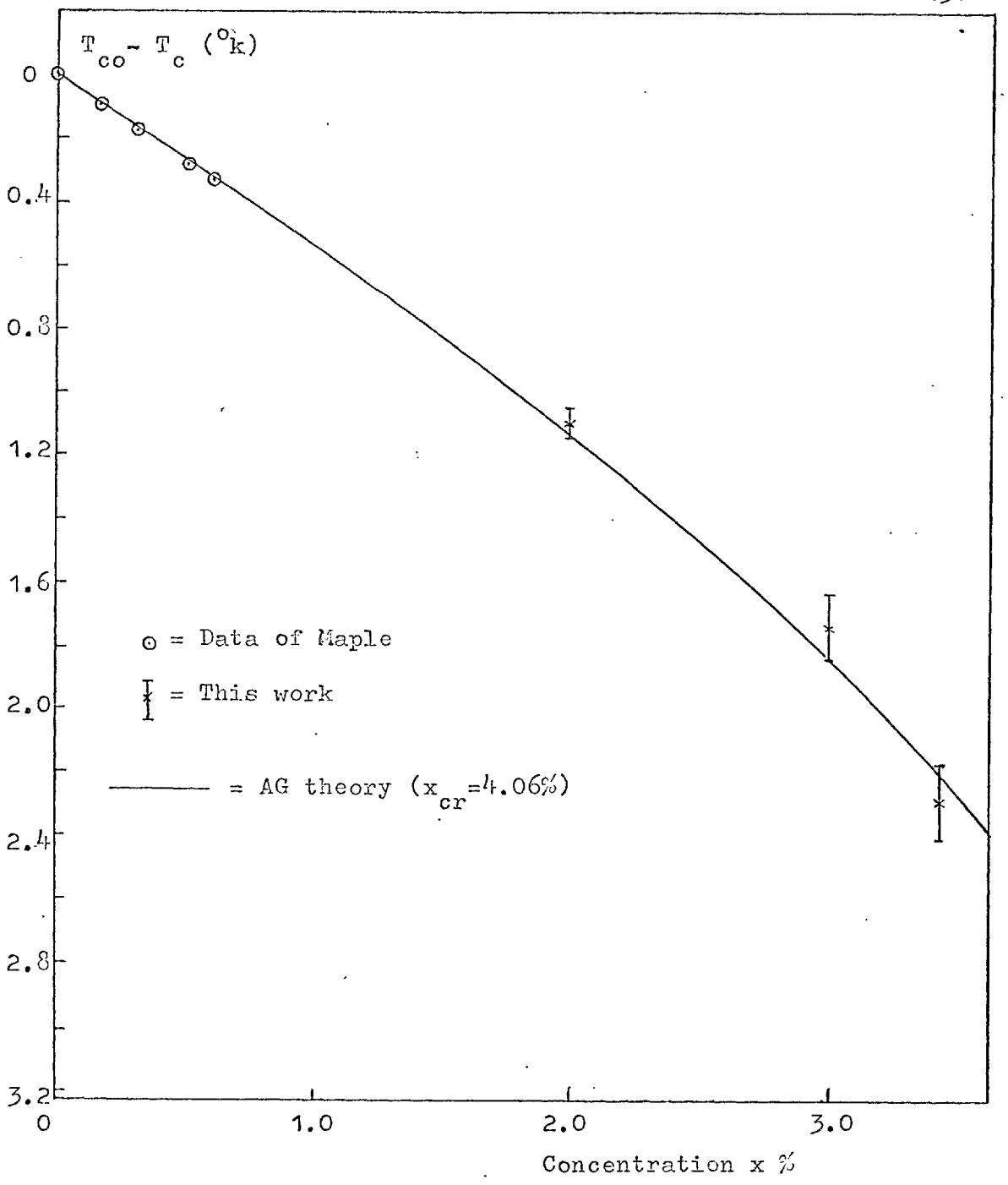

Fig. 4.6 $T_{co} - T_c$ vs. x(%) for $La_{1-x}Pr_xAl_2$

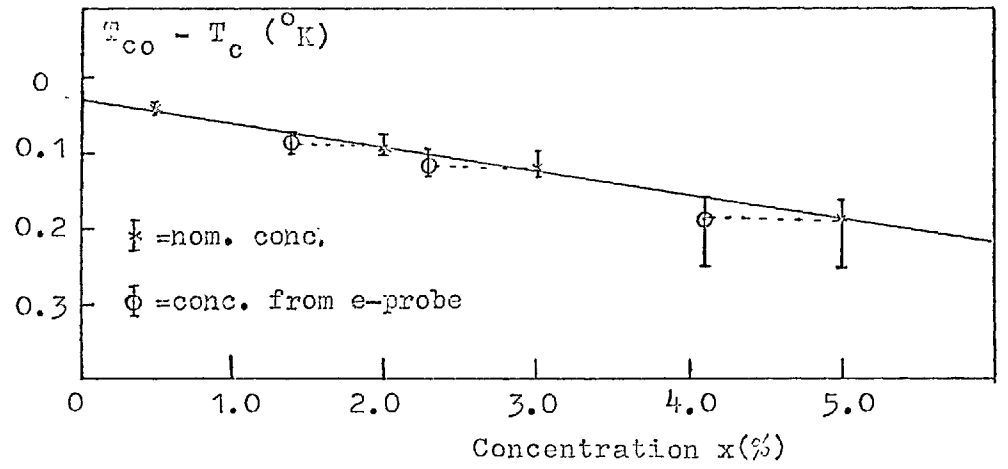

Fig. 4.7 $T_{co} - T_c$ vs. x(%) for $La_{1-x}Lu_xAl_2$

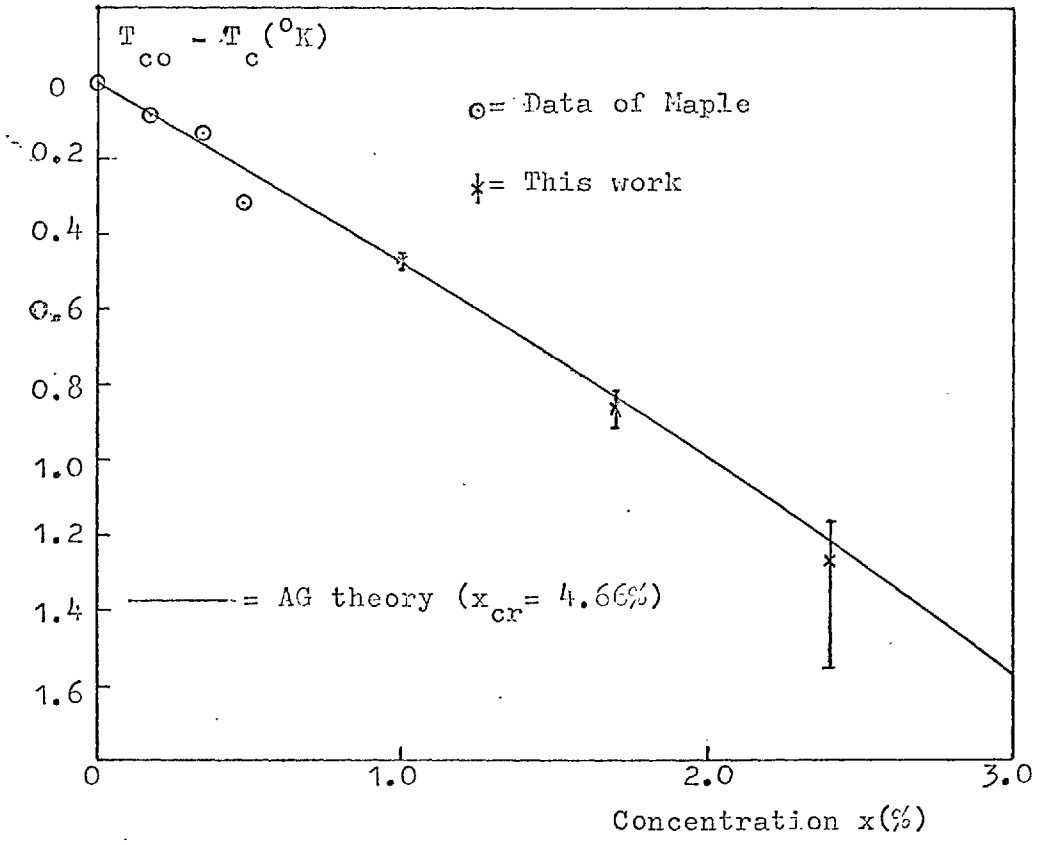

Fig. 4.8 $T_{co} - T_c$ vs. x(%) for $La_{1-x}Er_xAl_2$

is quite feasible bearing in mind the contraction in 4f shell radius towards the end of the series).

The same C_4, C_6 parameters have been used to predict the ground state and first excited states of the remaining rare earth impurities. These are given in table 4.2. For Er and Ho and Sm the predicted ground state isolation is large and the values of J_{eff} are in good agreement(10%) with that of gadolinium. For Ho the calculated level scheme for these parameters is different from that of Lea et al. This is because of an error in the values of the Stevens multiplicative factors (β, γ) for Ho used by these authors (110). At the other end of the series $La_{1-x}Pr_xAl_2$ has been found to obey the AG T_c law down to $0.9^{\circ}K$. (Fig. 4.6) The T_c results indicate that a magnetic ground state (Γ_5 triplet) lies lowest. This requires a larger value of $|C_4|$. For the same value of C_6 as for Tm ($-11^{\circ}K$). C_4 must be less than $-50^{\circ}K$. As mentioned previously, even in the absence of crystal field splitting larger values of $|J_{eff}|$ are required for Ce, Pr and Nd. However, with the postulated crystal field levels the latter two elements have respective J'_{eff} values of 2.2 and 1.5. Such a variation at the beginning of the series is consistent with that calculated by Freeman and Watson (70) for the Heisenberg exchange interaction. For the covalent mixing interaction the latter authors obtained

even stronger variations. Although the $\Gamma_8^{(1)}$ quartet ground state level has been postulated for Nd it is possible that the Γ_6 Kramers doublet does in fact lie lowest, and this will be shortly checked by looking for e.p.r. absorption (the $\Gamma_3^{(1)}$ level is anisotropic and a detectable resonance would not be expected in a polycrystalline or powdered specimen).

As can be seen from Table 4.2 the remaining elements, Dy and Tb, are expected to have a smaller ground state isolation. For the predicted levels the ground state isolations are both approximately $4^{\circ}K$. The Tb system is particulary interesting in that the Γ_3 non-magnetic doublet probably lies lowest and $\rho(T)$ falls by a factor of 4 for Tb from $3^{\circ}K$ to $1^{\circ}K$, although for both Tb and Dy the value of $\rho(T_{co})$ is consistent with $J'_{eff} = 1.1$ as for the nearby elements Ho and Er. Since $\rho(T)$ is still varying with temperature at T_{co} one would naively expect departures from the AG T_c versus x curve to occur for Tb and Dy . For this reason T_c has been plotted against x for Tb down to $0.7^{\circ}K$ (Fig. 4.3). It can be seen that the AG curve is followed down to $1.2^{\circ}K$ but there is one isolated point at a concentration greater than x_{cr} which, if correct, could be due to either crystal field or interaction effects. The two possible explanations for the behaviour of the Tb and Dy alloys assuming that the theory used here is correct,

(a third possibility which does not assume this, is given at the end of this chapter) are:

(i) The ground state isolation of the Γ_3 level in Tb (and probably in Dy also) is less than $1^{\circ}K$.

(ii) $J'_{eff} = 1.7$ for Tb and Dy, and also the $\Gamma_5^{(1)}$ level lies lowest for Tb.

Some Tb and Dy alloys are therefore being prepared and susceptibility measurements on $La_{1-x}Tb_xAl_2$ are being made at the time of writing, in order to distinguish between these two possibilities and the third one mentioned at the end of this chapter.

4.6 Results of Other Workers for $LaAl_2$ Based Systems.

(1) $La_{1-x}Ce_xAl_2$

The susceptibility of this system has been measured by White et al (62) and more recently by Maple and Fisk (80). The latter authors also measured T_c versus concentration and the electrical resistanceof these alloys.

The values of $\chi T/x$ obtained by the latter authors are independent of x up to x= .03. Above $4^{\circ}K$ the results could be fitted reasonably well to crystal field theory with $C_4=80^{\circ}K$ (6^{th} order fields have no effect for Ce^{+++}).

We have also calculated χT from the crystal field model with $C_4=93^{\circ}K$ and within the scatter of Maple's data ($\sim 2\%$) find

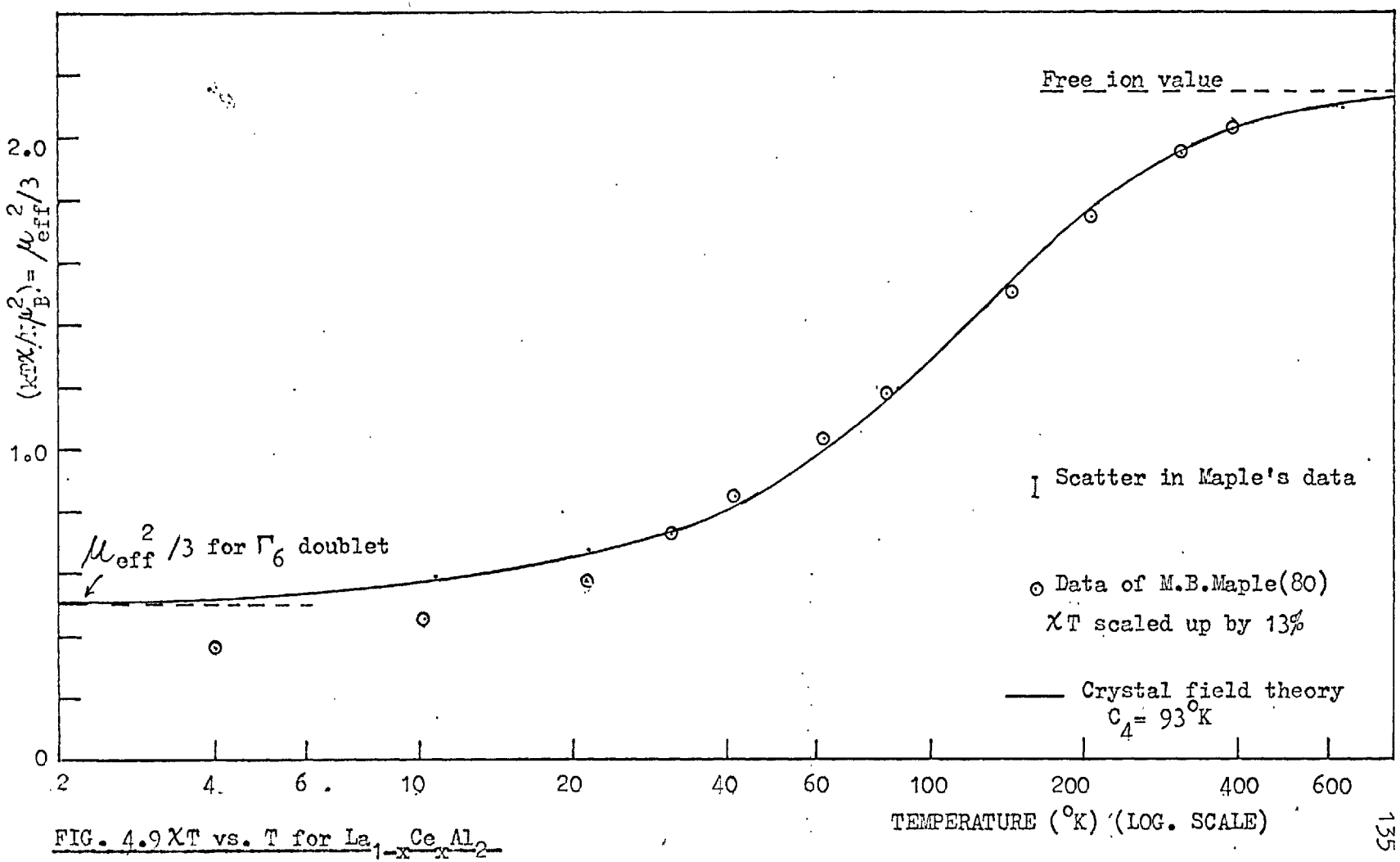

FIG. 4.9 χT vs. T for $La_{1-x}Ce_xAl_2$

excellent agreement with crystal field theory above 20°K, as shown in Fig. 4.9, if the measured values of χT are all scaled up by 13%.

The low temperature deviations have been interpreted as evidence for a Kondo-Nagaoka bound state by the authors.

Although there is still some uncertainty about the validity of a crystal field description of Ce it is interesting to note that the sign of C_4 is opposite to that for neighbouring Pr (C_4 must be negative for Pr, for any value of C_6, if a magnetic level is to lie lowest), and that this change in sign is associated with an increase in the 'covalent mixing' between the 4f electron and the conduction electrons.

(2) $La_{1-x}Pr_xAl_2$

The susceptibility of this sytem has been measured by Wallace et al (96). Their most dilute alloy (x=0.5) ordered ferromagnetically at 5°K. These authors concluded that the Γ_1 singlet ground state would lie lowest in the dilute limit but that higher states (specifically the Γ_4 triplet) were mixed in by the indirect ion-ion exchange interaction. Cooper (97) has shown that there will be no magnetic ordering at any temperature if a singlet ground state is sufficiently well isolated from the other levels. For this particular case his condition leads to $\Delta < 10$°K.

Where Δ is the energy difference between the Γ_1 singlet and the Γ_4 triplet. Wallace et al tried to fit their susceptibility data on the basis of a Γ_5 ground state for $1 < x < 0.8$ (here x is the Lea, Leask and Wolf (54) parameter not the concentration) and failed. Our results indicate that Γ_5 is lowest, but that x is between -0.7 and -1.0, a possibility not considered by the previous authors. The other possibility is that Wallace's result is correct, but then Γ_1 and Γ_4 would have to be extremely close together since, as can be seen from Fig. 4.6 , the T_c's of $La_{1-x}Pr_xAl_2$ obey the AG theory down to 0.9^oK, the lowest T_c measured. These two cases could easily be distinguished by susceptibility measurements on (say) a 1% $LaPrAl_2$ alloy.

4.7 Results of Other Workers for Similar Systems

Bucher, Andres et al (58) have measured the specific heat, susceptibility and superconducting transition temperatures of a series of intermetallic compounds having the cubic, Cu_3Au type, structure, namely $LaSn_3$, $LaPb_3$ and $LaTl_3$ doped with Tm or Pr impurities. The same authors have also made similar measurements on the ThPr and ThTm binary systems. Their results indicate that in all alloys except $La_{1-x}Pr_xSn_3$ the rare earth

ion does have a non-magnetic ground state. In this alloy $dT_c/dx = -10^{\circ}K$/at. % Pr (in La); the specific heat data gives $n(E_F) = 1.1$ states/eV/atom hence, using AG theory and assuming that the magnetic state Γ_5 lies lowest, and is well isolated, one finds $|J_{eff}| = 1.0$ eV/atom. This is extremely large for a rare earth ion and $J_{eff} < 0$ in this case. It should therefore be possible to see a resistance minimum in this alloy provided that the band of electrons mainly responsible for the electrical conductivity is also involved in the superconducting transition. This would be the first observation of a minimum associated with a rare earth ion (other than Ce) in the low concentration ($\sim$1%) regime.

The fact that dT_c/dx is anomalously large in $La_{1-x}Pr_xSn_3$ initially caused some confusion because Bucher et al had compared the values of dT_c/dx for $La_{1-x}Pr_xPb_3$ and $La_{1-x}Pr_xTl_3$ (see table 4.3) with this large value in commenting on the effect of a singlet ground state. There was still a small depression in T_c even for the singlet levels; and in addition the published $1/\chi$ vs T curves for the ternary compounds (e.g. $La_{1-x}Pr_xPb_3$), in contrast to those for $PrPb_3$ and $PrTl_3$, did not appear to show 'singlet' behaviour,

namely a temperature independent low temperature susceptibility. This point has now been cleared by further information from the authors and it seems that χ is indeed temperature independent below $4^{o}K$ for all binary and termary Pr and Tm compounds except $La_{1-x}Pr_{x}Sn_{3}$. The differences in χ that do arise are attributed to exchange fields which, on a molecular field model, give a concentration dependent displacement of the $1/\chi$ vs T curves along the $1/\chi$ axis. (ref.97).

The ThPr and ThTm systems exhibited unambiguous 'singlet' behaviour in $\chi(T)$. Since the ThGd and ThEr systems have also been measured by Finnemore et al (43) and by Guertin and Parks (40) respectively, $|J_{eff}|$ is known to be $\simeq 0.1$ eV for this system and, as shown in table 4.3, the measured depression in T_c for Pr and Tm impurities is considerably lower than that expected from a magnetic level. Nevertheless there is a residual depression in T_c, for all host matrices, whose origin is not understood. Bucher et al (58) were unable to explain this in terms of the effects of the temperature dependent population of higher crystalline field levels because these are too far away in energy ($\sim 220^{o}K$). Possibly there is a mechanism here involving spin fluctuations on the rare earth site, as in the Al Mn alloys,

1 $LaPb_3$, $LaTl_3$ and $LaSn_3$ - based Intermetallic Compounds

HOST ⟶ / Impurity ↓	$LaPb_3$ $\frac{dT_c}{dx}$(°K/%)	$LaTl_3$ $\frac{dT_c}{dx}$(°K/%)	$LaSn_3$ $\frac{dT_c}{dx}$(°K/%)	$LaSn_3$ J_{eff}(eV/at,)
Pr^{+++}	0.16	0.1	10	1.0,*
Tm^{+++}	–	–	.25	.17,*
Gd^{+++}	–	–	40	.36

* These are the J_{eff} values obtained from dT_c/dx, assuming well isolated Γ_5 levels lie lowest in both Pr and Tm.

2 Th - based alloys

Impurity	$\frac{dT_c}{dx}$(°K/%)	J_{eff}(eV/at.)	Calculated $\frac{dT_c}{dx}$(°K/%) (J_{eff}=0.1eV)	Assumed Ground State
Pr^{+++}	.04	–	.096	Γ_5
Tm^{+++}	.028	–	.09	$\Gamma_5^{(1)}$
Er^{+++}	.13	–	.137	Γ_6
Gd^{+++}	3.0	0.1	–	–

TABLE 4.3 dT_c/dx Values for Other Rare Earth/Superconductor Systems

which is responsible for the residual depression caused by the non-magnetic states.

Finally it can be seen from table 4.3 that the value of dT_c/dx in Th Er(face centred cubic) is consistent with that expected from a well isolated Γ_6 Kramers doublet level and $J_{eff} = 0.1$ eV. This indicates that (C_4, C_6) both have the same sign in Th as in Ag and Au although the magnitude of their ratio must be larger in Th. Such values of (C_4, C_6) would also give a singlet ground state (Γ_2 or Γ_3) for Tm^{+++} but would give the Γ_5 triplet for Pr^{+++} which is not observed. Therefore, in Th, as in the $LaAl_2$ and the noble metal based systems, some variation of C_4 and C_6 must occur along the series between Er and Pr. It should also be possible to see e.p.r. absorption corresponding to the Γ_6 doublet in the ThEr alloys.

4.8 Concluding Discussion and Summary for Rare Earth Impurities

1. T_c and Susceptibility Measurements

The susceptibility of $La_{1-x}Tm_xAl_2$ (x=.022) has been measured and fitted to the electrostatic crystal field model by suitable choice of the parameters (C_4, C_6). These parameters, $\sim(-40,-13)^\circ K$, have been used to predict the ground state and its isolation for the other rare earths in $LaAl_2$. It is found that the observed depression in T_c can be explained in terms of the AG theory when the predicted isolation is larger than about $12^\circ K$, that is for Tm, Er, Ho and Sm in $LaAl_2$ (and for Er in Thorium). The Heisenberg Exchange Interaction $-J_{eff}(g_J-1)\underline{J}.\underline{s}$ between the degenerate ground state levels and the conduction electrons has been used to give a spin-flip scattering cross section $1/\tau_s$ by simply calculating the matrix elements of the operator $\underline{J}.\underline{s}$ between these levels. Exact agreement with T_c measurements is obtained with an overall variation in J_{eff} of only 15% from Sm, through Gd, to Tm, the magnitude of J_{eff} being .084eV for Gd. For the elements at the beginning of the series, Pr amd Nd, a smooth increase in J_{eff}, probably associated with the increased 4f shell radius, and, for Pr, a

larger value of $|C_4|$ are required.

However, in the two cases Dy and Tb, where the predicted ground state isolations are both approximately $4^{\circ}K$, this simple picture is inadequate; although T_c for $La_{1-x}Tb_xAl_2$ follows the AG theoretical curve from $3.2^{\circ}K$ to $1.2^{\circ}K$. At the moment this could be explained in three possible ways which could be distinguished by susceptibility measurements on $La_{1-x}Tb_xAl_2$ and further T_c measurements on the Dy system, these are:

(1) The ground state isolation in Tb is $0.6^{\circ}K$ or less and that in Dy is $\leqslant 1.5^{\circ}K$.

(2) J'_{eff} ($J'_{eff} = J_{eff}/J_{eff}(Gd)$) values of at least 1.7 occur for Tb and Dy, and the levels are in fact well isolated. For Tb this would also require a magnetic $\Gamma_5^{(1)}$ level lowest and C_4/C_6 would therefore have to be a factor of two smaller.

(3) The simple theory used here, including inelastic scattering between crystal field levels is invalid when crystal field splittings $\sim 3.2\ ^{\circ}K$ (T_c for $LaAl_2$) occur. Even though a singlet state has an average value of J_z, $\langle J_z \rangle = 0$, there is still a finite probability of observing a non-zero J_z. That is, there are still fluctuations in the magnetic moment which only average to zero over times larger than $\hbar/kT_G$ where T_G is the ground state

isolation (^{o}K). When $T_G \sim T_{co}$ it is probable that the lifetime of these fluctuations should be allowed for.

Until more measurements are made further speculation is not very useful but explanation (3) seems the most likely. In addition it would also explain the residual depression in T_c observed for singlet ground states by Bucher et al and (probably) the absence up to now of any observable departures from AG in the T_c vs concentration plots due to crystal field splittings.

2. Crystal Field Effects

It is felt that the existence of a $J_{eff} \sim 0.1$ eV ($\simeq 1200^{o}$K) in the metallic state does support the view that the crystal field potential arises from the electrostatic repulsion between the conduction electrons of the host metal and the 4f ion core.

For

$$J_{eff}(\underline{k},\underline{k}) = \int \psi^{*}_{\underline{k}\uparrow}(\underline{r}_1)\, \psi^{*}_{4f\uparrow}(\underline{r}_2)\, \frac{e^2}{r_{12}}\, \psi_{\underline{k}\uparrow}(\underline{r}_2)\psi_{4f\uparrow}(\underline{r}_1)\, .\, d\tau_{12}$$

where $\psi_{\underline{k}\uparrow}$ is a conduction electron wavefunction (wave vector

$\underline{k}$,spin up) and $\Psi_{4f\uparrow}$ is a one electron 4f wave function. J_{eff} is known from T_c measurements to be ~ 0.1 eV/atom if $k \simeq k_F$, that is $J_{eff} \sim 1200^{\circ}K$. By analogy with the free ion case one expects associated energy terms such as:

$$V(\underline{k},\underline{k}) = \int |\Psi_{\underline{k}}(\underline{r}_1)|^2 \frac{e^2}{r_{12}} |\Psi_{4f}(\underline{r}_2)|^2 \, d\tau_{12}$$

to be one or two orders of magnitude larger.

In a metal (a) such terms will be strongly reduced by screening and (b) the 4^{th} and 6^{th} order contributions to the potential will be even smaller. Nevertheless this will still be equivalent to an electrostatic potential of cubic symmetry and of sufficient magnitude to give rise to the observed crystal field energies. Moreover, to the extent that the maximum value of $|\Psi_k|^2$ tends to be nearer the neighbouring positive charges, the electronic coulomb repulsion will give the opposite sign to, and larger parameters than, the point charge crystal field model, as found by experiment. This is very similar to the proposal of Williams and Hirst, (53) (WH), in their case they consider the Ψ_k's to be first perturbed by the impurity potential to give the correct screening charge (in the form of a 5d virtual level) which then interacts with the 4f level via the

interelectronic coulomb repulsion. This repulsion was estimated by them from the $4f^n$-5d repulsion in free rare earth ions. When the rare earth ion constitutes a large perturbation (as for a trivalent rare earth ion in Ag or Au) this is probably the best description. However when the rare earth ion replaces La it only constitutes a very small perturbation. Therefore the screening charge envisaged by WH is now replaced by the appropriate (possibly d-like) band of conduction electrons and the former description is more apt.

On this basis one would expect the crystal field parameters in La based alloys to be more constant along the series than in Ag and Au hostmetals, at least when J_{eff} is constant. It has already been noted that for both sorts of system crystal field parameters of about the same magnitude are observed experimentally.

Similar ideas can also be used to give a qualitative explanation of the effect of covalent mixing. It is known from general considerations of the Pauli principle that antiparallel electron spin alignment corresponds to a spatial electron distribution which is symmetric in the electron co-ordinates. Such a distribution maxmimises the total electron density in a certain region in space. If this is also a region of large attractive potential

(as in the H_2 molecule) the energy gained is sufficient to overcome the electron-electron repulsion, and covalent binding, associated with antiparallel electron spin alignment, results.

Similarly therefore, if the 4f electron - conduction electron mixing is sufficient to overcome their coulomb repulsion and give $J_{eff} < 0$ (as for Ce^{+++} in $LaAl_2$), the 4f charge distribution will tend to have maximum overlap with the conduction electrons and be pulled towards the nearby positive ions. Therefore, to the extent that s-f mixing can be represented by an electrostatic potential, it will give the opposite sign to the electron-electron repulsion case and agree with the predictions of the point charge model. This is a possible qualitative explanation of the change in sign of C_4 from Tm^{+++} and Pr^{+++} to Ce^{+++} in $La Al_2$ which has been deduced from the T_c and susceptibility measurements and is apparently correlated with the change in sign of J_{eff} for Ce^{+++}.

CHAPTER 5

DILUTE ALLOYS CONTAINING 3d TRANSITION ELEMENTS

5.1 Introduction

Accurate measurements on aluminium alloys containing less that 1 at. % of 3d transition elements have been made in this laboratory by Caplin and Rizzuto (98). Below $4.2^{\circ}K$ the resistivity of AlMn and AlCr alloys exhibited a small variation, proportional to T^2. This has now been associated with the occurrence of spin fluctuations on the impurity site, even though there is, on average, no magnetic moment. Measurements of $H_c(T)$ between $1^{\circ}K$ and $0.35^{\circ}K$ have been made on dilute AlT alloys (T=Mn, Cr, Zn) for the following reasons:

(1) It was hoped that the varying spin-flip scattering cross-section, indicated by the temperature dependent magnetic resistivity, would be revealed as departures of $H_c(T)$ from the BCS form.

(2) More mundane, but equally weighty, good single phase, homogeneous specimens were readily available, the same ones on which resistance measurements and T_c measurements (21) had been made.

At the time we intended to make $H_c(T)$ measurements on a series of thorium-based rare earth alloys, also having $T_c \sim 1^oK$, and this provided a convenient means of testing the apparatus.

As mentioned in chapter 2 a paper published by Zuckermann and Kiwi (27) after these measurements were made, showed theoretically that, within the model of Ratto and Blandin (11), no significant departures from BCS theory were expected in $H_c(T)$, apart from a small increase in H_o^2/T_c^2 associated with the increased density of states at the fermi level. This increase is associated with the virtual bound state and even for the most concentrated alloy used here, Al 0.1 at. % Mn, for which the density of states of the virtual bound state has its maximum at the fermi level, an increase of only 0.3% in γ is expected for a virtual bound state halfwidth, Γ, of 1 eV. However, these authors did find that anomalous tunnelling characteristics and even gaplessness should occur at low reduced temperatures.

To the writer's knowledge the thermodynamic properties have not yet been calculated for a model in which spin fluctuations are considered.

Another transition metal impurity system studied in this laboratory is the ε Cu Zn phase containing approximately 0.1 %

Fe impurity. This was first investigated by Waszink and more recently resistance and susceptibility measurements have been made by Caplin (111). The results indicate that there is a small ($\sim$1 Bohr magneton, μ_B) localised moment on the Fe site, its magnitude falls smoothly from about $1.4\mu_B$ to less than $0.3\mu_B$, as the composition of the ε Cu-Zn host matrix is altered from 21 at. % to 14 at. % Cu. The magnitude of the Kondo 'lnT' term in the resistance and the slope of the χ vs 1/T plot (Curie's Law is obeyed) are both consistent with such a moment. It would have been interesting to see the effect of this small moment on the superconducting transition temperature if ε Cu-Zn were a superconductor. For this reason attempts have been made to cool an ε CuZn(15 at % Cu) alloy using an adiabatic demagnetisation cryostat which will be briefly described at the end of this chapter.

I CRITICAL FIELD MEASUREMENTS ON AlT ALLOYS

5.2 Experimental Details

1. Measurement of H_c

The specimens were in the form of $\frac{1}{2}$ mm diameter wires about 2 cms long. Several pieces of each specimen were used and they were electrically insulated from each other with greased tissue paper. The transition of each one could in fact be distinguished and enabled a limit to the homogeneity to be found. For example the five pieces of Al .023 at. % Mn used all had the same concentration to within 1.5%.

In order to dispense with an unreliable copper cone joint and to accommodate the maximum number of specimens, four in all, on each run in the present cryostat, He^3 exchange gas was not used. This turned out to be unwise. Instead, as shown in Fig. 5.1, the specimens rested in $\frac{1}{4}$" deep holes, containing Apiezon 'N' grease, in a copper block and were clamped at that end with copper grub screws. This copper block was in turn screwed to the copper base of the He^3 pot.

The four pick up coils (each of 10,000 turns of 48 s.w.g. enamelled copper wire) and another, wound in series opposition,

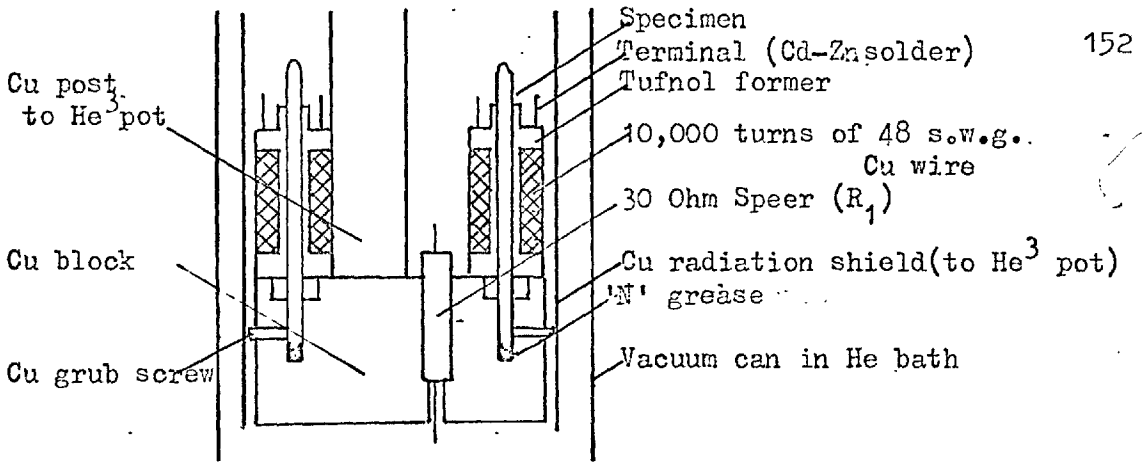

Specimen holder and pick-up coils

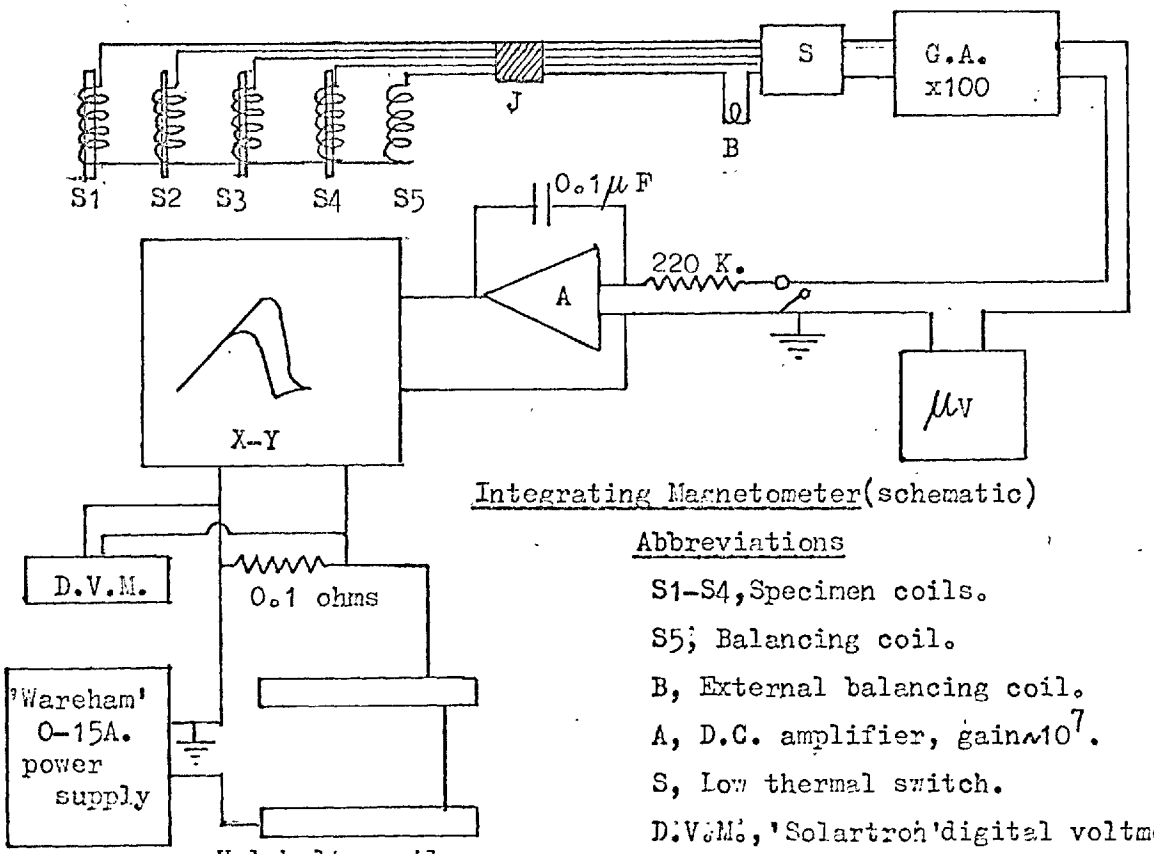

Integrating Magnetometer(schematic)

Abbreviations

S1-S4, Specimen coils.

S5; Balancing coil.

B, External balancing coil.

A, D.C. amplifier, gain~10^7.

S, Low thermal switch.

D.V.M., 'Solartron'digital voltmeter.

μV, Microvolt potentiometer.

J, Manganin-copper wire junction in cryostat.

G.A., Galvanometer amplifier, frequency response 0-14c/s, output drift ≃ 1μV/min.

FIG. 5.1 Apparatus used for $H_c(T)$ measurements on Al alloys.

could be connected in turn to the galvanometer amplifier and integrating magnetometer of Jones and Park (7). These coils were balanced with the series opposition coil at room temperature to within 100 turn cm^2, the remaining off balance signal could be compensated out during the run, when the specimens were normal, by rotating a small external bucking coil in the applied magnetic field.

The magnetisation curve could be plotted out at each temperature on an X-Y recorder as the external field was slowly swept up electronically. A fuller description of this system, which has been used by Jones and Park for sensitive measurements on the surface sheath of type I-II superconductors, is given in reference (7).

In practice, for accurate H_c measurements, the offset facility of the recorder was used to expand the sharp transition at H_c along the magnetic field (X) axis. The external field was provided by a pair of Helmholtz coils of 14 cm radius and was uniform to within 0.3 % over the experimental volume.

If was found that the sweep rate had to be extremely low, about 1.0 gauss per minute, otherwise the heat of magnetisation ($\sim$25 ergs), absorbed when the specimen started to go normal, cooled

the specimen and too high a value of H_c was obtained. The point at which the specimen became completely normal (point A in Fig. 5.2) was more sharply defined than the point where the transition first began, so this had to be used to define H_c. The slow sweep rates which had to be used made the measurements rather tedious. An approximate value of $H_c(T)$ was found with a faster sweep rate and this was then reduced to 1 gauss/minute just for the transition. The comparatively poor thermal contact between the specimens and the He^3 pot was responsible for this effect but it was aggravated by the very sharp (0.7 gauss in 100 gauss) transition at H_c..

2. Thermal contact measurements

Neglecting eddy currents in the normal regions of the specimen, the measured 'sweep rate effect' referred to above gives a value of 20 millidegrees K/microwatt (mdeg/μW) for the thermal resistance between the specimens and the He^3 pot. Measurements of thermal contact were also made using an unclamped aluminium specimen resting in 'N' grease on a similar copper block. A manganin heater, non-inductively wound on the specimen, was heated with a direct current of a few hundred microamps. At $0.4^{\circ}K$

the thermal resistance to the copper block measured by this method was determined to be 35 md/μW, in reasonable agreement with the previous value. This resistance fell by a factor of 10 when He^3 gas at a pressure of .02mm Hg (at 1^oK) was introduced into the specimen chamber.

Thus it can be seen that the use of exchange gas would have made the measurements easier in the long run by allowing faster sweep speeds to be used. Even with a resistance of 35 md/μW to the He^3 pot the calculated thermal time constant of the Al specimen at 0.4^oK was less than one second.

It was also established that the copper block was in adequate (1 md/μW resistance) thermal contact to the He^3 pot at 0.7^oK . Also the specimen temperature followed that of the block to within 1 md. when a power of 3μW was dissipated on the block. This was adequate since the total heat leak into the system, most of which would go directly to the He^3 pot, was 10μW at the lowest temperature.

3. Other experimental precautions

The earth's magnetic field was balanced out to .01 gauss (g) over the experimental volume by three pairs of coils. This was

checked on occasion by measuring $H_c(T)$, near T_c, in the reverse direction. The dilute specimens had a remanent moment (trapped flux) in zero field of less than 5% of H_c. Such a moment, it was calculated, would give a spurious magnetic field on the neighbouring specimens of .01 gauss at the most. Finally it was calculated that, if one specimen went superconducting, the upper limit to the field increase at the neighbouring specimen was .05 %.

4. Temperature measurement

Two 30 ohm Speer carbon resistors, one with the ceramic insulation ground away, were used as secondary thermometers and for the measurement of thermal gradients. Above 0.7°K the 1962 He^3 vapour pressure temperature scale (99) was used as a primary thermometer, the pressure being measured with an oil manometer connected to the pumping tube. No significant pressure gradients occurred along this tube, He^3 temperatures obtained when pumping were consistent with those obtained when the pump was shut off, as in both cases the same resistance-temperature curve was obtained for the 30 ohm Speer resistor (to within 1 md). Although temperatures down to 0.55°K could be measured this way and, in fact,

readings were taken, it was decided that the superconducting aluminium thermometer was more reliable below 0.7°K. The deviation between the two methods was 1 md at 0.7°K rising to 4 md at 0.55°K (the temperatures from the He^3 vapour pressure being lower) and probably arose from the Kapitza boundary resistance between the He^3 liquid and the floor of the copper pot. It was calculated that this gave a temperature drop of 2 md at 0.55°K, by using the measured heat leak into the He^3 pot of 10 μW. The area of contact was taken to be 2 cm^2 and the value of the boundary resistance used was that quoted by Rose-Innes (100) of $130/T^2$ (deg/cm^2/Watt).

To calibrate the aluminium thermometer the values of H_c above 0.7°K, measured by the same method as for the Al alloys, were used to find H_o. Temperatures below 0.7°K were then found from the measured values of H_c. In practice all the results were calculated in terms of I_c, the current through the coils corresponding to a field H_c. Two methods were used to find H_o (I_o) and hence T.

(1) I_o was chosen so that the usual deviation function $D(h)=1-h-t^2$ agreed with the data of Mapother and Harris (101) above 0.7°K. Here h and t are the reduced critical fields and temperatures.

$$t = T/T_c \text{ and } h = H_c/H_o = I_c/I_o$$

Mapother and Harris in turn based their data (for polycrystalline 6N Al) on temperatures found from the susceptibility of a chrome methylamine alum salt pill below 1.1^oK.

(2) The procedure of Sheahen (102) was followed and $H_c(T)$ was fitted to the formula:

$$1-h-t^2 = D_o \sin \pi(1-t^2),$$

by the method of least squares, for $T \geq 0.7$, regarding H_o and D_o as adjustable parameters.

This formula was then used below 0.7^oK to find T from the measured $H_c(T)$ values.

Both methods gave the same value of D_o and H_o within the experimental errors and hence the same temperatures, to within 2 md, below 0.7^oK. In both cases the measured value of T_c, which was found by a least squares fit of H_c vs T^2 near T_c, was used.

This was $\underline{T_c = 1.179 \pm .001^oK}$, in agreement with Mapother's value of $\underline{1.179 \pm .003^oK}$.

The values of I_o and D_o were:

$$I_o = \underline{5.944 \pm .015 \text{ amps}}$$

$$D_o = \underline{0.041 \pm .001}$$

The Helmholtz coil pair was later calibrated using a 'Bell and Howell' gaussmeter model 620 to give a coil constant of 17.65 ± .08 gauss/amp. Hence H_o = 104.9 ± .6 gauss. This is also in excellent agreement with Mapother's value of 104.93 ± 0.2 gauss.

5. Temperature control

The temperature was controlled manually by using a needle valve to bleed a small quantity of He^3 gas into the inlet of the Edwards 2M4 diffusion pump. Hence its effective pumping speed could be finely controlled and the temperature maintained constant to within 2 md over a period of several minutes.

6. Secondary thermometer

The ½ Watt 30 ohm Speer resistance was measured using a 3 lead AC Wheatstone bridge, which was operated at 260 c/s, and a home-made phase sensitive detector. Typically the resistance was 350 ohms at 1.3°K rising to 1000 ohms at 0.35°K. The resistor used was not always reproducible from run to run, sometimes changes of up to 5% occurred, on other occasions the calibration curve was reproducible. Small measurement errors also resulted

from changes in the phase shift produced by the highly tuned detection system over a period of time. In addition the sensitivity of the detection system fell for resistances above 1000 ohms and spurious quadrature signals increased. All in all the detection system and the resistor were not satisfactory for accurate ($\sim$1 md) temperature measurements, so in most cases pure aluminium and aluminium alloy critical field measurements were made consecutively. The resistance thermometer was then only used to correct for small temperature drifts during measurements. It was adequate for this purpose and at the low power level of 1/200 ergs/second the discrimination at 0.35^{o}K was 0.5 md.

5.3 Results and Analysis

1. Magnetisation curves

Magnetisation curves for the Al and Al .023% Mn specimens are shown in Figs 5.2 and 5.3. There is no surface sheath above H_c and there is some supercooling in both cases. The supercooling transition is not as sharp as usual, probably because of the low thermal conductance to the He^3 pot. Similar curves were obtained for the AlCr and AlZn alloys measured.

According to the Gorkov-Goodman formula (chapter 2 equation 2.2) even the most concentrated Al 0.1% Mn alloy has κ=0.1

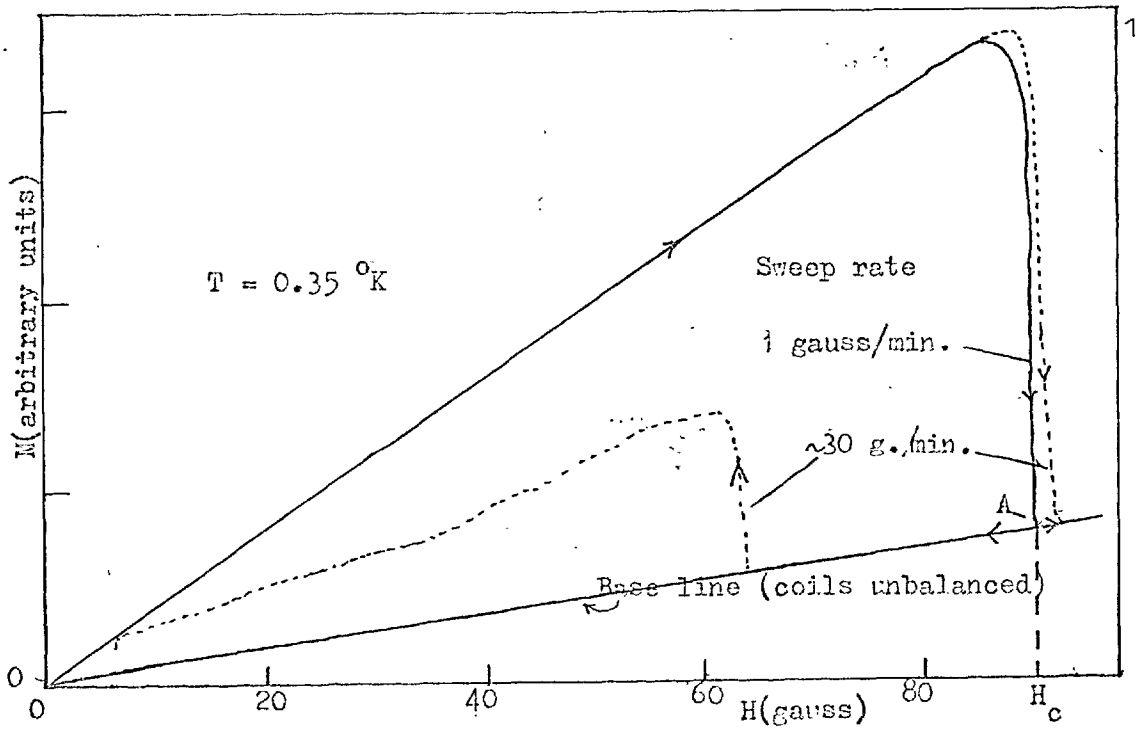

FIG. 5.2 M(H) curve for 5N Aluminium

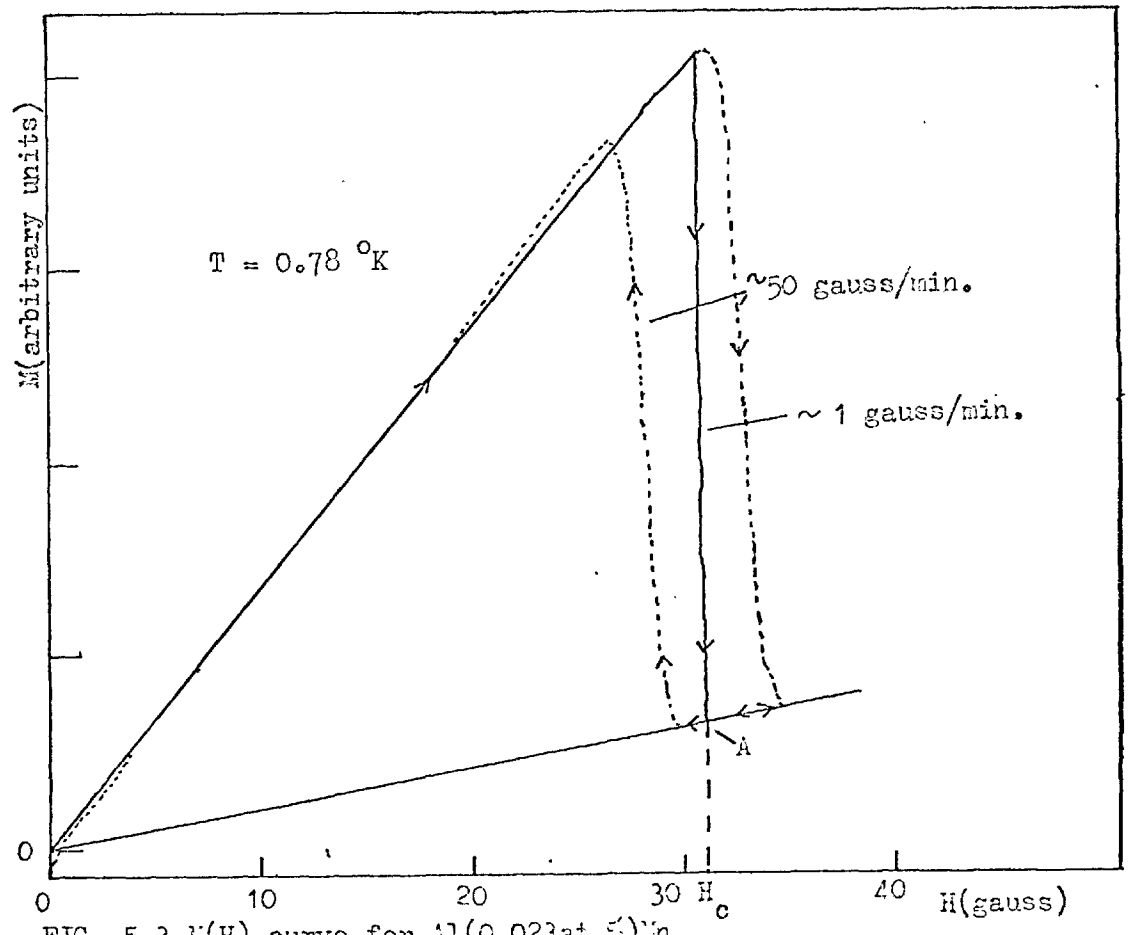

FIG. 5.3 M(H) curve for Al(0.023at.%)Mn

and should be type I. Unfortunately a detailed magnetisation curve was not kept for this alloy, it did show some supercooling but any possible tail associated with screening currents in the surface sheath would have been obscured by a combination of output voltage drift and imbalance of the detecting coils. It is just possible that the small amount of supercooling observed for this particular alloy was in fact hysteresis associated with the surface sheath.

2. Critical field measurements

Referring to Figs. 5.2 and 5.3, H_c was taken to correspond to the points marked A. In practice detailed magnetisation curves were not usually made, H_c was detected when the movement of the pen recorder in the y-direction suddenly slowed down, and the appropriate coil current was measured to 1 part in 104 using a standard 0.1 ohm resistor and a Solartron digital voltmeter.

The results are plotted in Figs. 5.4 to 5.9 in the form of $D(h) = 1-h-t^2$ vs t^2 curves.

To make these plots one needs to know both H_o and T_c. The latter quantity was found by least squares fitting H_c to T^2 for $t^2 \geqslant 0.9$ and extrapolating to $H_c=0$.

3. Methods of finding H_o

As discussed by Harris and Mapother (101), for reduced temperatures $t \leq 0.25$ the superconducting entropy $S_s(T)$ is negligible compared with that of the normal state $S_n(T)$.

The thermodynamic relation

$$S_n - S_s = \frac{-V_{mol}}{8\pi} \cdot \frac{d(H_c^2)}{dT}$$

therefore becomes

$$S_n = \gamma T = \frac{-V_{mol}}{8\pi} \quad \frac{d(H_c^2)}{dT}$$

Integrating:

$$H_c^2 = H_o^2 - \frac{4\pi}{V_{mol}} \cdot \gamma T^2$$

If data is available for sufficiently low temperatures then both H_o and γ (the coefficient of the electronic specific heat) can be found from a plot of H_c^2 vs T^2.

However, in this case the lowest values of t obtained were $\geqslant 0.3$ and some approximation for $S_s(T)$ has to be made to obtain H_o. One possible method would be to use the BCS form for $S_s(T)$ in the low temperature region (or equivalently the BCS numerical data for D(h)). It was shown by Sheahen (102) that for $t \geqslant 0.3$ the empirical formula:

$$1 - h - t^2 = .037 \sin\pi(1-t^2)$$

is equivalent to the BCS form of D(h) to within .001 in h. He also showed that nearly all experimental critical field measurements on superconductors can be adequately represented by the empirical formula: $1 - h - t^2 = D_o \sin \pi(1-t^2)$, with a suitable choice of D_o and H_o.

Furthermore, within the temperature range:

$$0.1 \leqslant t^2 \leqslant 0.2$$

that is $$0.31 \leqslant t \leqslant 0.44$$

which is just above the range where H_c^2 vs T^2 gives a straight line, it follows that the BCS theory (or Sheahen's approximation to it) becomes $h(t) = 1-(1+D_o\pi)t^2$, to within .003 in h.

Therefore in this limited temperature range H_o can also be obtained by extrapolation, this time by plotting H_c vs T^2 rather than H_c^2 vs T^2. The slope of the line is no longer simply related to γ ..

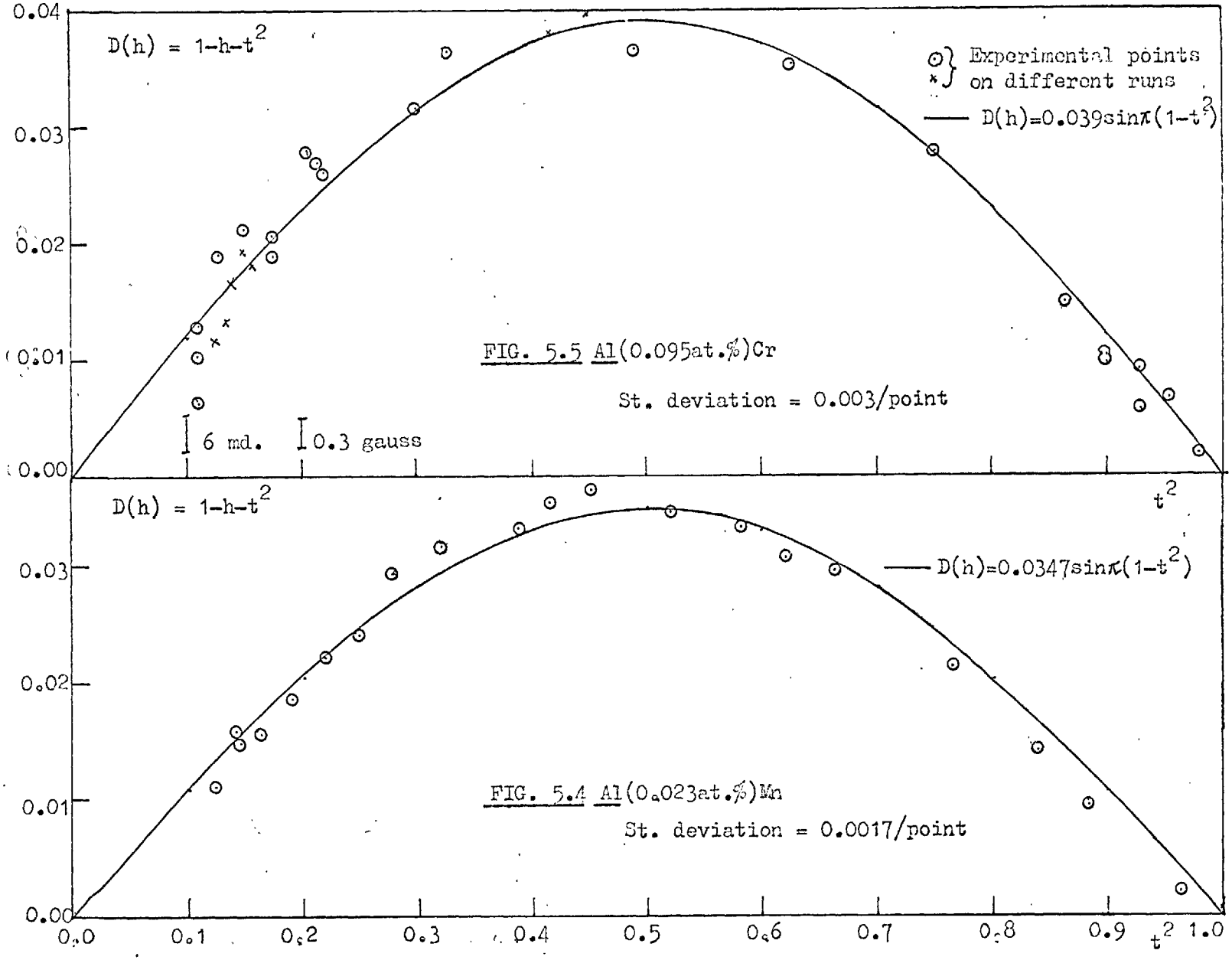

FIG. 5.5 Al(0.095at.%)Cr

St. deviation = 0.003/point

FIG. 5.4 Al(0.023at.%)Mn

St. deviation = 0.0017/point

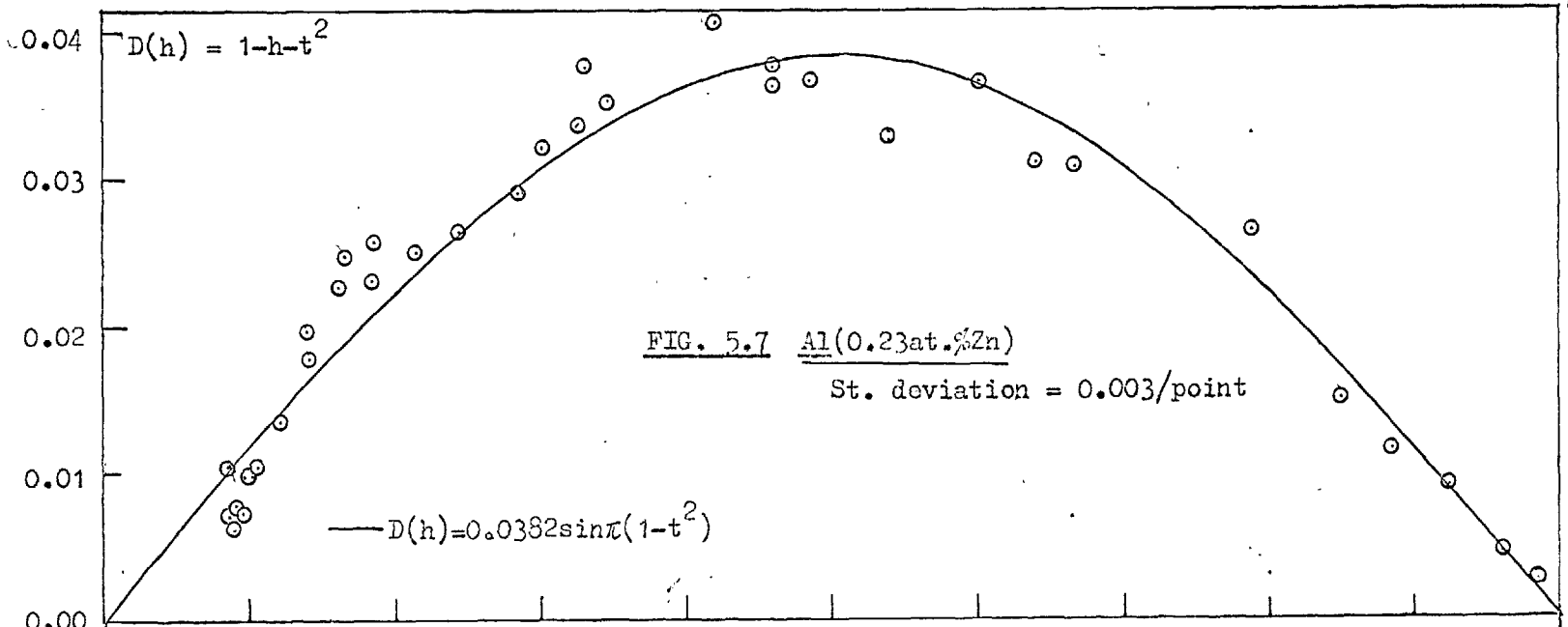

FIG. 5.7 Al(0.23at.%Zn)
St. deviation = 0.003/point

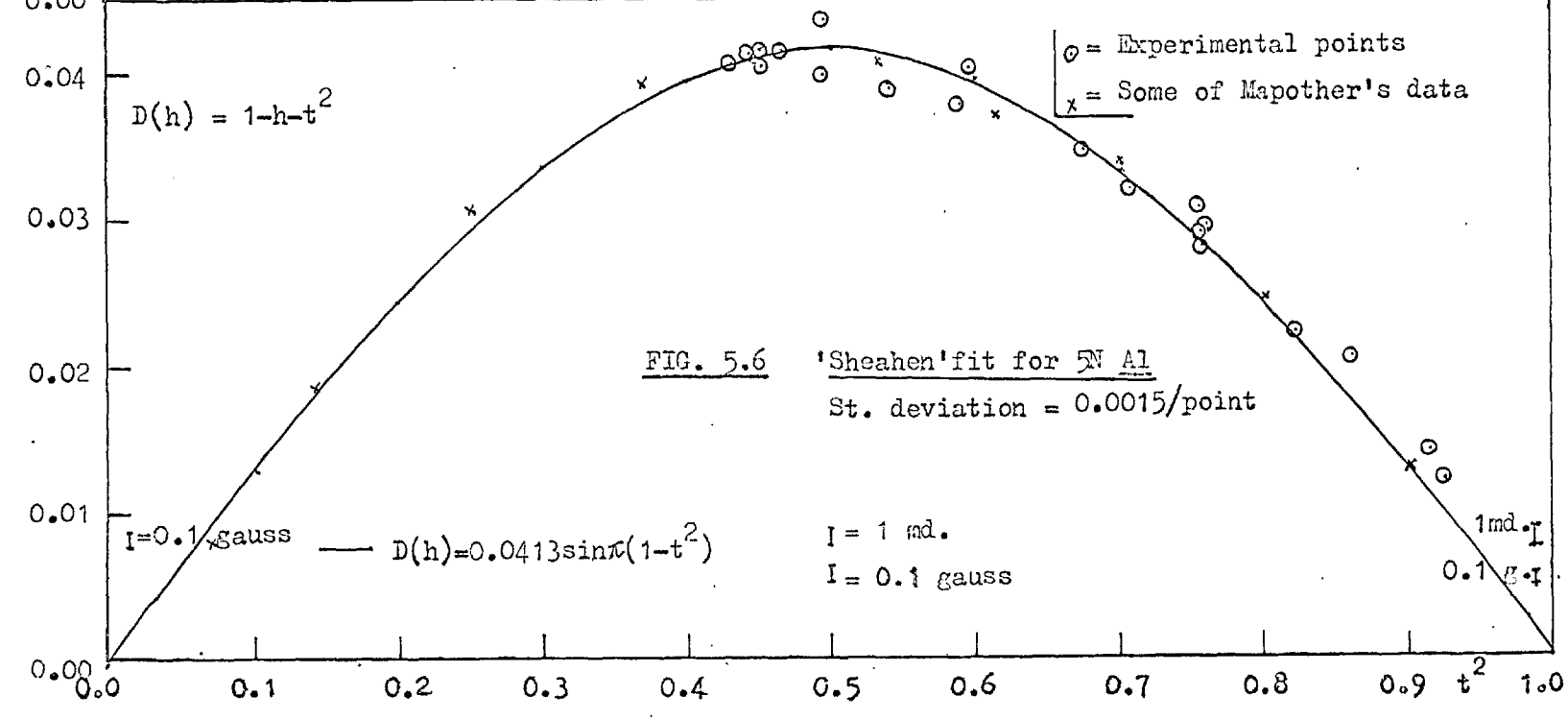

FIG. 5.6 'Sheahen'fit for 5N Al
St. deviation = 0.0015/point

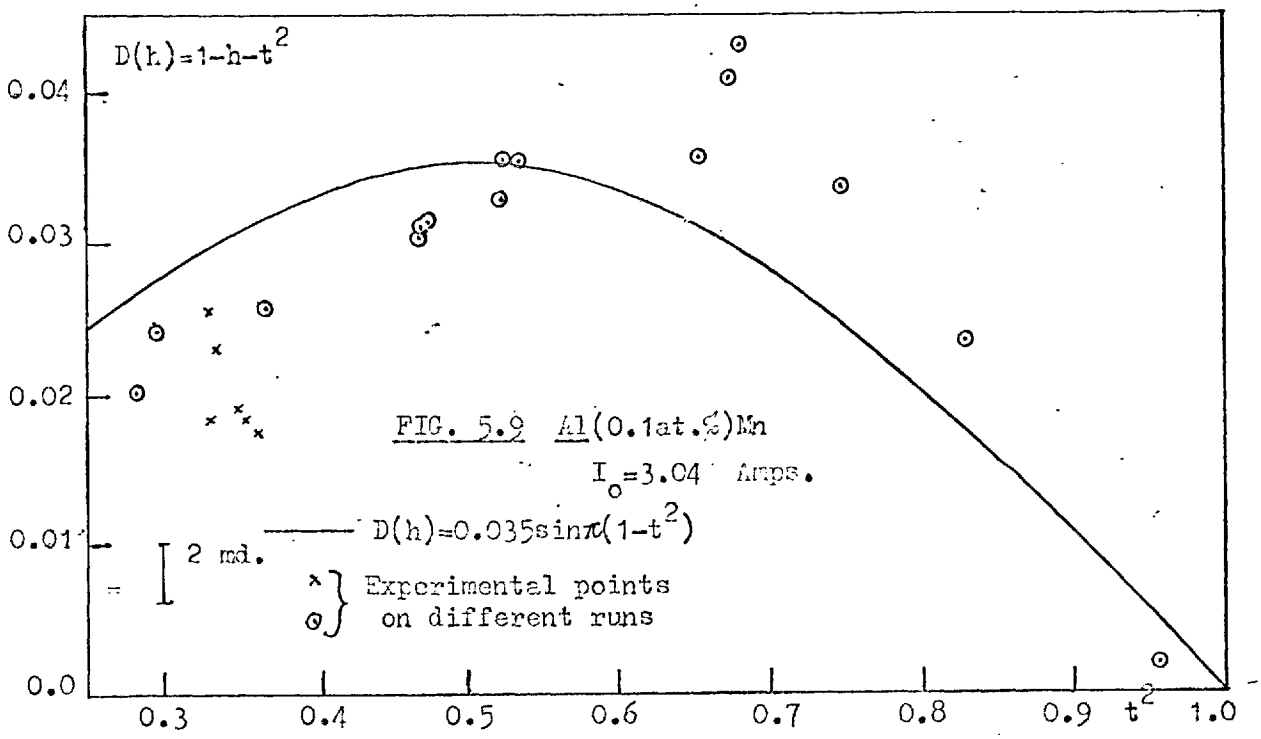

FIG. 5.9 Al(0.1at.%)Mn
I_o=3.04 Amps.

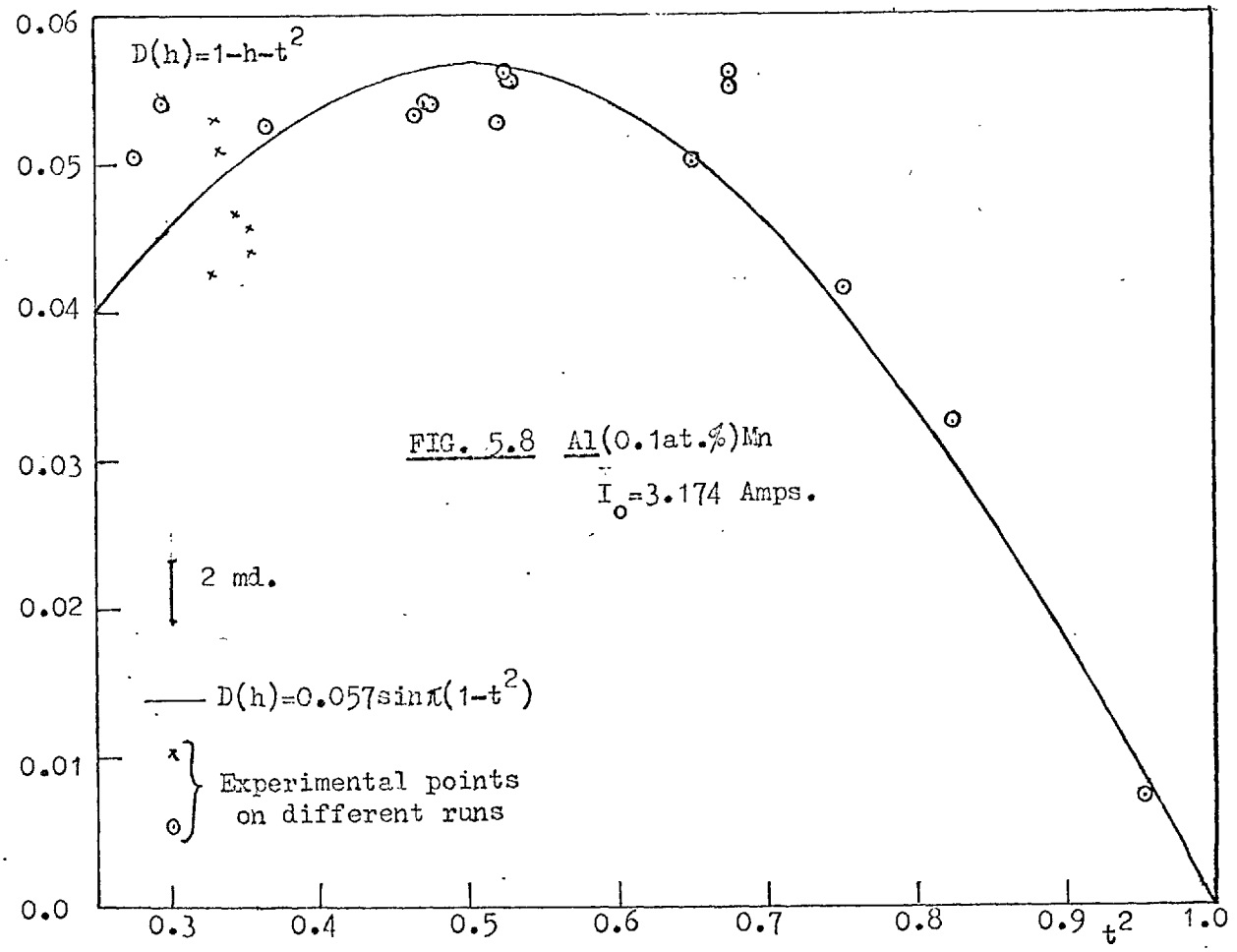

FIG. 5.8 Al(0.1at.%)Mn
I_o=3.174 Amps.

Specimen	T_c °K	Low Temperature Extrapolation $H_o^{(1)}$ (gauss)	'Sheahen' Fit $H_o^{(2)}$ (gauss)	% Increase in Ho^2/T_c^2 over Al	D_o	Resistance Ratio R4.2/R273	$\langle a^2 \rangle \times 10^{-2}$ Using Clem's theory	
							from D_o	from H_o^2/T_c^2
5N Al	1.179 ± .001	(104.9 ± .26*)	104.8 ± 0.4	0	.0413 ± .002	$< 5 \times 10^{-3}$	1.3 (from Hc)	1.2 (from T_c)
Al..023 at. % Mn (A)	.994 ± .001	90.9 ± .14	91.0 ± .12	5.8 ± .8	.0347 ± .0011	.074	1.8 ± .3	3.2 ± .4
Al 0.1 at. % Mn (B)	.592 ± .001	-	56.0 ± .4	12.8 ±2.2	.057 ± .005	.322	-	-
Al .095 at. % Cr (C)	.942 ± .001	86.2 ± .3	85.7 ± .14	5.0 ± .8	.039 ± .002	.337	0.8 ±0.7	2.5 ± .4
Al .23 at. % Zn (D)	1.149 ± .001	105.1 ±0.12	104.2 ± .12	4.2 ± .8	.0382 ± .0013	.14	1.5 ±1.0	2.8 ± .5

* Value obtained by fitting to Mapothers results above 0.7°K (NB the error given here is smaller than that given in the text because a systematic error in the gauss/amp ratio would not affect the relative values of H_o)

TABLE 5.1 Summary of $H_c(T)$ Data for Al and Al Alloys

With this in mind two methods were therefore used to find H_o.

(1) The data was fitted by least squares to the Sheahen formula $D(h) = D_o \sin \pi(1-t^2)$ over the whole temperature range. The standard deviations in D_o and H_o were also found by the usual method.

(2) For alloys with $T_c \simeq 1^oK$, H_c was fitted by least squares to the formula $H_c = H_o - AT^2$, by varying H_o and A, for $0.1 \leqslant t^2 \leqslant 0.2$.

The results for both methods are given in table 5.1.

5.4 Discussion of Results

1. Experimental errors

The estimated error in H_c was $\pm$ 0.1%, corresponding to the last figure on the digital voltmeter used for the measurement of current. That in the temperature was $\pm$ 1 md above 0.7^o, rising to $\pm$ 2 md at 0.35^oK as the superconducting thermometer became less sensitive. It can be seen from Figs. 5.4 to 5.9 that, especially for the low temperature points, in some cases the measured values of D(h) exhibit considerably more scatter that this, up to a factor of three more. This was partially due to the difficulty in holding the temperature constant for the long sweep times.

2. Values of H_o^2/T_c^2 and D_o obtained

Referring to table 5.1 it can be seen that the values of H_o found by both the methods described agree within the limits of error for alloys A and C. For alloy D(AlZn) there is a 1% difference, but from Fig. 5.7 for this alloy it can be seen that there is systematic departure from Sheahen's formula near t=0.4 which probably causes the discrepancy.

Ignoring the Al 0.1 at. % Mn alloy for the moment it can be seen from table 5.1 that all the values of H_o^2/T_c^2 are larger than that of pure aluminium by 5%. It was at first thought that this could be due to spin fluctuations and therefore the AlZn alloy was measured. This also had the same increase in H_o^2/T_c^2 indicating that the increase is probably a result of gap anisotropy in pure aluminium.

The results of Clem (16), for the change in the reduced quantity $H_o^2 = H_o^2/8\pi\gamma T_c^2$ on alloying, can be used to estimate $\langle a^2 \rangle$ the mean square anisotropy of the energy gap. Similarly his results can be used to find $\langle a^2 \rangle$ from the change in D_o. Both values of $\langle a^2 \rangle$ are listed in table 5.1 and unfortunately they do not agree.

The $\langle a^2 \rangle$ values obtained from H_o are consistent with $\langle a^2 \rangle = .028 \pm .004$. Those from D_o, with $\langle a^2 \rangle = .015 \pm .004$

Possible ways of accounting for this discrepancy are:

(1) There is also a mean free path effect on γ, increasing it by~2% for Zn, Mn and Cr impurities. Thus the correct value of $\langle a^2 \rangle$ is .015 ± .004 in agreement with Boato et al (21) and Mapother et al (101).

(2) The correct value of $\langle a^2 \rangle$ is .025 ± .003. This would be just consistent with all $\langle a^2 \rangle$ values except the one from D_o for AlCr. Although this would disagree with the results of Boato et al (21) (T_c measurements) and of Mapother et al (101) (H_c measurements for pure Al), in the first case only the quantity $\lambda_i \langle a^2 \rangle$ is found from T_c measurements. As mentioned in chapter 2, λ_i is an unknown parameter varying between 0.5 and 2.0 for different impurities; reducing all λ_i by a factor of two would again give agreement. As far as the critical field data of Mapother is concerned, it is possible that anisotropy is not the only cause of deviations from the BCS reduced field law in pure aluminium.

3. Conclusions for the alloys with $T_c \simeq 1^\circ K$

The critical fields $H_c(T)$ of three aluminium specimens AlMn, AlCr and AlZn, all with $T_c \simeq 1^\circ K$. have been measured to an accuracy of ± .003 in H_c/H_o down to $0.35^\circ K$. Within this

accuracy the alloys follow the BCS theory for a weak coupling superconductor. However, the values of H_o obtained are such that the quantity H_o^2/T_c^2 is 5.0 $\pm$.8% higher than for pure aluminium in all three cases. This is twice that expected from the theory of Clem using the accepted value for $\langle a^2 \rangle$ in pure aluminium obtained by T_c measurements on dilute Al alloys, and assuming that γ, the coefficient of the electronic specific heat, is the same for the alloys as for pure Al. The reason for this discrepancy is not known but despite this it is possible to say that, within the accuracy of the measurements, there is no difference in the $H_c(T)$ behaviour of the non-magnetic AlZn alloy, the non-magnetic alloy with short lifetime spin fluctuations AlCr and the non-magnetic alloy with longer lifetime spin fluctuations AlMn.

4. The Al 0.1 at. % Mn Alloy

Data was only available for this alloy above t=0.55, hence only the method of Sheahen could be used to find H_o. There is considerable deviation from BCS in both H_o and D_o obtained by this method, which cannot be caused by anisotropy.

In Figures 5.8 and 5.9 the D(h) curves are plotted for two values of H_o :

(1) H_o as determined by the Sheahen procedure, using the least squares program. For this case one then has:

$$I_o = 3.173 \pm .023 \text{ amps}$$

$$D_o = .057 \pm .0044$$

and

$$\delta(H_o^2/T_c^2) = +13\%$$

($\delta(H_o^2/T_c^2)$ is the increase in H_o^2/T_c^2 over the pure aluminium value)

(2) H_o is chosen so that $D_o = .035$, as for the more dilute AlMn alloy. The best fit with this constraint is $I_o = 3.04$ amps.

Hence

$$\delta(H_o^2/T_c^2) = +4.3\%$$

Although (1) is a better fit than (2), as one would expect from the calculated errors in D_o and H_o, there is considerable scatter in the data. It is possible in this case that the data is such a bad fit to the formula that the calculated errors are invalid. Therefore, on the basis of this one set of measurements, no firm conclusions can be drawn.

II THE DEMAGNETISATION CRYOSTAT

5.5 Introduction

The He^3 cryostat which has been used for the measurements reported in this thesis was designed with a large specimen chamber, 3 cms diameter and 20 cms long, and a wide helium dewar, in order to extend the temperature range down to 20 millidegrees K (md) or so by adding an adiabatic demagnetisation stage.

There are several advantages in having a lower initial temperature for adiabatic demagnetisation:

(1) For a paramagnet with a magnetic moment of 3 Bohr magnetons (μ_B) per magnetic atom , a field of 6 kilogauss at 0.4^oK produces the same entropy reduction (about a factor of 2) as 18 kg. at 1.2^oK.

(2) The heat leak into the system is much smaller, being proportional to T_i^2 (the initial temperature is T_i) for electronic conduction and T_i^4 for phonon conduction.

(3) Calibration of the thermometer (usually a cerium magnesium nitrate (CMN) thermometer) is easier, since the He^3 vapour pressure can be used.

Since 1963 when this project was first considered the position has altered in two respects. In the first case high

field superconducting solenoids are commercially available, negating (1) above. Secondly, and much more relevant, He^3-He^4 dilution refrigerators, which can maintain a temperature of about 30 md in the presence of a heat leak of about 1 μW, are now commercially available.

Several of the disadvantages of the present He^3 cryostat, for operation between 1.3°K and 0.4°K, for instance the difficulty in condensing He^3 and the relatively large (4 litres) quantity of liquid helium used per run, are a direct result of this change in design.

The demagnetisation system has been made to work despite this, although no new superconductors have been discovered. The system is briefly described here, mainly for the benefit of future users of the apparatus.

5.6 Design Criteria

Adiabatic demagnetisation is a well established technique and detailed accounts and further references are given in the books of Rose-Innes (100), White (103) and of Hoare, Jackson and Kurti (104). The design of the present system was based to some extent on the more recent work by Wheatley and co-workers (105-6).

The essential features of any refrigerating system are:

(1) the quasi-isothermal production of a more ordered state at one temperature, either continuously, for example the separation of He^3 and He^4 in the still of a dilution refrigerator, or once, for example, by magnetising a paramagnetic salt or condensing He^3 liquid.

(2) Thermal isolation of the ordered state.

(3) Production of a less ordered state, for example by mixing liquid He^3 and He^4, removal of the magnetising field or evaporation of He^3 liquid. Thus, since the total entropy is conserved in the absence of heat flux, the temperature of the system falls.

Since (1) always involves the production of heat, to achieve both (1) and (2) some form of heat switch is needed. The two methods commonly used in adiabatic demagnetisation are exchange gas and a superconducting heat switch. The original plan was to use a small quantity of He^3 exchange gas and to pump it away just before demagnetisation, relying on the cooled salt pill to absorb any remanent gas. However there are well-known difficulties in removing exchange gas from a very low temperature

($\sim 0.4^{o}K$) space, since the walls of the chamber outgas very slowly and because pumping speeds are very low for slow moving atoms. This was even more serious in our case because the narrow, 4 mm diameter, pumping tube also carried the measuring wires to the specimen chamber. For these reasons a superconducting heat switch made of 6 N lead wire was used. This was operated by the fringing field of the superconducting solenoid which provided the field for magnetisation..

1. Choice of Paramagnetic Salt

Basically one requires a salt whose magnetic entropy is increasing smoothly over the temperature range (T) of interest, this usually dominates all other entropy contributions below $1^{o}K$. This can be achieved by using a paramagnet with magnetic crystal field levels having energy differences $\Delta \sim kT$, by using a paramagnet which orders magnetically just below the range T, or by retaining a lower magnetic field so that level splittings in the field are $\sim kT$.

The first method is preferable since the entropy changes over a temperature interval Δ/k, giving an anomalously high 'Schottky' specific heat in that range, whereas long range order sets in over

a very limited temperature range. It is also difficult to make other measurements, for example susceptibility (for temperature measurements), in the proximity of a magnetically ordered salt, or in a magnetic field.

Subject to the restriction that the ordering temperature is not in the range of interest, it is usually better to have as large a concentration of magnetic ions as possible in the salt (except for a possible heat switch limitation mentioned later), and the magnetic moment per ion must be large enough to allow appreciable entropy reduction (about a factor of 2) at the magnetising temperature by the available magnetic field.

The salts considered were the commonly used hydrated ones, among them ferric ammonium alum, chrome potash alum (CPA) and cerium ethyl sulphate. It was decided by Dr. I. P. Morton of this laboratory that CPA, with a ground state isolation of .09^{o}K due to crystal field splitting, and an ordering temperature of 12 md, Hoare Jackson & Kurti (104), best satisfied the above requirements. All the above salts have the practical disadvantage that they lose their water of crystallisation over a period of time at room temperature and their magnetic properties change. CPA is no exception to this and, despite periodic coatings with General Electric (GE)

varnish, after several runs the CPA degenerated into an amorphous mauve powder.

It is perhaps worth mentioning briefly in this connection that the recent experiments on gold-based rare earth alloys in this laboratory (referred to in chapter 4), showing that interactions between rare earth ions are smaller than originally thought, raise the interesting possibility that these alloys could be used for adiabatic demagnetisation. Initial calculations show that for the 0.3% AuGd alloy mentioned previously (interaction temperature $|\Theta| < 50$ md) the magnetic entropy/cc is about 1/10 that of CPA at high temperatures. The thermal conductivity, which, together with the volume over which the magnetising field can be generated, limits the allowed volume of the paramagnetic material, is about 1,000 times larger in such an alloy than in CPA at 20 md. Therefore such an arrangement, using Au Ho say, with closely spaced, crystalline field split levels, may be useful in laboratories where 10 kg. magnetic fields are already available, for small scale experiments which do not justify the purchase of a dilution refrigerator. A superconducting heat switch could be soldered directly to the alloy and metallic specimens could be clamped firmly to it. Providing the magnetising field were reduced reasonably slowly

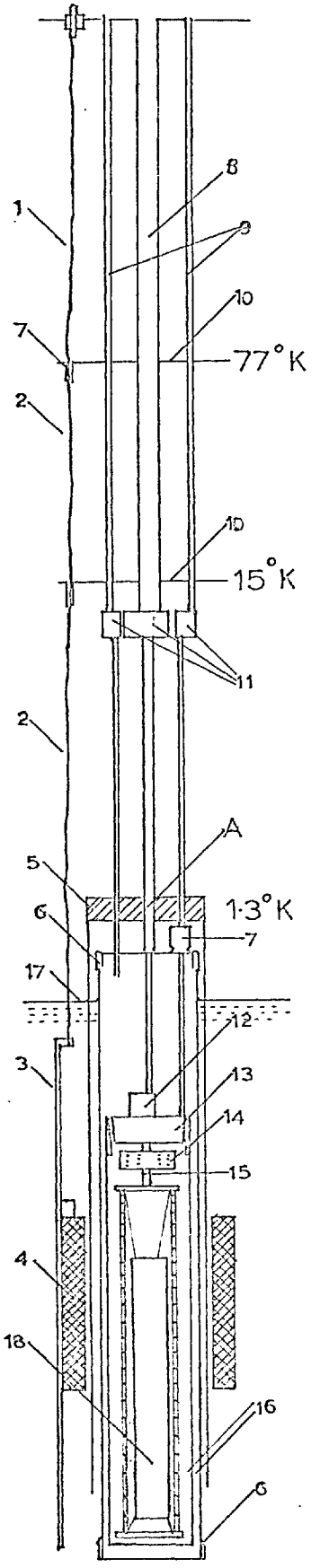

FIG. 5.10 The Demagnetisation Cryostat (scale 1:3)

Key

1. 3 x 28 s.w.g. copper wires
2. 1 x 26 s.w.g. copper wire
3. 1 x 12 s.w.g. enamelled copper wire
4. Superconducting solenoid
5. Demountable copper block holding 26 s.w.g. copper wires for thermal contact to He bath
6. Cd-Bi solder joint
7. Thermal anchor
8. 1 cm diam. He^3 pumping tube (Cu-Ni)
9. 4 mm diam. pumping tubes
10. Copper radiation shields
11. Radiation traps
12. He^3 pot
13. Copper cone joint
14. Terminal block
15. Stud to hold saltpill assembly
16. Vacuum spaces
17. Typical He level
18. Salt pill assembly (see Fig. 5.11)

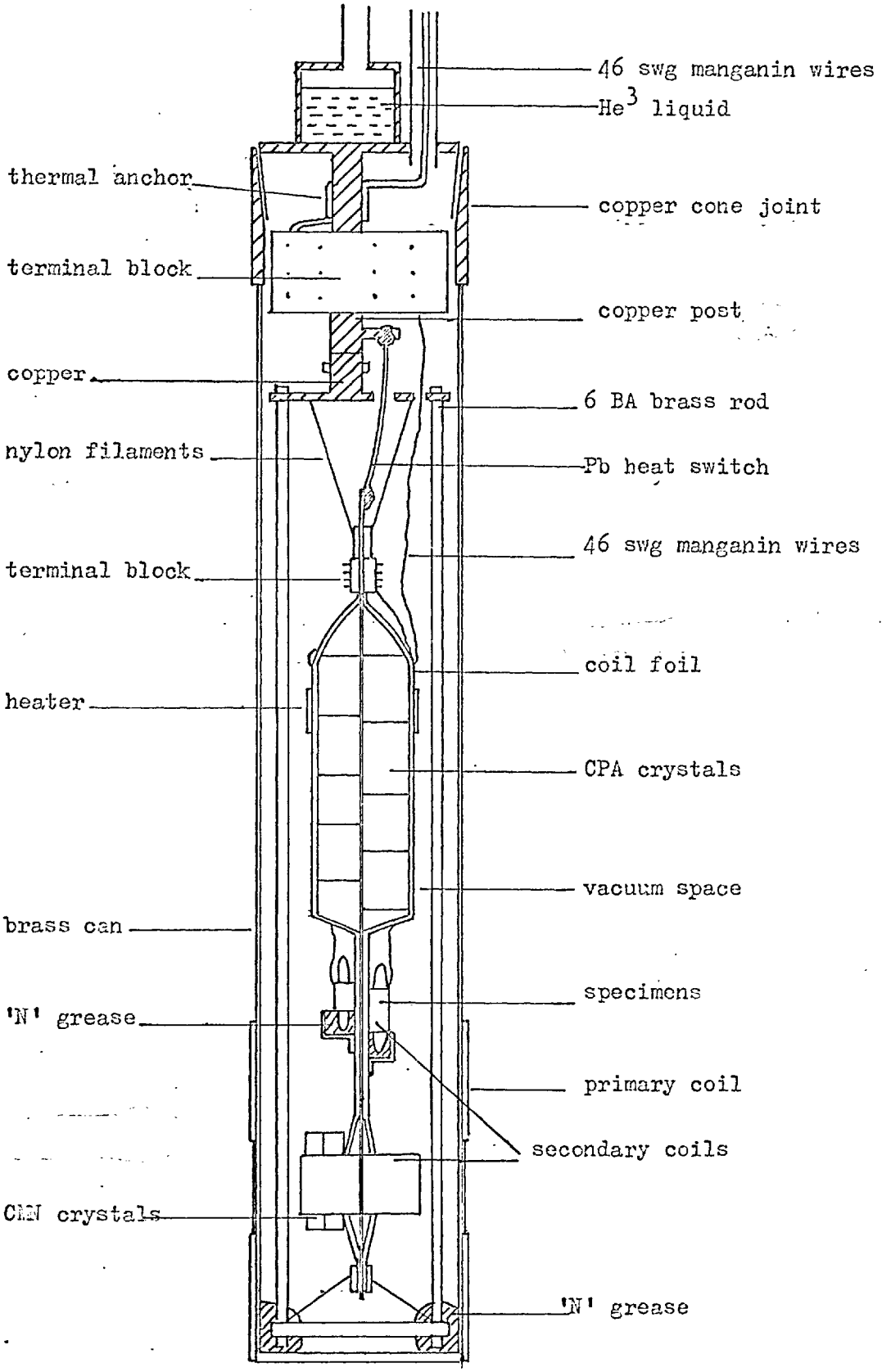

FIG. 5.11 The salt pill assembly (scale drawing)

(1 kilogauss/min) there would be no significant eddy current heating. In fact, according to ref. (58), the ThGd system (another system where the interactions are extremely weak) has already been used for this purpose, although the disadvantages associated with magnetic ordering presumably arise in this case.

5.7 Experimental details

The general overall arrangement used is shown in Fig. 5.10 and a more detailed diagram of the salt pill assembly is shown in Fig. 5.11.

1. The magnetising field

This field was obtained with a home-wound superconducting solenoid wound with Nb 25% Zr copper plated wire, which produced 770 gauss/amp at its centre over a 4 cm diameter bore. Because it was uniformly wound with a length/diameter ratio of only 2 the field was not uniform axially but this did not give significant temperature gradients in the CPA. The copper current leads to the superconducting solenoid had to be carefully designed, a substantial increase in the heat leak into the main helium bath could not be tolerated because this would have prevented the He^3 from condensing at the maximum backing pressure (3.5 cms Hg) of the 2M4

Edwards diffusion pump. In fact this pressure could be increased to 3.9 cms Hg for short periods by running the 2M4 at 245 volts. off a mains transformer. Even so, this He^3 vapour pressure corresponds to a temperature of 1.45°K and the yoke of 26 s.w.g. copper wires dangling into the helium bath was later provided, so that the point A (Fig. 5.10), where the He^3 condenses and drips down into the He^3 pot, was at about 1.3°K. Hence the latent heat of condensation of the He^3 could be removed in a reasonable time (30 to 60 minutes). The 12 s.w.g. copper wires shown in Fig. 5.10 were used to take the heat coming down the solenoid current leads directly into the helium bath rather than via A. Attempts were made to optimise the leads according to the paper of Mcfee (117) but these were unsuccessful and the best guide for the choice of wire gauge turned out to be the room temperature fusing currents for the various wire diameters. The wires used for various temperature intervals are shown in Fig. 5.10.

The solenoid was operated in the persistent mode during magnetisation. It was switched in and out of this by sending a superconducting short circuit (also of Nb 25% Zr), spot welded across its ends, normal with a heater. The circuit for this arrangement is shown in Fig. 5.12. As can be seen, two superconducting

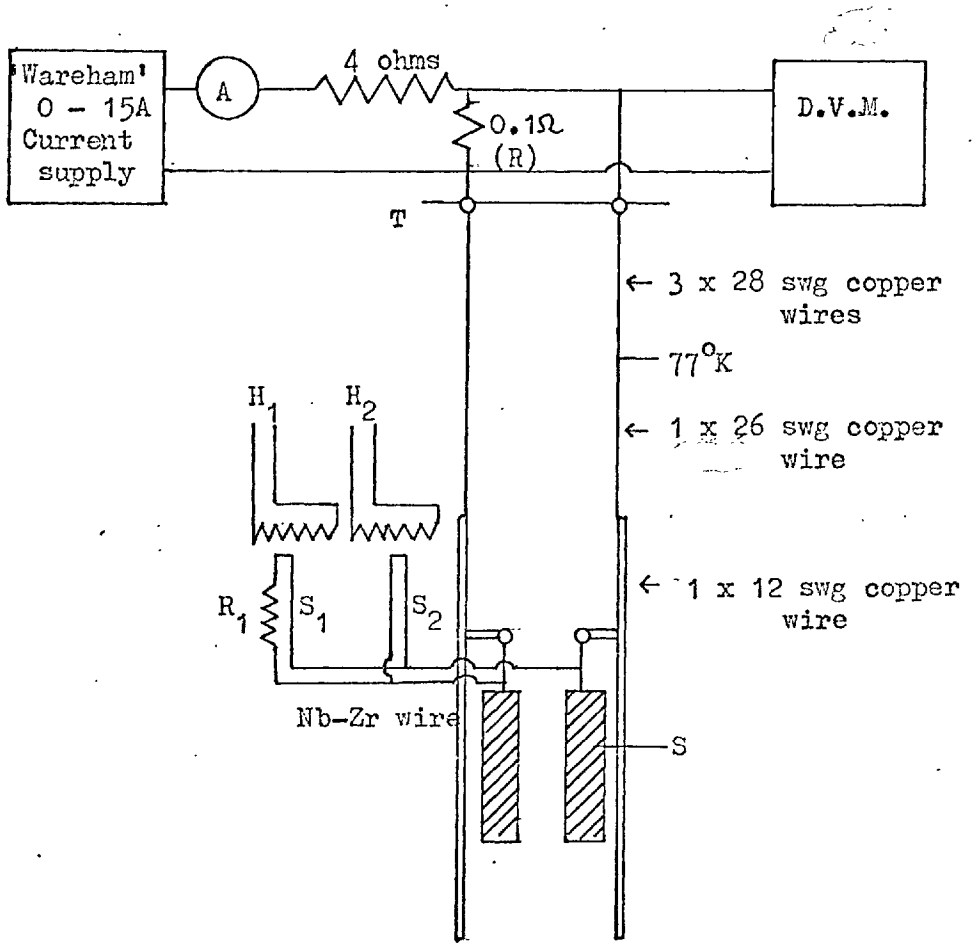

Key to Fig. 5.12

H_1 = heater 1

H_2 = heater 2

S_1 = superconducting short circuit 1

S_2 = superconducting short circuit 2

R_1 = 3 milliohms

D.V.M. = digital millivoltmeter

T = cryostat top-plate

FIG. 5.12 Current supply circuit for superconducting solenoid

switches were used in parallel. The self inductance of the solenoid was 0.3 Henries and a small resistance in series with one short gave a time constant of 100 secs with which the field was slowly reduced on demagnetisation. With both switches normal the time constant was 5 secs. These switches had to be kept out of the liquid helium on a stainless steel tube.

Referring to Fig. 5.12 the 0.1 Ω resistor, (R), provided a safeguard in the event of the solenoid going normal or a lead-in wire fusing, it effectively converted the constant current Wareham power supply into a constant voltage source. The millivoltmeter across it showed that the field was being established because it detected the 'back emf' in the solenoid; if the current in the 'persistent' mode fell the induced voltage in the solenoid could also be detected. At 13A total current about 1.3 Amps flowed through R so that the total power dissipation in the cryostat was 1.5 W, 30 times the normal heat leak. Preliminary experiments with an integrating fluxmeter were made to determine the best position for the Pb heat switch and the gauss/amp ratio of the superconducting solenoid.

2. <u>The saltpill assembly</u>

This is drawn in Fig. 5.11. The CPA crystals (about 20 cc)

were tightly bound and GE varnished between 3 strips of 'coil foil' as first used by Wheatley et al (105). This was made by winding 46 s.w.g. copper wire on a drum, coating with GE varnish and baking out at about 80°C. This combines the advantages of good thermal conductivity in one direction with low eddy current heating in changing magnetic fields. The whole assembly was supported from a threaded brass rod frame by pre-stretched nylon thread (0.2 mm diameter). The Pb heat switch, positioned so that its top end was just normal in the maximum magnetising field, was soldered at that end to a copper post on the He^3 pot and at the other end to the coil foil. Most of the details of this construction were obtained from the paper of Wheatley et al (105), which also contains useful information on thermal contact in such systems.

3. Temperature measurement and detection of superconductivity

A Hartshorn bridge, based on a Tinsley 0.1-1000 μH variable mutual inductor and operated with a home-made phase sensitive detector at 190 c/s, was used to measure both the mutual inductance of the CMN system and to detect superconductivity. The circuit used is shown in Fig. 5.13. The measuring field used was usually 1/10 g. p/p. Calculations showed that eddy current heating was negligible

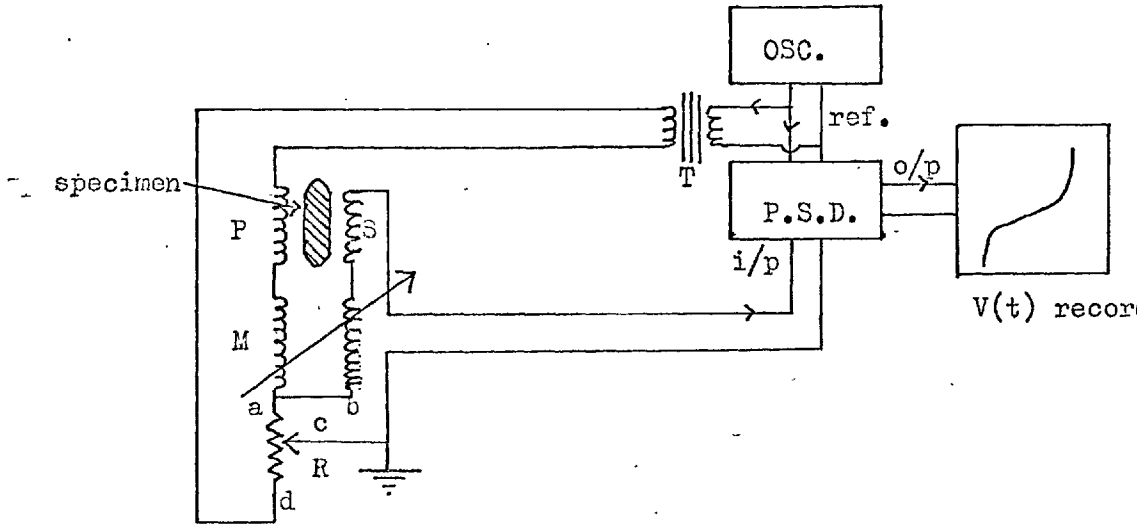

Schematic Diagram

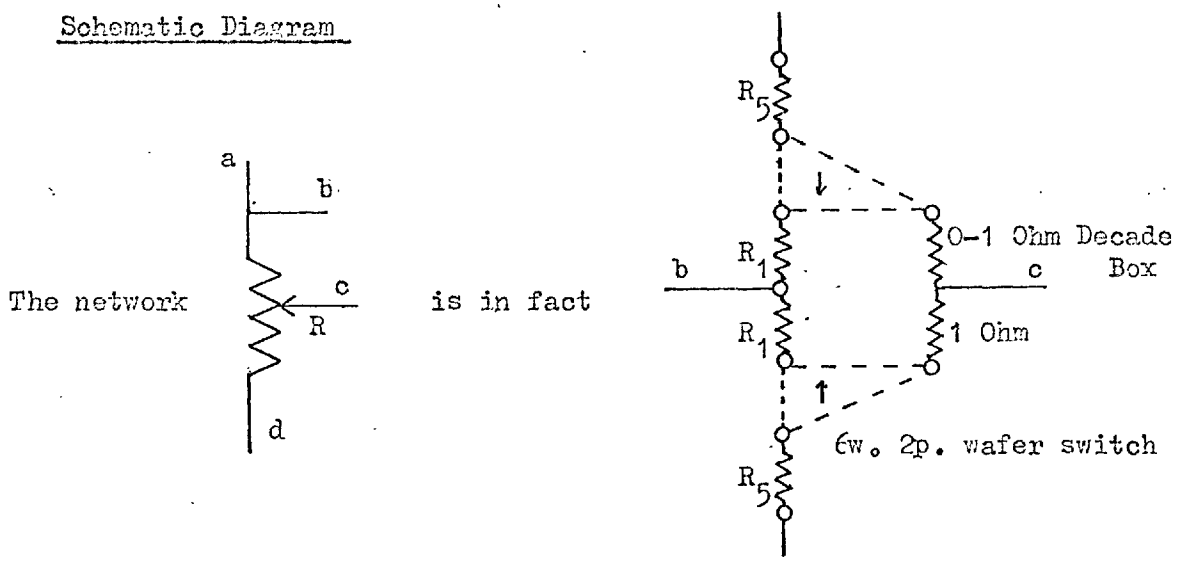

Key to Fig. 5.13

M = Tinsley 0.1 - 1000μH. variable mutual inductor

R_1 - R_5 are matched pairs of constantan wires (~10 - 1000 milli-ohms)

P =Primary coil in He^4 bath

S = Secondary coil containing specimen or CMN crystals

P.S.D. = Phase sensitive detector (usually operated at 190 c/s)

T = Isolating transformer

FIG. 5.13 The Hartshorn bridge circuit

for alloy specimens at this level, the discrimination at this power level was $\pm .05\ \mu$H. Since the usual change in mutual inductance (M) at T_c was about 50% of the normal state value of $\sim 10\ \mu$H there was plenty of sensitivity in hand and the measuring field could be reduced as desired. The primary coil was wound on the brass vacuum can, with overwound ends to produce a uniform field, according to the prescription of Garret (112). The secondary coils of the CMN were made of rectangular cross section (4,000 turns 48 s.w.g.). These were made rigid and formerless by coating alternate layers with GE varnish. To minimise magnetic interference from the CPA these had to be placed side by side, and flat pieces of CMN were varnished and tied to a piece of coil foil within one of the coils. CMN is highly anisotropic and this arrangement ensured that the coil axes were parallel to the direction of maximum susceptibility. The use of rectangular geometry was helpful in making good thermal contact between flat surfaces, the results of Wheatley et al (105) show that boundary effects are an important source of thermal resistance in such systems. With a 1 cm^2 cross sectional area of CMN, the measured mutual inductance M typically followed the law

$$M = \frac{-15 \pm 1}{T} + 30 \quad \mu H/^{\circ}K$$

This agreed with the calculated slope of about 20/T (μH/°K).

Each specimen had its own secondary coil (~500 turns 48 s.w.g.) wound directly on the metal and was tied tightly to the coil foil between the CPA and CMN crystals, and covered with 'N' grease.

4. Secondary Thermometers

On the first few runs a $\frac{1}{2}$ W. 30 ohm Speer carbon resistor was used as a secondary thermometer. This was rather insensitive, and too large physically for the demagnetisation apparatus, and in later runs a pair of matched 100 ohm $\frac{1}{4}$ W Speer resistors with the ceramic ground away were used. One of these was situated near the CPA and the other near the specimens in order to check that no significant thermal gradients occurred. These resistors were measured with the same 3 lead AC bridge described earlier in this chapter. The power dissipation used was 10^{-10}W, a factor of 30 higher than the maximum recommended by Wheatley et al (105). Although no self heating effects were detected down to the lowest temperature tested (70 md), further efforts will have to be made to reduce this dissipation for the lowest temperature range.

5.8 Performance of the Apparatus and Experimental Procedure

As has already been mentioned the CPA deteriorated after several runs with the result that the minimum obtainable temperature rose from 28 md to 70 md. The details given here refer to the first case when the CPA had its normal magnetic characteristics.

The He^3 liquid was condensed in the normal manner and by connecting the He^3 pot to the main storage cylinder a steady temperature of about $0.8^{\circ}K$ was maintained. The magnetising field was then applied and the solenoid was maintained in the persistent mode, giving a field of about 9 kilogauss. An external field of about 170 gauss also 'helped' the lead heat switch become non-superconducting. The He^3 was then pumped away at maximum speed to give a He^3 bath temperature of $0.4^{\circ}K$. Under these conditions the time constant of the assembly (with two Pb heat switches in parallel, each 2.5 cms long and 0.5 mm diam.) was about 10 mins. This was consistent with a measured resistance ratio of about 1,000 for the Pb wire used. The CPA reached a temperature of about $0.5^{\circ}K$ after about 30 mins. The external 170 g field was then reversed and by passing a current through heater H_1 (Fig. 5.12) the magnetising field was reduced with a time constant of 100 secs. The remaining flux was expelled quickly by heating H_1 and H_2, and the superconducting solenoid could

then be hoisted up so that it was about 20 cms away from the specimens. This was necessary (a) because in the persistent mode it prevented AC fields being established inside it and hence the mutual inductance measurements were greatly changed. (b) the solenoid retained some trapped flux. The remanent field at the specimens due to this (even with the solenoid raised) was later found to be 0.9 gauss..

The CMN reached its minimum temperature about 10 mins after demagnetisation and thereafter warmed up from about 30 md at a rate of 1 md/minute. This corresponds to a heat leak of 10 ergs/sec which was larger than envisaged, but calculations showed that this was to be expected from the lead heat switch used, which accordingly was later reduced in diameter. As the system warmed up measurements of mutual inductance for the CMN and the specimen secondary coils, and carbon resistance measurements, were made consecutively. (The superconducting transitions were usually plotted out on a chart recorder). Finally the CMN thermometer was calibrated against the He^3 vapour pressure by allowing He^3 exchange gas into the specimen chamber. (On some runs this vacuum chamber was not used and the He^3 vapour pressure could only be used between $1.2^{o}K$ and $1.4^{o}K$).

5.9 Results

As already mentioned, no new superconductors have been discovered in this temperature range. The 15% ℰ Cu-Zn alloy measured has been found to be normal down to 0.03°K although the remanent field (0.9 g) was not compensated on this run. Two specimens of iridium have been measured, one was in the form of a sintered 1.5 mm diameter rod and the other was a 0.5 mm diameter wire. By extrapolating their critical fields to zero (after allowing for the remanent field) respective transition temperatures of .107 and .096°K were found. These are consistent with the recent value of .105 ± .005°K found by Andres and Jensen (107). The slope of the critical field temperature curve at T_c indicates that $H_o \triangleq 2g$ for Ir. The AC transition showed a "peak" effect and there was some supercooling as the field was lowered, showing that both specimens were type I. H_c was taken to be the field at which the peak value of the inductive component (M) occurred.

Therefore the failure to compensate for the remanent field on the ℰ CuZn run was serious and the valid upper limit on a possible T_c is probably about 0.1°K, since the results for Ir show that T_c's of 0.1°K can be detected in the presence of this remanent field. As discussed by Wheatley et al in their paper on the

superconductivity of tungsten , (106) such fields can prevent the appearance of superconductivity, especially for very pure materials (with $K \ll 1$), even if they are considerably less than the thermodynamic critical field at that temperature, because of supercooling.

5.10 Conclusions and Final Suggestions

Although the adiabatic demagnetisation cryostat has been made to work there have been various difficulties associated (a) with the hydrated salt used and (b) with problems of remanent field. With the present heat switch used there is also not much advantage in using such a magnetically concentrated salt as CPA because on the warm-up the present measurements show that the dominant heat leak comes from the Pb heat switch itself. If less heat of magnetisation were generated then this could be made smaller and the overall warm up rate and time constant for magnetisation would be unaltered. Recent measurements have also revealed a small phase shift in the AC field caused by the brass vacuum can. (This is mentioned in chapter 6).

This should not have affected the relative values of the CMN mutual inductance at high and low temperatures, but it would be better to use a lower operating frequency than 190 c/s in future,

so that the occurrence of any other AC losses (for instance in the CMN itself) could be detected. Provision exists for raising the solenoid right to the top of the cryostat but at the moment this is not possible because of the radiation shields in the main helium dewar. This would certainly eliminate the remanent field problem.

CHAPTER 6

INTERMETALLIC COMPOUNDS OF TRANSITION METALS

6.1 Reasons for Interest

The effect of the screened coulomb repulsion U_{eff} between electron states within the d bands of transition metal superconductors has been mentioned in chapter 2. Especially towards the end of the 4d and 5d series U_{eff} becomes large enough to give long range spin fluctuations which strongly depress T_c. Such fluctuations are also associated with an enhanced Pauli paramagnetic susceptibility χ_p and give an extra contribution, in addition to the electron-phonon enhancement, to the electronic specific heat γT. An example of this behaviour is shown in Fig. 6.1 where T_c, γ and χ_p are plotted against electron density for several alloys of 4d and 5d elements at the end of the transition series. (This graph has been taken from a review by Muller (115) 1969). Both γ and χ_p are plotted here in states/eV/ c.c.

The free electron formulae:

$$\chi_p = \mu_B^2 \; n_\chi(E_F) \qquad 6.1$$

and

$$\gamma = \tfrac{1}{3}\pi^2 k^2 \, n_\gamma(E_F) \qquad 6.2$$

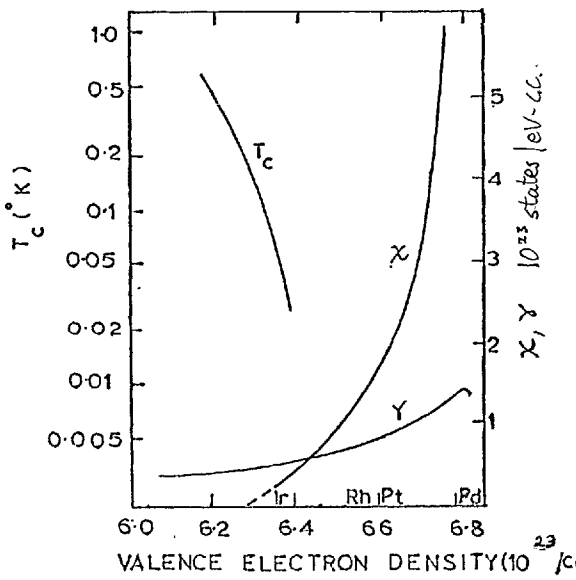

FIG. 6.1 T_c, χ and γ vs. Electron Density for some 4d and 5d alloys

have been used to find $n_{\chi}(E_F)$ and $n_{\gamma}(E_F)$, the enhanced 'susceptibility' and 'specific heat' density of states for both spin directions, from the measured values of χ_p and γ :
(k is Boltzmann's constant and μ_B is the Bohr magneton).

It can be seen that T_c falls rapidly just as enhancement in the susceptibility first occurs. The specific heat, γ , continues to rise towards the end of the series, probably because of the effects of spin fluctuations. Therefore the empirical rule linking the increase in T_c with an increase in $n_{\gamma}(E_F)$, which is obeyed for alloys between earlier members of the 4d and 5d transition series (116)is not obeyed here because of the spin fluctuations.

It is of interest to see whether similar considerations apply to some intermetallic compounds of transition elements. The Laves phase compounds XCo_2 and XRu_2 (X is an early member of the 3d, 4d, 5d or 4f transition series) were a promising system for such a study. For, while it is known that YCo_2 is a 'weak' ferromagnet with a Curie temperature of approximately 300°K and a saturation moment of approximately $1\mu_B$ per atom (59), other XCo_2 compounds based on nearby elements, for example Ti and Zr, have a temperature independent paramagnetic susceptibility (113).

In these AB_2 compounds both the larger A atoms and the smaller B atoms can be replaced by neighbouring elements over a large range of concentration. It should be possible to introduce spin fluctuations by the addition of Y to $ZrCo_2$(say), YCo_2 being equivalent to Pd in the previous example.

Furthermore, if such compounds were superconducting it would be of interest to compare them with the behaviour of the $CeCo_2$ and $CeRu_2$ compounds with the $MgCu_2$ structure, studied by Smith et al (92). These authors showed that Ce is 4-valent in these compounds, thus one might expect the iso-structural XCo_2 compounds of 4-valent Ti , Zr, and Hf to be superconducting.

6.2 Experimental Details

The He^3 cryostat and the AC detection system described previously were used. There were slight differences from the measurements described in Chapter 3. The extra vacuum can, sealed with a copper cone joint, was employed and contained about .01 mm Hg pressure (at 1^oK) of He^3 exchange gas to make thermal contact between the specimens and the He^3 pot.

The Hartshorn Bridge used to measure the mutual inductance of the small coils containing the specimens was usually balanced at 174 c/s. These coils had about 300 turns but a smaller cross-sectional area than before. The standing mutual inductance (M) was typically 40μH. At the superconducting transition temperature this fell by about 10μH for an intermetallic compound specimen of 20 $(mm)^3$ volume. Sometimes smaller pieces contained in a 3 mm diameter plastic tube were used and these gave a change of about 4μH at T_c. At 174 c/s the discrimination of the bridge was at least $\pm$ 0.05 μH for the measuring field used (0.5 gauss peak to peak). Occasional measurements were made at 30 c/s, for which the standing mutual inductances (and the changes at T_c) were 20% larger. An empty coil measurement showed that this was due to eddy currents in the brass vacuum can rather than in the specimens. Eddy currents in

the specimen only gave a significant reduction in the change in mutual inductance (ΔM) at T_c for a 5N aluminium specimen. ΔM was reduced by a factor of ten but even so was still easily detectable ($\Delta M \sim 0.4 \mu H$). The resistance ratio of the Al specimen was later measured and was so large that only an upper limit (2000) could be found. Therefore there was nc possibility of a transition in one of the intermetallic compounds not being detected, or even being reduced significantly because of induced eddy currents at 174 c/s. During a run the procedure was usually as follows:

The mutual inductances (M) of the six specimen coils were measured at 300°K, 77°K and 14°K (the triple point of H_2, where the exchange gas used to precool the He^3 pot solidified). The He^3 liquid was condensed and M measured at 1.3°K and 0.4°K. In the absence of any transitions the values of M at 14°K, 1.3°K and 0.4°K were usually the same to within about $0.1 \mu H$. If any transitions had occurred these were then plotted out on a pen recorder, allowing the specimens to warm up. As described in chapter 5 the 1962 He^3 and 1958 He^4 vapour pressure temperature scales were used to calibrate the 30 ohm Speer carbon resistance thermometer. This had been previously calibrated below 0.6°K

against $H_c(T)$ for aluminium, again as described in chapter 5.

This procedure has been described in such detail because it will become apparent from the next section that many results are negative, in that superconductivity was not detected, but with the present arrangement there is almost no possibility of a transition being missed. Sometimes a small amount of second phase was detected by microscopic analysis. If the matrix were not superconducting down to $0.4^{\circ}K$ then, providing the second phase exceeded about 5% of the total volume, any superconductivity in this phase would also have been detectable. Finally, there was no ambiguity about whether the flux was expelled (superconducting transition) or whether there was an increase in flux through the specimen (ferromagnetic transition), and any ferromagnetic and (possibly) antiferromagnetic transitions in the specimen should have been detectable.

6.3 Results and Discussion

The results of T_c measurements are given in table 6.1. Surprisingly, none of the more recently made $CeCo_2$ alloys were superconducting down to the temperature (T_n) shown. Two superconducting $CeCo_2$ alloys which had previously been measured

Table 6.1

Tc Measurements on Intermetallic Cobalt Compounds

1 Non-Superconducting Specimens

Specimen	Source	Tn(^{o}K)	Remarks
$TiCo_2$	1	0.4	~100 p.p.m. Fe impurity
$Ti_{0.8}Zr_{0.2}Co_2$	1	0.4	All Ti and Zr specimens used for χ_p(T) measurements (113)
$Ti_{0.5}Zr_{0.5}Co_2$	1	0.4	
$Ti_{0.2}Zr_{0.8}Co_2$	1	0.4	
$ZrCo_2$	1	0.4	~100 p.p.m. Fe impurity
$HfCo_2$	2	0.38	
$ScCo_2$	2	0.38	
$NbCo_2$	2	0.38	
$Ce_{24}Co_{11}$	2	0.4	

$CeCo_2$ - non stoichiometric specimens all homogenised by I. R. Harris

$Ce_{.33}Co_{.67}$	2	0.4	
$Ce_{.3333}Co_{.6667}$	2	0.4	~100 p.p.m. Fe impurity
$Ce_{.34}Co_{.66}$	2	0.4	5% Ce rich second phase ~100 p.p.m. Fe impurity
$Ce_{.3475}Co_{.6525}$	2	0.4	
$Ce_{.35}Co_{.65}$	2	0.4	
$Ce_{.355}Co_{.645}$	2	0.4	

2 Superconducting Specimens

Specimen	Source	T_c °K	80% transition width (md)	Remarks
$Ce_{.34}Co_{.66}$	2	1.07(5)	± 15	No detectable Fe impurity (i.e.<10p.p.m.)
$Ce_{.355}Co_{.645}$	2	0.97(5)	± 25	
ZrCo	2	1.5	± 120	1/10 expected ΔM at T_c
$LaRu_2$	3	3.12	± 60	Two more broad transitions at 2.2°K and 1.4°K.

KEY TO TABLE

1 Specimens kindly supplied by Professor R. S. Craig, University of Pittsburg

2 Specimens kindly supplied by T. F. Smith (Harwell) and I. R. Harris (Birmingham University)

3 Specimen made here by arc melting

in another He^3 cryostat by T. F. Smith were therefore measured here. These were measured on the same run as some of the newer alloys and the transition temperatures agreed with those of Smith. Subsequently some of the specimens were examined by emission spectroscopy in the Analytical Services Laboratory, Imperial College. As shown in table 6.1 the two non-superconducting $CeCo_2$ alloys examined were found to contain approximately 100 p.p.m. Fe, whereas the superconducting one did not. This result must be treated with some caution because a considerable number of the stronger lines in the Fe spectrum were obscured by Ce lines. The nominal purity of the starting materials is not known but presumably was the best commercially available "off the shelf", namely 99.9% Ce. In fact a new batch of Ce was used for the non-superconducting alloys. Assuming 100-1000 p.p.m. of Fe in solid solution is responsible for the depression in T_c then the depression is $\sim 10^3$ to 10^4 ^oK/at % for Fe in $CeCo_2$. This is extremely large (to the writer's knowledge the largest depression found up to now is 300^oK/at % for Mn in Zn) and so the $CeCo_2$-Fe system would be worthy of further investigation.

The two $Ce_{.34}Co_{.66}$ alloys (one superconducting, the other

not) were also examined by electron probe analysis which confirmed that the bulk of the alloy was $CeCo_2$. Microscopic examination of these two alloys revealed about 5% of a Ce rich second phase at the grain boundaries, despite the homogenisation of the non-superconducting alloy carried out by I. R. Harris. This phase was presumably not detected by his X-ray measurements. The second phase is insufficient to give a superconducting transition of the observed magnitude (the Ce rich phase does not appear to be multiply-connected and in any case, a powdered specimen was also superconducting) but could be responsible for the observed increase in χ_p at low temperatures.

While on the subject of the homogeneity of the specimens it should be noted that none of $LaRu_2$, $CeRu_2$ or $CeCo_2$ melt congruently (60), that is, the phase diagram near these compositions has the form:

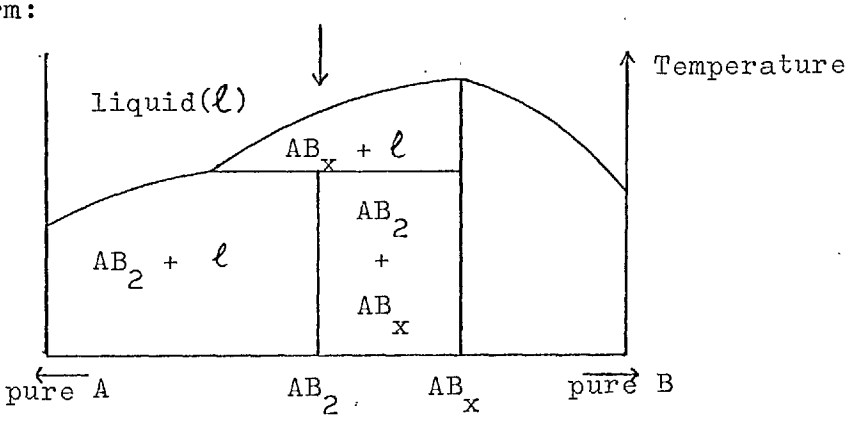

Thus on cooling an alloy of composition AB_2 from the melt there is bound to be some AB_x and an A-rich phase formed as well as AB_2. For $CeCo_2$ this results in only a small amount ($\sim$5%) of unwanted second phase, but we have been unable to make even reasonably single phase $LaRu_2$ or $CeRu_2$ by arc melting. (We have also examined a $La_{.94}Gd_{.06}Ru_2$ alloy used by Peter et al (77) for susceptibility and e.p.r. measurements, this contains approximately equal amounts of three phases).

The three-phase $LaRu_2$ alloy which was tested for superconductivity in fact had three transitions, the main one being at 3.12°K, none of which agreed with the published value of 1.63°K (114). It seems that X-ray diffraction is not a sensitive enough method for detecting other phases and any results obtained for intermetallic compounds which do not melt congruently must be viewed with caution in the absence of further annealing treatment and metallographic analysis by optical microscopy.

With the present limited amount of data it is difficult to give a detailed discussion of the other XCo_2 compounds. The known paramagnetic susceptibilities at 300°K of the alloys measured are given in table 6.2. For comparison that of a

non-transition metal cubic Laves phase compound, $LaAl_2$, is given as well. (χ_p for this alloy has been taken from the work of Maple (80) and is corrected for the core diamagnetism).

Table 6.2

Paramagnetic Susceptibilities of $MgCu_2$ Structure Intermetallic Compounds at 300°K

Compound	χ_p(300) emu/mole	$n_\chi(E_F)$ States/eV/atom	Reference
$TiCo_2$	1.5×10^{-3}	16	(113)
$ZrCo_2$	1.5×10^{-3}	16	(113)
$CeCo_2$	1.2×10^{-3}	13	(108)
$LaAl_2$	0.075×10^{-3}	0.8	(80)

In table 6.2, formula 6.1 has been used to calculate $n_\chi(E_F)$. For $LaAl_2$ $n_\chi(E_F)$ is a factor of two lower than the value obtained in chapter 3 ($n(E_F)$=1.4 states/eV/atom, corresponding to m/m^*=3) but χ_p does increase by a factor of two from 300°K to 20°K (80) so that exact agreement cannot be expected.

If one compares the values of $n_\chi(E_F)$ given in table 6.2

with those of Fig. 6.1, where $T_c \simeq 0.02^{\circ}K$ for $n\,\chi(E_F) \simeq 2$ states/eV/atom, it is understandable that $TiCo_2$ and $ZrCo_2$ are not superconducting downto $0.4^{\circ}K$, the question is, why is $CeCo_2$ a superconductor ?

Both 4-valent Ce and 3-valent La have an empty 4f shell and the possibility of a different mechanism for superconductivity in La (and U), involving occupation of virtual 4f levels, has been raised by some authors, for example Kuper et al (109) (1963). Alternatively Peter et al, (77) (1967), suggested that $LaRu_2$ could be a two-band superconductor. The large, enhanced Pauli paramagnetic susceptibility could be a property of a "d-like" band and superconductivity could arise from pairing of electron states within an "s-like" band.

The only superconducting compounds with the cubic $MgCu_2$ structure which have been found to be superconducting up to now are those containing La and Ce, although the hexagaonal, $MgZn_2$ structure compounds $ScRu_2$, YRu_2 and $ZrRu_2$ are superconducting (24). Some other $MgCu_2$ structure phases $TaCo_2$, $TiRu_2$, $HfRu_2$ and $NbRu_2$ have yet to be tested. Before further speculation is made about $CeCo_2$ it would be interesting to know,

(a) If the Pauli paramagnetic susceptibility of superconducting $ScRu_2$, YRu_2 and $ZrRu_2$ is as large as that of $CeCo_2$,

(b) If the remaining, $MgCu_2$ structure, XRu_2 and XCo_2 compounds are superconducting and yet also have large values of $n_\chi(E_F)$.

If (a) or (b) were true then the '4f mechanism' would not be needed to explain the superconductivity of the Ce- and La- based compounds.

The measurements on $ScCo_2$ indicate that there may be magnetic ordering in this compound at low temperatures. In contrast to $HfCo_2$ and $NbCo_2$ where M was constant (to within $0.1\mu H$) from 14^oK to 0.4^oK, for $ScCo_2$ there was a smooth increase of $0.5\mu H$ in M from 14^oK to 1^oK and then a decrease of $0.5\mu H$ down to 0.4^oK. The corresponding variation in AC (174 c/s) susceptibility is $\sim 5 \times 10^{-3}$ emu/cc, $\sim 10^{-1}$ emu/mole. This is far too small for a ferromagnetic transition but could possibly be due to antiferromagnetic ordering.

In view of the effect of $\sim$ 100 p.p.m. Fe impurity on $CeCo_2$ the remaining XCo_2 alloys should have been tested for Fe. Unfortunately most of the alloys were returned to the Solid State Division, Harwell, before this was done and only $TiCo_2$ and $ZrCo_2$ have been tested. This has been done recently and, as for $CeCo_2$, $\sim$ 100 p.p.m. of Fe impurity was found by emission spectroscopy.

Although Abel and Craig (113) made measurements of $\chi(T)$ down to $4.2^{o}K$ on these alloys such a small concentration of Fe impurity, even with a giant moment $\sim 5\mu_B$/atom would not have given a detectable contribution to χ compared with $\chi_p(T)$. Therefore it is still possible that higher purity $ZrCo_2$ and $TiCo_2$ will be superconducting.

In conclusion then, further measurements on the XCo_2 and XRu_2 systems are required. For measurements of T_c care must be taken to ensure that contamination with Fe does not occur. For measurements of χ the specimen must be truly single phase. These should then throw some light on the superconductivity of the $CeCo_2$, $CeRu_2$ and $LaRu_2$ compounds and on that of neighbouring $MgZn_2$ structure compounds.

APPENDIX I

Transition Temperatures of $LaAl_2$ and $La_{1-x}R_xAl_2$ Alloys

Unless stated otherwise these temperatures were determined by the AC method.

Key to tables: a, b, c, d refer to metallurgical features (i) to (iv) respectively in Chapter 3, section 3.4.

hh, electron probe analysis indicates overall homogeneous impurity distribution, to within 10%.

h, indicates homogeneous impurity concentration in $LaAl_2$ matrix only (to within 20%), there are small regions ($\sim 10\%$) of higher impurity content.

i, inhomogeneous impurity concentration.

1 $LaAl_2$ Samples

Spec. No.	T_c ^oK	80% width md.	Metall. examination	Elect. probe analysis	Source	Remarks
1	3.19	± 5	a	h	La Jolla	
1	3.24		a,b			anneal 24 hrs 850°C T_c obtained from $H_c(T)$
2	3.24	± 8	a,b,d		1	
3	3.32 3.28	± 10 ± 5	a		1	He level very low, transition on warm up was at lower temp.
4	3.28	± 11	a,d		1	
5	3.23	± 15	a		1	
6	3.19	± 30			Harwell	arc melted button
7	3.1 2.1				Harwell	powdered specimen
8	3.25	± 30			B'ham	
#1L	2.86	-90 +50			1	new batch La
#2L	3.24	± 8			1	same batch La as #1L

2 $La_{1-x}Tm_xAl_2$

Nom. Conc. x %	T_c °K	80% width md	Metall. examination	Elec. probe analysis	Source	Remarks
3.0	2.89	± 50	a		La Jolla	Later powdered, used for $\chi(T)$
2.0	3.01	+ 60 − 20	a	h	1	x=1.3%, e-probe
4.0	2.74	+ 90 − 50	a,d	h	1	x=5.3%, e-probe
0.89	3.106	± 12	a		1	
4.2	2.76	± 40	a,b,c,d,	h	1	
5.7	2.64	± 18	a,b,c,d	h	1	
7.2	2.17	± 20	a,b,c,d	i	1	off $T_c(x)$ graph
7.2	2.39	+ 160 − 130	a,b,d		1	
5.0	<1.3		a			Small specimen trans. not detect.
8.73	2.30	± 12	a,d	h	1	x=9.0%, e-probe
0.5	3.04	± 30			Harwell	powdered before measurement
0.9	3.06	± 30			B'ham	

$La_{1-x}Tm_xAl_2$ (contd)

Nom. Conc. x %.	T_c °K	80% width md	Metall. examin-ation	Elec. probe analysis	Source	Remarks
0.5			a,b		La Jolla	
	The remaining specimens were made from 99.7% La					
4.0	2.33 ± 100					Only 1 arc melt
4.0	1.54 ± 100					After 2 hrs @ 600°C
4.0	2.9 – 2.2					After 48 hrs @ 1000°C
5.2	(a)2.38 ± 2 (b)2.86 ± 150					2 transitions, (b) is very small
6.3	2.14 ± 50					
8.7	2.74 ± 30					Off T_c graph

3 $La_{1-x}Lu_xAl_2$

Spec. No.	Nom. Conc. % x	T_c °K	80% width md	Metall. examin- ation	Elec. probe analysis	Source	Remarks
	0.5	3.20	± 7			La Jolla	
	2	3.15	± 15	a,b,c	h	1	Lu inclusions present, nom. concentration 1.2-1.5x larger than those from e-probe.
	3	3.12	± 16	a,b,c	h	1	
	5	3.06	+ 24 − 72	a,b,c	h	1	

4 $La_{1-x}Pr_xAl_2$

	2.0	2.14	± 50	a,b	h	1	accurate e-probe analysis not possible because of coincident La, Pr, X-ray lines
#1L	2.98	1.49	± 100			1	
#2L	4.02					1	
#3L	3.42	0.925	± 3			1	

5 $La_{1-x}Tb_xAl_2$

#2L	0.8	1.28	± 70	a,d		1	used for $\chi(T)$
#3L	0.6	1.88	+ 8 − 80	a,d	hh	1	e-probe x=.69%

5 $La_{1-x}Tb_xAl_2$ (Contd)

Spec. No.	Nom. Conc. % x	T_c °K	80% width md	Metall. examin-ation	Elec. probe analysis	Source	Remarks
#4L	0.37	2.43	+ 6.5 - 13	a,d	hh	1	
#5L	1.87			a,d		1	
#6L	1.16					1	
#7L	1.22	0.77	+ 80 - 160			1	

6 $La_{1-x}Ho_xAl_2$

#1L	2.41	<0.4				1	
#2L	3.01	<0.4				1	
#3L	2.0	1.42	± 90			1	used for e.p.r.
	1.57	2.09	± 80	a	hh	La Jolla	1.88% from e-probe

7 $La_{1-x}Dy_xAl_2$

#1L	1.42	<0.4				1	
#2L	1.62	<0.4				1	
#3L	1.09%					1	Not measured yet

8 $La_{1-x}Er_xAl_2$

Spec. No.	Nom. Conc. % x	T_c °K	80% width md	Metall. examin-ation	Elec. probe analysis	Source	Remarks
	0.47	2.88	± 9	a,d	hh	La Jolla	
	0.5	2.96	± 30			Harwell	used (powder) for M(H)
	1.03	2.77	± 26	a,d		1	
#1L	1.7	2.38	− 30 + 40			1	
#2L	3.75	2.0	+ 200 − 300			1	off $T_c(x)$ graph
	The remaining specimens from 99.7 % La						
	2.4	1.67	− 300 + 100			1	one melt only
	2.4	1.67	− 300 + 100			1	after 24hrs @ 600°C
	2.4	2.01 1.83	± 90 ± 40	d		1 1	48 hrs @ 1000°C 2 transactions
	2.4	1.87	− 60 +100			1	surface removed

REFERENCES

1 J. BARDEEN, L. N. COOPER and J. R. SCHRIEFFER Phys. Rev. 108 1175 (1957)

2 A. A. ABRIKOSOV JETP 5 1174 (1957)

3 L. P. GORKOV JETP 9 1364 (1959)

4 K. MAKI Physics 1 21 (1964)

5 G. EILENBERGER Phys. Rev. 153 p 584 (1967)

6 D. SCHOENBERG 'Superconductivity' Cambridge University Press (1952) p. 126

7 JONES D. P. PhD Thesis, University of London (1969)

8 V. ESSMANN and M. TRÄUBLE Phys. Letters 24A 526 (1967)

9 B. COQBLIN and A. BLANDIN Adv. in Physics Vol. 17 No 67 (1968) p 312

10 W. L. MACMILLAN Phys.Rev. 167 331 (1968)

11 C. F. RATTO and A. BLANDIN Phys. Rev. 156 p 513 (1967)

12 P. W. ANDERSON Phys. Rev. 124 p 41 (1961)

13 K. MAKI Phys. Rev. 153 428 (1967)

14 H. SUHL Phys. Rev. 141 483 (1966)

15 D. MARKOWITZ and L. P. KADANOFF Phys. Rev. 131 p 563 (1963)

16 J. R. CLEM Phys.Rev. 148 p 392 (1966)

17 P. W. ANDERSON J. Phys. Chem. Solids 11 p26 (1959)

18 P. FULDE Phys. Rev. 139 p 726 (1965)

19 "Handbook of Math. Functions" M. ABRAMOWITZ and I. A. STEGUN Dover publications (NY) (1965)

20 S. DONIACH and S. ENGLESBERG Phys. Rev. Letters 17 750 (1966)

21 G. BOATO, G. GALLINARO and C. RIZZUTO Phys. Rev. 148 353 (1966)

22 P. G. De GENNES "Superconductivity of Metals and Alloys" W. A. Benjamin Inc. (1966)

23 B. T. MATTHIAS, T. H. GEBALLE and V. B. COMPTON Rev. Mod. Phys. Vol 35 p 1 (1963)
(see also B. R. COLES, Rev. Mod. Phys. Vol 36 p 139 (1964))

24 B. W. ROBERTS "Superconductive Intermetallic Compounds" General Electric Research Report No. 64-RL-3540M (Jan. 1964)

25 K. H. BENNEMANN J. W. GARLAND and F. M. MUELLER (to be published)

26 J. W. GARLAND Phys. Rev. Letters 11 111 (1963)

27 M. J. ZUCKERMANN and M. KIWI Phys. Rev. 164 818 (1967)

28 For example:
(a) A. D. CAPLIN and C. RIZZUTO Phys. Rev. Letters Vol 21 p 746 (1968)
(b) M. A. JENSEN, D. SCALAPINO, S. DONIACH and P. LEDERER (to be published)
(c) M. J. ZUCKERMANN Lectures at VII Annual Winter School of Theoretical Physics, Karpacz, Poland (1969)

29 J. R. SCHRIEFFER, J. Appl. Phys. 38 1143 (1967)

30 C. RIZZUTO in proceedings of Solid State Physics Conference, Inst. of Physics, Manchester (1969)

31 J. R. SCHRIEFFER and B. COQBLIN, (to be published)

32 A. A. ABRIKOSOV and L. P. GORKOV Soviet Phys. JETP 12 1243 (1961)

33 S. DONIACH in Proceedings of the 'Enrico Fermi' School of Physics, Course 37, Varenna (1966), Academic Press, New York (1967)

34 S. H. LIU Phys. Rev. 121 451 (1960)

35 M. B. MAPLE Phys. Letters 26A, No 10 p 513 (1968)

36 HEIN R. A., R. L. FALGE, B. T. MATTHIAS and E. CORENZWIT Phys. Rev. Letters 2 500 (1959)

37 J. E. CROW and R. D. PARKS Phys. Letters 21 No 4 p 318 (1966)

38 A. M. TOXEN, P. C. KWOK and R. J. GAMBINO, Phys. Rev. Letters 21 792 (1968)

39 K. YASUKOCHI, Y. KUWASAWA and K. SEKIZAWA Phys. Letters 28A 12 (1968)

40 R. P. GUERTIN and R. D. PARKS Solid State Comm. Vol 7 p 59 (1969)

41 K. H. BENNEMANN Phys. Rev. Letters 17 No 8 438 (1966)

42 D. K. FINNEMORE, L. K. WILLIAMS, F. H. SPEDDING and D. C. HOPKINS Phys Rev. 176 p 712 (1968)

43 W. R. DECKER, D. T. PETERSON and D. K. FINNEMORE Phys. Rev. Letters 18 No 21 899 (1967)

44 F. REIF and M. A. WOOLF Phys. Rev. 137 A557 (1965)

45 A. S. EDELSTEIN Phys. Rev. Letters Vol 19 1184 (1967)

46 L. P. GORKOV and A. I. RUSINOV JETP 19 922 (1964)

47 P. FULDE and K. MAKI Phys. Rev. 141 275 (1966)

48 N. BARTH, H. E. HOENIG and P. FULDE Solid State Comm. Vol 5 p 459 (1967)

49 K. H. BENNEMANN and J. W. GARLAND Phys. Rev. 159 p 369 (1967)

50 D. K. FINNEMORE, D. C. HOPKINS and P. E. PALMER Phys. Rev. Letters 15 891 (1965)

51 D. GRIFFITHS and B. R. COLES Phys. Rev. Letters 16 1093 (1966)

52 L. L. HIRST, G. WILLIAMS, D. GRIFFITHS and B. R. COLES J. Appl. Physics 39 844 (1968)

53 L. L. HIRST and G. WILLIAMS (to be published in Phys. Rev.)

54 K. R. LEA, M. J. M. LEASK and W. P. WOLF J. Phys. Chem. Solids Vol 23 1381 (1962)

55 W. LOW Solid State Physics Suppl. 2, Section 20, Academic Press (1960)

56 B. G. WYBOURNE "Spectroscopic Properties of Rare Earths" Chapter 6 Wiley (Interscience)(1965)

57 P. W. ANDERSON S.S.P. Suppl. 14 (1963) (Academic Press)

58 E. BUCHER, K. ANDRES, J. P. MAITA and W. HULL Helv. Phys. Acta, Vol. 41 p 723 (1968)

59 A. R. PIERCY and K. N. R. TAYLOR J. Phys. Soc. C. Vol 2 p 1112 (1968)

60 K. A. GSCHNEIDER, "Rare Earth Alloys" (1960) D. V. Van Nostrand Ltd.

61 C. RIZZUTO (Private Communication)

62 J. A. WHITE, M. J. WILLIAMS, J. H. WERNICK and R. C. SHERWOOD Phys Rev. 131 p 1039 (1963)

63 K. H. J. BUSCHOW Phillips Res. Reports 20 337-348 (1965)

64 T. SUGAWARA and H. EGUCHI J. Phys. Soc. Japan 23 965 (1967)

65 J. D. LIVINGSTON Phys. Rev. 129 1943 (1963)

66 J. SILCOX and R. W. ROLLINS App. Phys. Letters 2 231 (1963)

67 E. HELFAND and N. R. WERTHAMER Phys. Rev. 147 p 291 (1966)

68 T. SUGAWARA, H. EGUCHI J. Phys. Soc Japan 21 725 (1966)

69 A. P. MURANI PhD Thesis, University of London (1969)

70 A. J. FREEMAN, R. E. WATSON, S. KOIDE and M. PETER Phys. Rev. 139 A167 (1965)

71 B. G. WYBOURNE "Spectroscopic Properties of Rare Earth" (ref. (56))

72 P. G. DE GENNES J. Phys. Rad. 23 (1962) 520 (in French)

73 M. PETER, J. DUPRAZ and H. COTTET Helv. Phys. Acta Vol 40 301 (1967)

74 K. H. J. BUSCHOW and H. J. VAN DAAL Solid State Comms. Vol 7 p 217 (1967)

75 V. JACCARINO J. Appl. Phys. 32 (1961) 102 S. and V. JACCARINO, A. C. GOSSARD and J. H. WERNICK Journ. Phys. Soc. Japan Vol 17 S. B1 p 88 (1962)

76 For example: K. YOSIDA Phys. Rev. 106 893 (1957)

77 H. COTTET, P. DONZE, J. DUPRAZ, B. GIOVANNINI and M. PETER Zeit fur Angewandte Physik Vol 24 p 249 (1968)

78 A. J. FREEMAN and R. E. WATSON Phys. Rev. 152 p 567 (1966)

79 S. DONIACH (private communication)

80 M. B. MAPLE PhD Thesis, University of California (1969) and M. B. MAPLE and Z. FISK Proc. LT. 11. Edinburgh (1968)

81 J. KONDO Prog. Theor. Phys. Japan Vol 22 No 1 p 37 (1964)

82 B. BLEANEY Proc. Roy. Soc. 276 28 (1963)

83 J. H. VAN VLECK "Electric and Magnetic Susceptibilities" Oxford University Press (first edition 1932)

84 E. U. CONDON and G. H. SHORTLEY "The Theory of Atomic Structure" Cambridge University Press (1968)

85 V. HEINE "Group Theory and Quantum Mechanics" Pergamon Press

86 K. W. H. STEVENS Proc. Phys. Soc. A 65 209 (1952)

87 A. J. FREEMAN and R. E. WATSON 'Magnetism' Vol IIA p 385 Academic Press (1965) (Ed. G. T. Rado and H. Suhl)

88 For example: L. D. LANDAU and E. M. LIFSHITZ "Electrodynamics of Continuous Media" Pergamon Press (1963) p 58

89 G. T. TRAMMELL Phys. Rev. 131 (1963) p 932

90 B. BLEANEY Proc. Roy. Soc. 23 939 (1959)

91 H. STATZ and G. F. KOSTER Phys. Rev. 115 p 1568 (1959)

92 T. F. SMITH and I. R. HARRIS J. Phys. Chem. Solids Vol 28 p 1846 (1967)

93 L. L. HIRST Solid State Comm. Vol 5 No 9 p 752 (1967)

94 J. ZIMAN "Electrons and Phonons" Oxford University Press (1960)

95 M. J. ZUCKERMANN (Private communication)

96 W. E. WALLACE and K. H. MADER (to be published in J. Phys. Chem. Solids)

97 B. R. COOPER Phys. Rev. 163 444 1967

98 A. D. CAPLIN and C. RIZZUTO Phys. Rev. Letters 21 746 (1968)

99 R. H. SHERMAN, S. G. SYDORIAK, T. R. ROBERTS Report No LAMS 2701 available from: Office of Technical Services, U.S. Dept of Commerce, Washington 25 DC

100 A. C. ROSE-INNES "Low Temperature Techniques" English Universities Press Ltd (1964)

101 D. MAPOTHER and E. P. HARRIS Phys. Rev. 165 522 (1968)

102 T. P. SHEAHEN Phys. Rev. 149 368 (1966)

103 G. K. WHITE "Experimental Techniques in Low Temperature Physics" Clarendon Press, Oxford (1959)

104 F. E. HOARE, L. C. JACKSON and N. KURTI "Experimental Cryophysics," Butterworth (1961)

105 W. R. ABEL, A. C. ANDERSON and J. C. WHEATLEY Rev. Sci. Inst. Vol 35 p 444 (1963)

106 R. T. JOHNSON, O. E. VILCHES, J. C. WHEATLEY and S. GYGAX Phys. Rev. Letters Vol 16 No 3 101 (1966)

107 K. ANDRES and M. A. JENSEN Phys. Rev. 165 533 (1968)

108 T. F. SMITH (Private Communication)

109 C. G. KUPER, M. A. JENSEN and D. C. HAMILTON Phys. Rev. Vol. 134 A13 (1964).

110 L. L. HIRST (Private Communication)

111 A. D. CAPLIN Proc. Phys. Soc. 92 p 739 (1967)

112 M. W. GARRET J. Appl. Phys. 22 1091 (1951)

113 A. W. ABEL and R. S. CRAIG Journ. Less Common Metals (to be published)

114 MATTHIAS B. T. and COMPTON V.B. Acta. Cryst. 651 (1959)

115 J. MULLER, CERN Lecture Notes, CERN 69-9, Geneva (1969)

116 B. R. COLES, Rev. Mod. Phys. Vol 36 No 1 p 139 (1964)

117 R. MCFEE, Rev. Sci. Inst. Vol. 30 No 2 p 98 (1959)